Novel Nonlinear Processes, Higher-Order Molecular Coupling and Multiphoton Interactions: A Quantum Electrodynamical Formulation©

Jamie Mark Leeder

As part requirement for the qualification of PhD

University of East Anglia

School of Chemistry

Submitted August 2011

This copy of the thesis has been supplied on the condition that anyone who consults it is understood to recognise that its copyright rests with the author and that no quotation from the thesis, nor any information derived therefrom, may be published without the author's prior, written consent.

Abstract

This thesis presents novel developments in the theory of distinct matter-radiation interactions, specifically resonance energy transfer (RET) and radiation-induced fluorescence. These processes and all associated mechanisms are accommodated within a fully quantized system, founded within a quantum electrodynamical (QED) formulation. The opening investigation concerns the photophysical relationship between electronically excited molecules and their neighbours, succeeding in demonstrating how such interactions differ from ground-state counterparts. A range of processes are considered, including RET, all of which are dependent on intermolecular interactions resulting from electric dipole coupling. Additional mechanisms including laser-assisted energy transfer are also assessed subject to interaction with off-resonant light. A system is subsequently developed in which the interplay of all such interactions is characterised. While RET is typically described through electric dipole (E1) coupling, exceptions exist in which the donor and/or acceptor exhibit E1-forbidden transitions, perhaps the result of inherent molecular symmetry. An alternative transfer mechanism occurs through higher-order multipole transitions and the relative significance of such couplings are assessed in systems where such interactions may be prominent. Progressing to laser-based studies of fluorescence, it is known that polarisation features of the emission convey rich information on structural details of a sample. It is shown how polarisation-resolved measurements can secure detailed information on the degree of rotational order within a system of chromophores oriented in three dimensions. The theory is extended, accommodating the signal produced by nonlinear polarisations, induced by one-, two- and three-photon absorptions. Results indicate that multiphoton imaging

can discriminate micro-domains within samples that exhibit orientational correlation. Finally, a novel development in radiation-induced fluorescence, namely “laser-controlled fluorescence”, is explored, whereby the character of emission is modified by a laser-controlled, nonlinear input. The result is a decay rate that can be controllably modified, the associated change affording new, chemically-specific information and novel technological application via all optical switching.

Contents

Publications

The content of this thesis, whilst related by a common theoretical foundation, is structured into chapters, each addressing a distinct development in QED theory. As a result of this work, a number of journal articles and conference proceedings have been published, the findings of which are summarised and in some cases expanded upon within these pages. Whilst each publication is cited in text where appropriate, a comprehensive bibliography is presented below, listing all work in chronological order:

1. Bradshaw, D.S., Leeder, J.M., Rodriguez, J. & Andrews, D.L. *Proc. SPIE* **6905**, 690503 (2008).
2. Bradshaw, D.S., Leeder, J.M., Rodriguez, J. & Andrews, D.L. *Proc. SPIE* **7034**, 703408 (2008).
3. Bradshaw, D.S., Leeder, J.M., Rodriguez, J. & Andrews, D.L. *Phys. Chem. Chem. Phys.* **10**, 5250 (2008).
4. Leeder, J.M. & Andrews, D.L. *J. Chem. Phys.* **130**, 034504 (2009).
5. Leeder, J.M. & Andrews, D.L. *J. Chem. Phys.* **130**, 184504 (2009).
6. Bradshaw, D.S., Leeder, J.M. & Andrews, D.L. *Proc. SPIE* **7571**, 75710B (2010).
7. Leeder, J.M. & Andrews, D.L. *Proc. SPIE* **7569**, 756922 (2010).
8. Bradshaw, D.S., Leeder, J.M. & Andrews, D.L. *Proc. SPIE* **7712**, 77121R (2010).
9. Bradshaw, D.S., Leeder, J.M. & Andrews, D.L. *Proc. SPIE* **7571**, 75710B (2010).

10. Andrews, D.L., Dávila Romero, L.C., Leeder, J.M. & Coles, M. *Proc. SPIE* **7762**, 776202 (2010).
11. Leeder, J.M. & Andrews, D.L. *J. Chem. Phys.* **134**, 094503 (2011).
12. Bradshaw, D.S., Leeder, J.M. & Andrews, D.L. *J. Phys. Chem. B* **115**, 5227 (2011).

The inclusion of reference 10 in the list above requires an additional note in that it addresses novel work on optically controlled molecular motors. Due to the preliminary nature of this research, current progress is not reported within this thesis, however research currently continues within the Norwich QED group.

Acknowledgements

I would first like to offer my gratitude to Professor David Andrews in recognition of his limitless knowledge, expert guidance, faultless organisation and superhuman patience. More importantly I am infinitely grateful for the genuine friendship you have offered me over the past four years. It has made this experience productive, highly enjoyable and truly unforgettable. Thank you David!

I offer my thanks and appreciation to all members, past and present, of the QED group in Norwich. In particular, I wish to highlight the talents of Dr David Bradshaw and Dr Luciana Dávila Romero-Smith, recognising just how much help you have both offered me throughout my studies.

I wish you all happiness, success and prosperity in your future endeavours

On a more personal note, I am grateful of the endless love and support offered by my family and friends. Without you all, this adventure would have never started. In particular I would like to offer thanks to my mum and my fiancée Lyndsey:

Mum, your guidance throughout my life is appreciated far more than I can ever express.

Lyndsey, you are simply stunning in everyway. Thank you for all the help!

Chapter 1 – General Introduction: Quantum Electrodynamics

In a recent review addressing the current state of high precision physics, Karshenboim poignantly and concisely summarised a brief history of classical mechanics and the inevitable development of quantum mechanical theory with regards to bound systems.[1] To elaborate, early advances in the physical theory of bound systems are often associated with Kepler, who studied the movement of planetary bodies within our solar system, theorising that such movement must adhere to a form of mathematical harmony. Whilst unable to prove this by observation, Kepler did successfully characterise previously unknown regularities in planetary orbital motion and his findings, presented as Kepler's Laws, became fundamental in advancing the theory of gravitation, mechanics and subsequently classical mechanics as a whole.

Comparisons can be drawn to developments made at the molecular scale, centuries later. Initially, the structure and properties of atoms were investigated within a model consistent with a heliocentric solar system, the nucleus (as the sun) being surrounded by electrons (planets) travelling in fixed orbits. Having failed to predict and verify known properties of simple atomic systems utilizing this classical approach, scientists slowly began to establish a new theoretical framework, that of quantum mechanics. Initially focussed on explaining the emission properties of atomic hydrogen, quantum mechanics has seen many developments since its inception, from Bohr theory, to both relativistic and non-relativistic quantum

mechanics and more recently quantum electrodynamics (QED).[2-5] The latter establishes the framework for the work that follows, QED having been recognised as the single most successful quantum theory to date, tested to a higher degree of precision than any other in modern physics. Notable accomplishments include the successful theoretical determination of the fine structure constant, the magnitude of the magnetic moment of the electron, and the Lamb shift.[1,6] The latter describes the small energy difference between the $^2S_{1/2}$ and $^2P_{1/2}$ energy levels, often associated with the hydrogen atom, yet subsequently characterized within helium as well as so called super-heavy elements.[1,7,8]

One of the hallmarks of QED, in contrast to both classical and semi-classical representations, is that it furnishes each mode of a fully quantized radiation field with a zero-point energy, consistent with quantum fluctuations in the corresponding electric and magnetic fields. As a physical consequence, these vacuum fields give rise to electromagnetic field quanta that can contribute to the dynamical behavior of a system. Cast in the framework of molecular QED, the dispersion interaction between electrically neutral molecules affords a good example. Within the short-range regime, *i.e.* where molecules are separated by a distance less than an optical wavelength, the interaction potential is known to vary with the inverse sixth power of the intermolecular separation, R^{-6}. Whilst such a result can be delivered by calculations performed on either a semi-classical or QED basis, only the latter form correctly accommodates retardation effects. As a consequence of field quanta propagating at the finite speed of light, QED predicts that the form of the interaction

potential exhibits a change to an R^{-7} dependence beyond short-range molecular separations and the success of this interpretation is vindicated by experimental measurement.[9]

Further to the unrivalled accuracy and precision of QED, the application of the theory also proves to be highly flexible, greatly facilitating the identification of fundamental links between effects that are physically different, but share a common form of mathematical development. One example is the similarity in the theoretical constructs of Raman scattering and two-photon absorption.[3,10,11] Another case is the formal link between fluorescence resonance energy transfer (FRET) and sequential Raman scattering.[12] Exploiting all these advantages, a QED framework is now constructed in which a variety of newly theorised photophysical mechanisms are explored and novel developments within established processes are investigated.

1.1 Development of a Fully Quantized System

For any QED analysis, discussion generally begins with the complete system Hamiltonian:

$$H = \sum_{\xi} H_{mol}(\xi) + \sum_{\xi} H_{int}(\xi) + H_{rad}\,, \tag{1.1}$$

in which $H_{mol}(\xi)$, H_{rad} and $H_{int}(\xi)$ correspond to fully quantized molecular, radiation and interaction Hamiltonians respectively. Noting the absence of any

term describing direct molecule-molecule interaction, equation (1.1) specifically represents the multipolar form of the system Hamiltonian in which all intermolecular interactions are deemed to occur solely through the exchange of photons.[13,14] The general representation of $H_{mol}(\xi)$ is well known, the Hamiltonian being expressible as the sum of all potential and kinetic quantum operators within the system:

$$H_{mol} = \sum_{\xi} \left\{ \frac{1}{2m} \sum_{\alpha} \left(\boldsymbol{p}_{\alpha}(\xi) \right)^2 + V(\xi) \right\}. \tag{1.2}$$

In the above expression, α labels each of the charged particles within molecules arbitrarily labeled ξ and it is noted that the featured Schrödinger operators incorporate terms relating to both nuclei and electrons. As previously discussed, the inclusion of H_{rad} in equation (1.1) is unique to a QED formulation, as opposed to a classical or semi-classical interpretation. Whilst first principle derivation of the quantized radiation field is beyond the remit of this introduction, the methods employed are discussed in detail in a number of prominent publications.[5,15-19] Proportional to the squares of both the quantized electric displacement and magnetic induction, H_{rad} is defined in terms of both the transverse electric displacement field, $\boldsymbol{d}^{\perp}(\boldsymbol{r})$ and the magnetic induction, $\boldsymbol{b}(\boldsymbol{r})$ as:

$$H_{rad} = \frac{1}{2} \int \left\{ \varepsilon_0^{-1} \left(\boldsymbol{d}^{\perp}(\boldsymbol{r}) \right)^2 + \varepsilon_0 c^2 \left(\boldsymbol{b}(\boldsymbol{r}) \right)^2 \right\} \mathrm{d}^3\boldsymbol{r}, \tag{1.3}$$

where ε_0 is the permittivity of free space. For brevity, it is assumed that both the quantized molecular and radiation terms in equation (1.1) are either known or are determinable, therefore it is the mutual interaction between the molecular system and quantized electromagnetic field, described by the interaction Hamiltonian, $H_{int}(\xi)$, that is of primary interest. Explicitly, $H_{int}(\xi)$ can be represented in the following generalized form, cast using the convention of summation over repeated Cartesian (subscript) indices:

$$H_{int}(\xi) = -\varepsilon_0^{-1} \sum_{\xi} E^{(l)}_{i_1 i_2 \ldots i_l}(\xi) \nabla_{i_2} \ldots \nabla_{i_l} d^{\perp}_{i_1}(\boldsymbol{R}_{\xi}), \tag{1.4}$$

where $E^{(l)}_{i_1 i_2 \ldots i_l}(\xi)$ represents an l^{th} order electric multipole operator coupled to the transverse electric field operator, $d^{\perp}_i(\boldsymbol{R}_{\xi})$ at position vector $\boldsymbol{R}_{\xi}$. In principle it is necessary to consider not only electric but also magnetic multipole contributions, however the latter are disregarded since magnetic contributions are typically several orders of magnitude smaller than their electric equivalents.[20-22] Whilst $E^{(l)}_{i_1 i_2 \ldots i_l}(\xi)$ acts on the system molecular states, $d^{\perp}_i(\boldsymbol{R}_{\xi})$ correspondingly operates on the system radiation states, being expressible in the following vectorial form:

$$\boldsymbol{d}^{\perp}(\boldsymbol{R}_{\xi}) = i \sum_{\boldsymbol{p},\lambda} \left(\frac{\hbar c p \varepsilon_0}{2V} \right)^{\frac{1}{2}} \Big[\boldsymbol{e}^{(\lambda)}(\boldsymbol{p}) a^{(\lambda)}(\boldsymbol{p}) \exp(i\boldsymbol{p}.\boldsymbol{R}_{\xi}) - \overline{\boldsymbol{e}}^{(\lambda)}(\boldsymbol{p}) a^{\dagger(\lambda)}(\boldsymbol{p}) \times \exp(-i\boldsymbol{p}.\boldsymbol{R}_{\xi}) \Big]. \tag{1.5}$$

Above, $\boldsymbol{e}^{(\lambda)}(\boldsymbol{p})$ is the electric field unit vector with complex conjugate $\overline{\boldsymbol{e}}^{(\lambda)}(\boldsymbol{p})$, whilst a and $a^{\dagger}$ respectively represent the photon annihilation and creation operators that act upon the eigenstates $n(\boldsymbol{p},\lambda)$ of H_{rad}. Specifically, a and $a^{\dagger}$ modify the number of photons n, each summed over all wave-vectors $\boldsymbol{p}$ and polarisations λ, that exist within an arbitrary quantization volume, V through the following expressions:

$$a|n\rangle = n^{1/2}|n-1\rangle, \tag{1.6}$$

$$a^{\dagger}|n\rangle = (n+1)^{1/2}|n+1\rangle. \tag{1.7}$$

Subsequently since equation (1.4) is linear with respect to $\boldsymbol{d}^{\perp}(\boldsymbol{R}_{\xi})$, each operation of $H_{int}(\xi)$ acts to destroy or create a single photon.

1.1.1 Ideal Dipole Approximation

Inclusion of $E^{(l)}_{i_1 i_2 \ldots i_l}(\xi)$ in equation (1.4) requires that any interaction between matter and radiation states is expressible as a complete sum over all electric multipole orders. The necessarily expanded expression for $H_{int}(\xi)$ follows as:

$$H_{int}(\xi) = -\varepsilon_0^{-1}\sum_{\xi}\left(\mu_i(\xi)\, d_i^{\perp}(\boldsymbol{R}_{\xi}) + Q_{ij}(\xi)\nabla_i d_j^{\perp}(\boldsymbol{R}_{\xi}) + \ldots\right), \tag{1.8}$$

in which $\mu_i(\xi)$ and $Q_{ij}(\xi)$ feature as components of the electric dipole (E1) and quadrupole (E2) transition moments respectively.[3,14,23,24] It is assumed that the molecular dimensions of a system treated by QED analysis are small relative to the wavelength of any interacting radiation. As a result, whilst additional higher order operators including the electric octapole (E3) and hexadecapole (E4) moments can be incorporated into equation (1.8), such contributions become increasingly small. Typically under such conditions on the molecular dimensions, the ideal dipole approximation is implemented whereby all observed molecular state transitions are considered to develop exclusively through electric dipole moments and consequently $H_{int}(\xi)$ becomes expressible in the following simplified form:

$$H_{int}(\xi) = -\varepsilon_0^{-1} \sum_{\xi} \mu_i(\xi) d_i^{\perp}(\boldsymbol{R}_{\xi}). \tag{1.9}$$

To clarify, the ideal dipole approximation is inferred for all discussion presented throughout this thesis and subsequently the interaction Hamiltonian is considered to be completely represented by equation (1.9). The only exception to this is in Section 3, where certain electric dipole transitions will be considered weak or entirely forbidden as a result of high molecular symmetry. Only in this case will $H_{int}(\xi)$ be portrayed by equation (1.8) where $\mu_i(\xi)$ shall represent the first term of a multipolar series with $Q_{ij}(\xi)$ corresponding to a significant lead correction.

1.1.2 Media Influence

To conclude laying foundations for the analyses to follow, it is appropriate to dwell on the influence of any host medium within which any photophysical process may occur. The explicit incorporation of such a medium in the theory develops the system Hamiltonian portrayed in equation (1.1), duly modifying all subsequent expressions. To begin, the total system is separated into two separate subsystems. The first such subsystem describes the "participating environment," in which the observed photophysical process occurs, subsequently following the pattern of theory previously established, *i.e.* the associated Hamiltonian comprises a sum of the molecular quantum operators for all molecules within the participating environment. The other subsystem represents all remaining matter existing outside this space, examples of which may include a protein scaffold, host crystal lattice or solvation shell etc. that modifies the total system Hamiltonian as:

$$H = \sum_{\xi'} H_{mol}\left(\xi'\right) + \sum_{\xi'} H_{int}\left(\xi'\right) + H_{bath}\,, \tag{1.10}$$

where ξ' represents all molecules within the participating environment and H_{bath} is the "bath" Hamiltonian. The latter operator comprises the radiation Hamiltonian as well as the Schrödinger and interaction operators for all remaining molecules represented by ξ'' existing outside the participating environment:

$$H_{bath} = H_{rad} + \sum_{\xi''} \left(H_{mol}\left(\xi''\right) + H_{int}\left(\xi''\right) \right). \tag{1.11}$$

Any observed photophysical process is now considered to be mediated by induced fluctuations of the bath as opposed to the vacuum electromagnetic field. Generally, intermolecular interactions within the participating environment are strong compared to the coupling between the two subsystems and in such instances an established treatment utilising perturbation theory is employed.[3,5,25] It should be noted that the procedures required to evaluate medium effects are well established, their application generally leading to the inclusion of Lorentz local-field factors and other corrections based on the complex refractive index of the host;[26] however, these steps shall be left implicit in order to simplify the form of all ensuing results. Instead, all matter-radiation interactions are considered *in vacuo*, with subsequent details of the perturbative approach to be discussed in Section 1.2.1.

1.2 Quantum Probability Amplitudes

In most applications, QED theory is utilized within molecular systems to determine transition probabilities and energy shifts that occur as a result of radiation field interactions. Such factors are accordingly addressed through quantum probability amplitudes that determine the relative coupling strengths between defined initial and final system states linked through any possible combination of intermediate state transitions. In the language of QED, such quantum probability amplitudes are commonly cast in the form of “matrix elements” as they are in principle derivable

for any specified initial and final state. For diagonal matrix elements, the initial and final system states represented by $|I\rangle$ and $|F\rangle$ respectively are identical and assuming at least a single matter-radiation interaction occurs, such transitions signify observable energy shifts, the aforementioned Lamb shift being a prominent example. In all off-diagonal contributions, where initial and final system states differ, the determined quantum probability amplitude is associated with a photophysical process. In such cases, the process efficiency (determined by Fermi's Golden Rule) is proportional to the modulus square of the matrix element, written as $|M_{FI}|^2$ so that:[27]

$$\Gamma = \frac{2\pi\rho_F}{\hbar}|M_{FI}|^2. \tag{1.12}$$

In the above expression, Γ is the rate of the observable process and ρ_F represents a density of states, defined as the number of molecular levels per unit energy associated with $|F\rangle$. In the development of theory relating to novel and potentially observable photophysical processes, the determination of associated off-diagonal matrix elements is significant and therefore such derivation becomes the focus of all following sections within this chapter.

1.2.1 Time-dependent Perturbation Theory

As previously established, providing that matter and field coupling remains sufficiently small with respect to intramolecular bond energies, *i.e.* propagating radiation regardless of its source does not disrupt the molecular structure of any participant within the system, the physical consequence of $H_{int}^{(\xi)}$ can be treated as a perturbation, partitioned from the unperturbed sum of all molecular and radiation operators, H_0, such that:

$$H = H_0 + \sum_{\xi} H_{int}(\xi). \tag{1.13}$$

Since both $H_{mol}(\xi)$ and H_{rad} are known quantities, the basis within which the effect of the coupling between matter and radiation states is determined is defined by the eigenstates $|Q\rangle$ of H_0 such that:

$$|Q\rangle = |mol_Q; rad_Q\rangle. \tag{1.14}$$

The perturbation is subsequently cast as an infinite series as:

$$M_{FI} = \sum_{q=1}^{\infty} \langle F | H_{int}(\xi) \left(T_0 H_{int}(\xi)\right)^{q-1} | I \rangle. \tag{1.15}$$

Above, $T_0 \approx \left(E^I - H_0\right)^{-1}$, with E^I the initial system energy. The parameter q, which denotes the power of $H_{int}(\xi)$ in each term of the expansion, has significant physical meaning; as an inherent result of the photon creation and annihilation operators present in $H_{int}(\xi)$, q corresponds to the number of fundamental matter-radiation interactions.

In order to demonstrate the discussed approach, the process of spontaneous one-photon emission, in which an excited state molecule undergoes transition to a ground state configuration whilst spontaneously emitting a photon into the vacuum field, is now detailed as an example. Initial conditions for the process require that the associated matter exists in an excited state, having been previously excited as the result of a laser input that plays no further role in the process, *i.e.* all radiation modes are unoccupied prior to the spontaneous emission. Since only a single matter-radiation event occurs, the necessary matrix element requires that $q = 1$ and is represented following substitution into equation (1.15) as:

$$M_{FI} = \langle F | H_{int}(\xi) | I \rangle, \tag{1.16}$$

where specifically for one-photon emission, $|I\rangle = |\xi^{\alpha}; n(\boldsymbol{p}, \lambda)\rangle$ and $|F\rangle = |\xi^{0}; (n+1)(\boldsymbol{p}, \lambda)\rangle$. Such details highlight an additional complication in constructing the matrix element for any photophysical process; that of self energy corrections relating to self-interaction terms. Whilst one-photon emission has so far

been characterized as a $\left|\xi^{0};(n+1)(\boldsymbol{p},\lambda)\right\rangle \leftarrow \left|\xi^{\alpha};n(\boldsymbol{p},\lambda)\right\rangle$ system state transition involving a single matter-radiation interaction, alternative pathways between the initial and final states involving multiple matter-radiation events are plausible. For example, the transition can be described by substitution of $q=3$ into equation (1.15) providing that one of the three implicit matter-radiation interactions represents single photon annihilation. Owing to the absence of any external laser input, the $q=3$ component of the matrix element for one-photon emission describes both the creation and annihilation of a single virtual photon, originating from a fluctuation in the background vacuum field and also the creation of one real photon. Subsequently, the $q=3$ term represents an additional correction to the complete matrix element, which is expressible as a series of terms:

$$M_{FI}=\left\langle F\left|H_{int}(\xi)\right|I\right\rangle+\sum_{R,S}\frac{\left\langle F\left|H_{int}(\xi)\right|S\right\rangle\left\langle S\left|H_{int}(\xi)\right|R\right\rangle\left\langle R\left|H_{int}(\xi)\right|I\right\rangle}{\left(E^{I}-E^{R}\right)\left(E^{I}-E^{S}\right)}+\ldots \tag{1.17}$$

in which $\left|R\right\rangle$ and $\left|S\right\rangle$ relate to system intermediate states with corresponding energies E^{R} and E^{S}. In this and all other examples, the lead term dominates over subsequent contributions, the former typically in the region of three orders of magnitude more significant. The $q=3$ term in the above expression and all further self energy corrections represented by additional contributions are therefore duly ignored.

The generalized form of equation (1.17) is worthy of additional note in that the presented matrix element equally portrays the process of one-photon absorption. As previously discussed, the application of QED therefore greatly facilitates the identification of fundamental links between processes that are physically different, but share a common form of mathematical development. Such links are explored in greater depth as the focus of Section 2.

1.2.2 Time-ordered Diagrams

Evident in processes involving multiple matter-radiation events, there is an additional factor in deriving required matrix elements, that all possible matter-radiation interaction combinations are considered as required by the sum over states form of perturbation theory; the complete matrix element of any process being the sum of all such contributions. In such cases it becomes useful to visualize all such combinations through the use of time-ordered "Feynman" diagrams.

All time-ordered diagrams presented in this thesis share a number of common features. Each represents time along the vertical dimension with the initial and final conditions portrayed at the bottom and top of the diagram respectively. Solid, vertical lines, often referred to as "world lines," illustrate changes to the electronic state of molecules during the exhibited process. Photons are represented by wavy lines, the evolution of which has a component within the horizontal axis, considered to represent spatial dimensions. Consequently, the intersection of a wavy line and a

world line represents an interaction vertex in which the processes of one-photon annihilation and creation are illustrated. Accounting for all such features, Figure 1.1 portrays one-photon emission as represented by the first term of equation (1.17).

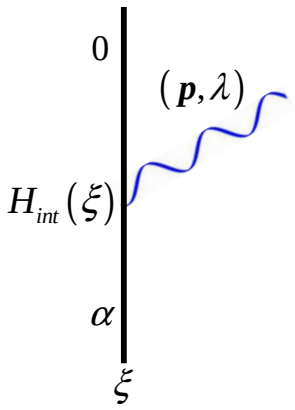

Figure 1.1 Time-ordered diagram of spontaneous one-photon emission.

Progressing upwards, the figure initially represents ξ in an electronically excited state ξ^{α} which as a result of interaction with the vacuum radiation field, as characterized by $H_{int}(\xi)$, undergoes a decay transition to a ground state configuration ξ^{0} whilst a photon of mode $(\boldsymbol{p},\lambda)$ is emitted. The diagram is unique as only one matter-radiation interaction occurs, however the second term of equation (1.17), although considered a self energy correction, provides a example in which numerous matter-radiation combinations must be considered to account for the entire process. Having already discussed that the self-interaction term incorporates three events, being the creation and annihilation of a single virtual photon and the emission of a single real photon, the order of such events is as yet

undefined. The three possible combinations of events are represented by Figure 1.2.

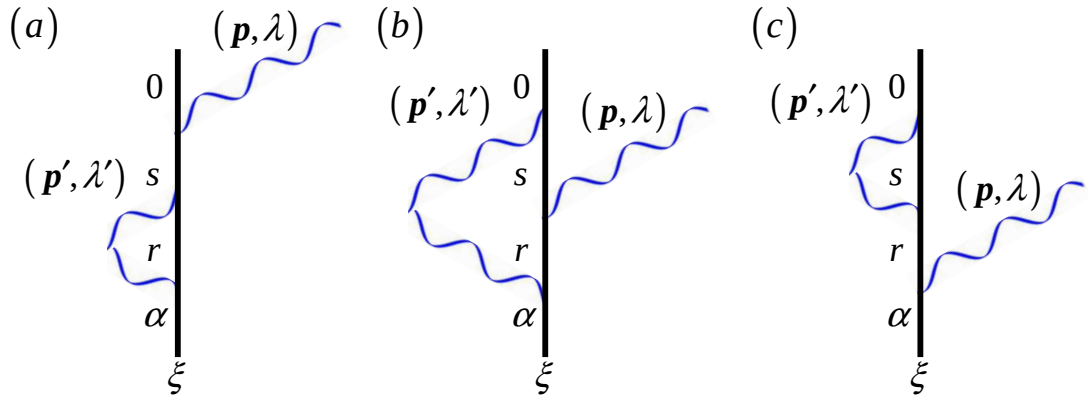

Figure 1.2 Time-ordered diagrams illustrating self energy corrections to one-photon emission.

As before, in all representations portrayed in Figure 1.2, the molecule ξ begins and ends in molecular states ξ^{α} and ξ^{0} respectively, however, inclusion of two additional matter-radiation interactions determine that the transitions progress through two molecular intermediate states ξ^{r} and ξ^{s}. Being a self-interaction contribution, the molecular transitions coincide with both the absorption and emission of a single virtual photon of mode $(\boldsymbol{p}',\lambda')$. Figures 1.2(*a*), 1.2(*b*) and 1.2(*c*) portray the process of single, real photon emission occurring after, during and prior to the emission and subsequent absorption of the virtual photon respectively. The energy required to create the virtual photon is drawn from fluctuations in the vacuum field, and providing the energy is replaced quickly, by re-absorption of the same virtual photon, the time-energy uncertainty principle permits the violation of energy conservation. Subsequently, the three time-orderings in Figure 1.2, each

represent equally valid corrections to the lead matrix element contribution portrayed by Figure 1.1 and if self-energy corrections had not been disregarded, the resulting contribution of each term would feature in the complete matrix element for spontaneous one-photon emission.

1.3 Rotational Averaging

As previously established, all the research to follow is broadly categorized within two main topics, each of the subsequent chapters either representing an original development in molecular energy transfer or laser induced fluorescence. Whilst both processes are fundamentally distinct, they share a common experimental variable, that each to a degree is dependent on the orientation of its associated chromophores. For the former, the orientation of an energy donor relative to a neighbouring acceptor is a crucial factor in determining the overall efficiency of an observed energy migration. In the case of the latter, the polarisation of an induced fluorescence output is known to vary with chromophore orientation relative to the polarisation of the input excitation. As a means to keep the presented results general and not otherwise restricted to the description of fixed and/or highly ordered molecular systems, it is considered in all subsequent examples that molecular matter is free to rotate in response to any imposed external stimulus and consequently, chromophores are assumed at all times to be randomly orientated in three dimensions. Under such conditions, results are typically determined by means of an isotropic orientational average, the basic procedure for which is now outlined.

In the continued example of one-photon emission, the process matrix element is first derived, requiring substitution of equation (1.9) into equation (1.17) and noting that only the lead term where $q=1$ is considered in the case of the latter:

$$M_{FI}=\left\langle A^{0};1(\boldsymbol{p},\lambda)\right|-\varepsilon_{0}^{-1}\mu_{i}(A)\,d_{i}^{\perp}(\boldsymbol{R}_{A})\left|A^{\alpha};0(\boldsymbol{p},\lambda)\right\rangle. \tag{1.18}$$

For simplicity, the summed contribution over an ensemble of molecules ξ is dropped in favor of a matrix element specifically determined for a single molecule, A. For further clarity, the matter and radiation terms are partitioned, allowing equation (1.18) to be re-expressed as:

$$M_{FI}=-\varepsilon_{0}^{-1}\left\langle A^{0}\left|\mu_{i}(A)\right|A^{\alpha}\right\rangle\left\langle 1(\boldsymbol{p},\lambda)\left|d_{i}^{\perp}(\boldsymbol{R}_{A})\right|0(\boldsymbol{p},\lambda)\right\rangle. \tag{1.19}$$

By substitution of equation (1.5) into the above expression, the matrix element is subsequently portrayed as:

$$M_{FI}=i\sum_{\boldsymbol{p},\lambda}\left(\frac{\hbar cp}{2\varepsilon_{0}V}\right)^{\frac{1}{2}}\bar{e}_{i}^{(\lambda)}(\boldsymbol{p})\,\mu_{i}^{0\alpha}(A)\exp\left(-i\boldsymbol{p}.\boldsymbol{R}_{A}\right), \tag{1.20}$$

where the electric dipole transition moment $\mu_{i}^{0\alpha}(A)\equiv\left\langle A^{0}\left|\mu_{i}\right|A^{\alpha}\right\rangle$, portrays the molecular transition $A^{0}\leftarrow A^{\alpha}$, in which the operator follows the convention of writing the initial and final molecular states as the right and left superscript

characters respectively. The subscript indices associated with the electric polarisation and dipole moment terms can each assume the Cartesian values of *x*, *y* or *z* with respect to a chosen frame, determining that both $\overline{e}_i^{(\lambda)}(\boldsymbol{p})$ and $\mu_i^{0\alpha}(A)$ are the salient parameters of study for the purpose of an orientational average. For clarity, equation (1.20) is therefore defined as:

$$M_{FI} = K\left(\overline{e}_i^{(\lambda)}(\boldsymbol{p})\mu_i^{0\alpha}(A)\right), \tag{1.21}$$

introducing a constant of proportionality K. The Fermi Golden Rule is utilized as a final step before the averaging procedure and by substitution of equation (1.21) into equation (1.12), the rate of spontaneous one-photon emission from A is presented as:

$$\Gamma = K'\left(\overline{e}_i^{(\lambda)}(\boldsymbol{p})e_j^{(\lambda)}(\boldsymbol{p})\mu_i^{0\alpha}(A)\overline{\mu}_j^{0\alpha}(A)\right), \tag{1.22}$$

where $K' = 2K\pi\rho_F(\hbar)^{-1}$. In the adopted notation, both the matter and radiation terms in equation (1.22) are currently portrayed within the same arbitrary space-fixed frame of reference. The initial step in implementing an orientational average is to first uncouple both sets of parameters by assigning to the former a molecule-fixed frame of reference, labeled by Greek indices such that:

$$\langle\Gamma\rangle = K'\left(\overline{e}_i^{(\lambda)}(\boldsymbol{p})e_j^{(\lambda)}(\boldsymbol{p})\mu_\lambda^{0\alpha}(A)\overline{\mu}_\mu^{0\alpha}(A)\langle\ell_{i\lambda}\ell_{j\mu}\rangle\right). \tag{1.23}$$

where angular brackets denote the rotational average. The space- and molecule-fixed reference frames are now linked through a product of direction cosines $\ell_{i\lambda}\ell_{j\mu}$, where $\ell_{i\lambda}$ for example is the cosine of the angle between the space-fixed axis i and the molecule-fixed axis λ. Conventionally, the average would proceed by re-expressing the direction cosines in terms of Euler angles, the end result being determined by means of mathematical integration. However, such methods are only feasible for tensors of low rank; the above example exhibiting an implicit sum over two separate Cartesian indices is resolved through second-rank, *i.e.* $n = 2$ orientational averaging. In later examples that require the deployment of averaging protocols up to the eighth-rank, an alternative integration free method based on isotropic matrix elements must instead be utilized. The analysis requires implementation of fourth-, sixth- and eighth-rank tensor averages, of which only the former two are widely documented;[3,28-30] nonetheless their calculational principles have been deployed across a wide range of photophysical processes, recently including coupled systems and interactions such as quantum dot assemblies, van der Waals dispersion energies and Casimir effects.[31-34]

As a rotationally invariant parameter, it is possible to represent $\left\langle \ell_{i\lambda}\ell_{j\mu} \right\rangle$ as a linear combination of tensors, each of which is also invariant under rotation. Such combinations are the product of two isotropic tensors, one referred to the space-fixed frame and the other to the molecule-fixed frame. In three dimensions, each isotropic tensor is representable as a product of at least two fundamental tensors, the well known Kronecker delta δ_{ij} and the Levi-Civita antisymmetric tensor, ε_{ijk}.

Since all rotational averages presented in the following work are of even rank, the associated isotropic tensors will each be the product of $\frac{n}{2}$ Kronecker deltas, the Levi-Civita antisymmetric tensor featuring only in averages of odd rank that most often arise in quantum interference terms. For the continued example of one-photon emission, having already been determined as a second rank average, both the space- and molecule-fixed isotropic tensors are represented by a single Kronecker delta, the corresponding average following as:

$$\left\langle \ell_{i\lambda} \ell_{j\mu} \right\rangle = \frac{1}{3} \delta_{ij} \delta_{\lambda\mu}, \tag{1.24}$$

By substitution of equation (1.24) into equation (1.23), the Kronecker delta functions operate on the matter and radiation terms that feature in the latter, effecting two changes. First, the fundamental tensor δ_{ij} contracts the electric polarisation terms, such that $\delta_{ij}\left(\overline{e}_i^{(\lambda)}(\boldsymbol{p}) e_j^{(\lambda)}(\boldsymbol{p})\right) = \overline{e}_i^{(\lambda)}(\boldsymbol{p}) e_i^{(\lambda)}(\boldsymbol{p}) = 1$. Similarly, $\delta_{\lambda\mu}$ contracts the molecular transition dipole moments so that $\delta_{\lambda\mu}\left(\mu_\lambda^{0\alpha}(A)\overline{\mu}_\mu^{0\alpha}(A)\right) = \mu_\lambda^{0\alpha}(A)\overline{\mu}_\lambda^{0\alpha}(A) = \left|\mu^{0\alpha}(A)\right|^2$. Subsequently, the rotationally averaged rate of single photon emission is determined as:

$$\left\langle \Gamma \right\rangle = \frac{1}{3} K' \left|\boldsymbol{\mu}^{0\alpha}(A)\right|^2. \tag{1.25}$$

Whilst in the above example, the second rank average presented as equation (1.24) clearly features only one possible product of the two isotropic tensors, higher ordered averages require the consideration of multiple possible combinations or isomers. In the case of fourth-rank averaging for example, each of the space- and molecule-fixed isotropic tensors are written as the product of two Kronecker deltas, an isomer of each being $\delta_{ij}\delta_{kl}$ and $\delta_{\lambda\mu}\delta_{\nu\sigma}$ respectively. Focusing on the former, by permuting the four indices, two additional isomers $\delta_{ik}\delta_{jl}$ and $\delta_{il}\delta_{jk}$ are generated. Following similar permutation in the molecule-fixed isotropic tensors, nine possible combinations of products between the two frames now exist. In order to concisely represent all possible arrangements, the generalized form of all higher rank averages are typically presented as matrix equations, where for example the generalized fourth-rank average, $\left\langle \ell_{i\lambda}\ell_{j\mu}\ell_{k\nu}\ell_{l\sigma} \right\rangle$ is represented generally as:[3,28]

$$\left\langle \ell_{i\lambda}\ell_{j\mu}\ell_{k\nu}\ell_{lo} \right\rangle = \frac{1}{30}\begin{pmatrix} \delta_{ij}\delta_{kl} \\ \delta_{ik}\delta_{jl} \\ \delta_{il}\delta_{jk} \end{pmatrix}^{T} \begin{pmatrix} 4 & -1 & -1 \\ -1 & 4 & -1 \\ -1 & -1 & 4 \end{pmatrix} \begin{pmatrix} \delta_{\lambda\mu}\delta_{\nu\sigma} \\ \delta_{\lambda\nu}\delta_{\mu\sigma} \\ \delta_{\lambda\sigma}\delta_{\mu\nu} \end{pmatrix}, \tag{1.26}$$

where T indicates a transpose matrix. Utilised in Sections 3, 4 and 5, the sixth rank orientational average $\left\langle \ell_{i\lambda}\ell_{j\mu}\ell_{k\nu}\ell_{l\sigma}\ell_{m\tau}\ell_{n\rho} \right\rangle$ features fifteen distinct isomers and is representable as:[3,28]

$$\left\langle \ell_{i\lambda}\ell_{j\mu}\ell_{k\nu}\ell_{l\sigma}\ell_{m\tau}\ell_{n\rho}\right\rangle = \frac{1}{210}\begin{pmatrix} \delta_{ij}\delta_{kl}\delta_{mn} \\ \delta_{ij}\delta_{km}\delta_{ln} \\ \delta_{ij}\delta_{kn}\delta_{lm} \\ \delta_{ik}\delta_{jl}\delta_{mn} \\ \delta_{ik}\delta_{jm}\delta_{ln} \\ \delta_{ik}\delta_{jn}\delta_{lm} \\ \delta_{il}\delta_{jk}\delta_{mn} \\ \delta_{il}\delta_{jm}\delta_{kn} \\ \delta_{il}\delta_{jn}\delta_{km} \\ \delta_{im}\delta_{jk}\delta_{ln} \\ \delta_{im}\delta_{jl}\delta_{kn} \\ \delta_{im}\delta_{jn}\delta_{kl} \\ \delta_{in}\delta_{jk}\delta_{lm} \\ \delta_{in}\delta_{jl}\delta_{km} \\ \delta_{in}\delta_{jm}\delta_{kl} \end{pmatrix} M^{(6)} \begin{pmatrix} \delta_{\lambda\mu}\delta_{\nu\sigma}\delta_{\tau\rho} \\ \delta_{\lambda\mu}\delta_{\nu\tau}\delta_{\sigma\rho} \\ \delta_{\lambda\mu}\delta_{\nu\rho}\delta_{\sigma\tau} \\ \delta_{\lambda\nu}\delta_{\mu\sigma}\delta_{\tau\rho} \\ \delta_{\lambda\nu}\delta_{\mu\tau}\delta_{\sigma\rho} \\ \delta_{\lambda\nu}\delta_{\mu\rho}\delta_{\sigma\tau} \\ \delta_{\lambda\sigma}\delta_{\mu\nu}\delta_{\tau\rho} \\ \delta_{\lambda\sigma}\delta_{\mu\tau}\delta_{\nu\rho} \\ \delta_{\lambda\sigma}\delta_{\mu\rho}\delta_{\nu\tau} \\ \delta_{\lambda\tau}\delta_{\mu\nu}\delta_{\sigma\rho} \\ \delta_{\lambda\tau}\delta_{\mu\sigma}\delta_{\nu\rho} \\ \delta_{\lambda\tau}\delta_{\mu\rho}\delta_{\nu\sigma} \\ \delta_{\lambda\rho}\delta_{\mu\nu}\delta_{\sigma\tau} \\ \delta_{\lambda\rho}\delta_{\mu\sigma}\delta_{\nu\tau} \\ \delta_{\lambda\rho}\delta_{\mu\tau}\delta_{\nu\sigma} \end{pmatrix}, \tag{1.27}$$

requiring the 15×15 numerical matrix, $M^{(6)}$ as follows:

$$M^{(6)} = \begin{pmatrix}
16 & -5 & -5 & -5 & 2 & 2 & -5 & 2 & 2 & 2 & 2 & -5 & 2 & 2 & -5 \\
-5 & 16 & -5 & 2 & -5 & 2 & 2 & 2 & -5 & -5 & 2 & 2 & 2 & -5 & 2 \\
-5 & -5 & 16 & 2 & 2 & -5 & 2 & -5 & 2 & 2 & -5 & 2 & -5 & 2 & 2 \\
-5 & 2 & 2 & 16 & -5 & -5 & -5 & 2 & 2 & 2 & -5 & 2 & 2 & -5 & 2 \\
2 & -5 & 2 & -5 & 16 & -5 & 2 & -5 & 2 & -5 & 2 & 2 & 2 & 2 & -5 \\
2 & 2 & -5 & -5 & -5 & 16 & 2 & 2 & -5 & 2 & 2 & -5 & -5 & 2 & 2 \\
-5 & 2 & 2 & -5 & 2 & 2 & 16 & -5 & -5 & -5 & 2 & 2 & -5 & 2 & 2 \\
2 & 2 & -5 & 2 & -5 & 2 & -5 & 16 & -5 & 2 & -5 & 2 & 2 & 2 & -5 \\
2 & -5 & 2 & 2 & 2 & -5 & -5 & -5 & 16 & 2 & 2 & -5 & 2 & -5 & 2 \\
2 & -5 & 2 & 2 & -5 & 2 & -5 & 2 & 2 & 16 & -5 & -5 & -5 & 2 & 2 \\
2 & 2 & -5 & -5 & 2 & 2 & 2 & -5 & 2 & -5 & 16 & -5 & 2 & -5 & 2 \\
-5 & 2 & 2 & 2 & 2 & -5 & 2 & 2 & -5 & -5 & -5 & 16 & 2 & 2 & -5 \\
2 & 2 & -5 & 2 & 2 & -5 & -5 & 2 & 2 & -5 & 2 & 2 & 16 & -5 & -5 \\
2 & -5 & 2 & -5 & 2 & 2 & 2 & 2 & -5 & 2 & -5 & 2 & -5 & 16 & -5 \\
-5 & 2 & 2 & 2 & -5 & 2 & 2 & -5 & 2 & 2 & 2 & -5 & -5 & -5 & 16
\end{pmatrix}. \tag{1.28}$$

Whilst both the fourth and sixth rank averages have previously been implemented in a host of applications, Sections 4 and 5 each also utilize the generalised eighth rank isotropic average, the form of which does not feature explicitly due to its size; the $M^{(8)}$ matrix is representable as a 105×105 grid of characters.[29]

1.4 Summary of Theoretical Framework

It is prudent to conclude this opening chapter by means of a summary, reviewing all salient features of the background information presented thus far. Any further development in either the established theory or employed method, including any

specific deviation from the general points to follow, will be addressed in detail as required.

All novel research is founded within a recognized QED theoretical framework and thus accommodates a fully quantized system; both matter and radiation field are subject to the postulates of quantum mechanics. The system Hamiltonian is presented in the multipolar form and therefore in the description of intermolecular interactions, no direct matter-matter coupling exists. Instead, all such interactions are facilitated through the surrounding radiation field, mediated by the exchange of transverse photons. Whilst both the quantized molecular and radiation Hamiltonians are required parameters for any complete interpretation of a given system, such features for brevity are assumed to be known or determinable. It is therefore the mutual interaction of the molecular system and electromagnetic field, whose transitions are individually described by the electric multipole and transverse displacement field operators respectively, that are of primary concern.

In addressing molecular transitions, the system dimensions in all worked examples are considered compatible with the ideal dipole approximation therefore generally excluding the need to comment further on the contribution of magnetic or higher-order electric multipole transitions. For the radiation field, it is assumed at all times that interaction photons travel at the speed of light *in vacuo*. Under such conditions, the present work elicits clear physical behaviour of complex systems

whilst further providing a sound basis for developing a further tier of theory to account for any modifications introduced by media influences.

In the development of theory pertaining to innovative photophysical processes, it is envisaged throughout that the strength of coupling between matter and radiation field is comparatively weak relative to the Coulombic fields that maintain the internal structure within atoms or molecules. Matrix elements derived through time-dependent perturbation theory are therefore always valid and remain so even in later examples addressing the application upon a molecular system of high intensity pulsed laser inputs. Whilst it has been shown that matrix elements may be represented as the sum of an infinite number of terms through the inclusion of self-interaction contributions, it is always the lead term that dominates, such that subsequent higher-order additions are duly disregarded.

Finally, it is well known that chromophore orientation represents a dependent variable for both the processes of RET and laser induced fluorescence that together represent the two main topics of discussion. In all cases, such chromophores are assumed to be randomly orientated in three dimensions and free to rotate in response to any imposed external stimulus. Under such conditions, results are determined by means of an isotropic average, requiring the utilisation of either the fourth-, sixth- or eighth-rank orientational averages as previously presented.

References

1. Karshenboim, S.G. *Phys. Rep.* **422**, 1 (2005).
2. Healy, W.P. *Non-Relativistic Quantum Electrodynamics*. (Academic: London, 1982).
3. Craig, D.P. & Thirunamachandran, T. *Molecular Quantum Electrodynamics*. (Dover: New York, 1998).
4. Salam, A. *Int. Rev. Phys. Chem.* **27**, 405 (2008).
5. Salam, A. *Molecular Quantum Electrodynamics*. (Wiley: Chichester, 2009).
6. Gabrielse, G., Hanneke, D., Kinoshita, T., Nio, M. & Odom, B. *Phys. Rev. Lett.* **97**, 030802 (2006).
7. Drake, G.W. *Nucl. Phys.* **737**, 25 (2004).
8. Mokler, P.H. *Radiat. Phys. Chem.* **75**, 1730 (2006).
9. Sukenik, C.I., Boshier, M.G., Cho, D., Sandoghdar, V. & Hinds, E.A. *Phys. Rev. Lett.* **70**, 560 (1993).
10. Andrews, D.L., Blake, N.P. & Hopkins, K.P. *J. Chem. Phys.* **88**, 6022 (1988).
11. Andrews, D.L. & Blake, N.P. *J. Mod. Optic.* **37**, 701 (1990).
12. Andrews, D.L. & Allcock, P. *Chem. Phys.* **198**, 35 (1995).
13. Andrews, D.L. & Bradshaw, D.S. *Eur. J. Phys.* **25**, 845 (2004).
14. Salam, A. *J. Chem. Phys.* **122**, 044112 (2005).
15. Loudon, R. *The Quantum Theory of Light*. (Oxford University Press: Oxford, 2000).

16. Woolley, R.G. in *Handbook of Molecular Physics and Quantum Chemistry*. (Wiley: Chicester, 2003), p. 657 .
17. Novotny, L. & Hecht, B. *Principles of Nano-Optics*. (Cambridge University Press: Cambridge, 2006).
18. Cohen-Tannoudji, C., Dupont-Roc, J. & Grynberg, G. *Photons and Atoms: Introduction to Quantum Electrodynamics*. (Wiley: Chichester, 2007).
19. Grynberg, G., Aspect, A. & Fabre, C. *Introduction to Quantum Optics*. (Cambridge University Press: Cambridge, 2010).
20. Daniels, G.J., Jenkins, R.D., Bradshaw, D.S. & Andrews, D.L. *J. Chem. Phys.* **119**, 2264 (2003).
21. Andrews, D.L. *Can. J. Chem.* **86**, 855 (2008).
22. Baer, R. & Rabani, E. *J. Chem. Phys.* **128**, 184710 (2008).
23. Scholes, G.D. & Andrews, D.L. *J. Chem. Phys.* **107**, 5374 (1997).
24. Andrews, D.L. & Allcock, P. *Optical Harmonics in Molecular Systems: Quantum Electrodynamical Theory*. (Wiley-VCH: Weinheim, 2002).
25. Löwdin, P.O. *Perturbation Theory and its Applications in Quantum Mechanics*. (Wiley: New York, 1965).
26. Juzeliūnas, G. & Andrews, D.L. in *Resonance Energy Transfer*. (Wiley: Chicester, 1999), p. 65.
27. Mandel, L. & Wolf, E. *Optical Coherence and Quantum Optics*. (University Press: Cambridge, 1995).
28. Andrews, D.L. & Thirunamachandran, T. *J. Chem. Phys.* **67**, 5026 (1977).
29. Andrews, D.L. & Ghoul, W.A. *J. Phys. A* **14**, 1281 (1981).

30. Wagniere, G. *J. Chem. Phys.* **76**, 473 (1982).

31. Scholes, G.D. *J. Chem. Phys.* **121**, 10104 (2004).

32. Salam, A. *J. Phys. B* **39**, S651 (2006).

33. Salam, A. *J. Phys. B* **39**, S663 (2006).

34. Huxter, V.M. & Scholes, G.D. *J. Chem. Phys.* **132**, 104506 (2010).

SECTION 1 – Quantum Electrodynamical Development of Resonance Energy Transfer

The following section consists of two chapters each exploring distinct developments in theory pertaining to resonance energy transfer (RET); a mechanism of remarkable relevance across a wide range of physical, chemical and biological systems, described as the transportation of electronic excitation between donor and acceptor units (ions, atoms, molecules or chromophores) following photoexcitation.

Chapter 2 investigates a range of photophysical processes that fundamentally depend on intermolecular interactions resulting from electric dipole coupling, the most familiar being static dipole-dipole interactions, RET, and intermolecular dispersion forces. Additional forms of intermolecular interaction including radiation-induced energy transfer and optical binding are also considered in molecules subjected to off-resonant light. Within the established QED formulation, all these phenomena are cast in a unified description that establishes their inter-relationship and connectivity at a fundamental level. Theory is then developed for systems in which the interplay of these forms of interaction can be readily identified. Throughout this work, a primary consideration is that electronically excited molecules interact with their neighbors differently from their ground-state counterparts, therefore any migration of the excitation between molecules should

modify the observed intermolecular forces, reflecting changes to the local potential energy landscape.

While RET is typically described as a coupling of electric dipole (E1) transition moments, a significant number of exceptions exist in which donor decay and/or acceptor excitation processes are E1-forbidden. Possible alternative transfer mechanisms that can apply in such cases include roles for higher multipole transitions, exciton- or phonon-assisted interactions, and non-Coulombic interactions based on electron exchange. Chapter 3 provides a rigorous basis to assess the first of these, deemed the most generally applicable alternative to E1-forbidden RET. Specifically, the significance of higher multipole contributions to the process of energy transfer is considered in donor-acceptor systems where E1-transitions are precluded by symmetry.

Resonance Energy Transfer

The primary result of photon absorption in any complex dielectric material is the population of electronic excited states, in individual atomic or molecular sites. Typically, each such absorption is followed by a rapid but partial degradation of the acquired energy, dissipative losses due to intramolecular or lattice nuclear vibrations ultimately being manifest in the form of heat. The majority of the excitation energy, held in a localized electronic excited state, may be acquired by a

neighboring atom or molecule with a suitably disposed electronic state, through RET.[1-3]

The process of RET operates across a chemically diverse and extensive range of material systems. Perhaps the most important and widely known example occurs naturally in plants and photosynthetic organisms as the photochemical harvesting of solar energy.[4-8] In an attempt to mimic such photosynthetic units and exploit the Sun in solving our own energy crisis, a number of synthetic alternatives have been proposed. Polymer systems such as dendrimers along with dye loaded zeolite crystal structures are just two possible media for the efficient capture and relocation of optical energy to desirably located acceptor cores.[8-17] As an additional advantage, the one-directional nature of such energy transfers opens the technology to a range of applications including organic light-emitting diodes and luminescence detectors.[18,19]

Beyond energy harvesting and channelling, there has recently been a resurgence of interest in RET used as a structural probe utilising the mechanisms well known sensitivity to transfer distance. Time-resolved decay measurements of biomaterials such as proteins suitably labeled with fluorescent chromophores allow the study of dynamic conformational changes within biological systems, exploiting the distance dependence as a so-called "spectroscopic ruler".[20-26] Similar application of the technology is applied to elucidate physical and morphological interface properties

of complex polymer blends.[27-31] Several ultra-sensitive molecular imaging applications are also based on the same underlying principles.[32-38]

Irrespective of the specific application, the elementary process of RET can be summarised by the expression $A^{\alpha} + B^{0} \rightarrow A^{0} + B^{\beta}$ featuring two, usually neighboring chromophores, A and B which operate respectively as donor and acceptor of the electronic excitation.

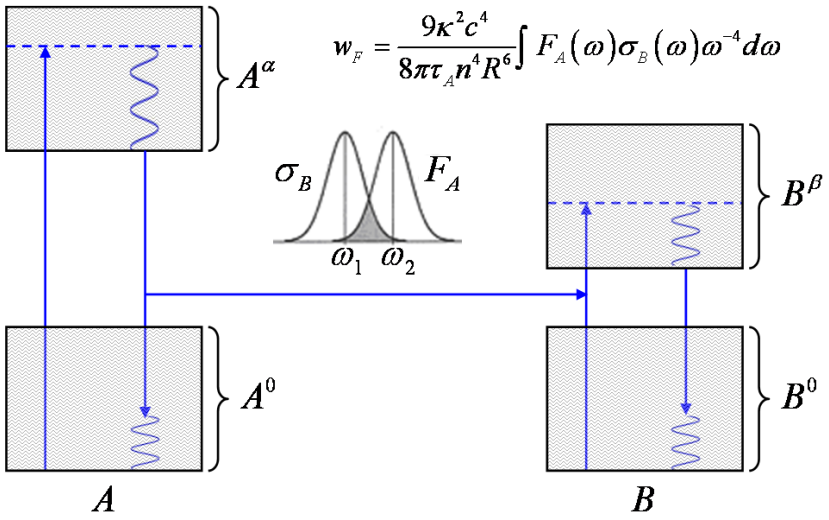

Figure 1.3 Energetics and spectral overlap features for RET. Electronic states for *A* and *B* and their vibrational manifolds are signified by the boxes. Wavy lines indicate processes of non-radiative, vibrational relaxation.

As portrayed in Figure 1.3, the energy transfer process through RET proceeds through resonance coupling between the donor and the acceptor. The short-range rate equation first proposed by Förster is presented in the figure, introducing the fluorescence and absorption spectra, F_A and σ_B of the donor and acceptor

respectively. The refractive index of the host media is represented by *n*, the donor excited state lifetime by τ_A and the relative orientation of donor and acceptor molecules is included through the orientation factor κ.

After initial electronic excitation, the donor in an excited state A^{α} undergoes a downward energy transition to the electronic ground state whilst the acceptor is promoted from its ground state configuration to an excited state B^{β}. In principle, relaxation of the donor and excitation of the acceptor can engage any available electronic states of the participating molecules providing that the donor and acceptor necessarily have emission and absorption spectra exhibiting a degree of overlap. Generally a rapid internal reorganisation following the energy transfer usually puts the acceptor into an energy level from which its subsequent decay has relatively small overlap with the donor absorption profile, establishing a spectroscopic gradient that limits back-transfer.[39] At short distances, where the wavefunctions of the two species have significant overlap, an electron exchange mechanism usually associated with the name of Dexter can operate.[40] Additionally, the coupling of electric multipoles persists into and well beyond the point where wavefunction overlap can be disregarded. The nature of the latter interaction is the primary focus of work in this section.

The mechanism for RET is most accurately described within a QED framework, analysis by which delivers a rate equation for the energy migration that incorporates both near- and far-zone behavior as limits of a more general dependence on inter-

chromophore separation.[41] Within the short-range limit, Coulombic RET is commonly described as a radiationless (Förster) process linking dipole-allowed transitions, and the rate of transfer has an R^{-6} dependence.[42] As the chromophore separation increases to and beyond the optical wavelength scale, QED theory correctly establishes a seamless linkage to the far-zone limit where an R^{-2} relationship, associated with radiative transfer, is observed.

References

1. Andrews, D.L. *Resonance Energy Transfer*. (Wiley: Chichester, 1999).
2. Scholes, G.D. *Annu. Rev. Phys. Chem.* **54**, 57 (2003).
3. Andrews, D.L. *Can. J. Chem.* **86**, 855 (2008).
4. Cogdell, R.J., Gardiner, A.T., Roszak, A.W., Law, C.J., Southall, J. & Isaacs, N.W. *Photosynth. Res.* **81**, 207 (2004).
5. Melkozernov, A.N. & Blankenship, R.E. *Photosynth. Res.* **85**, 33 (2005).
6. Grimm, B., Porra, R.J., Rüdiger, W. & Scheer, H. *Chlorophylls and Bacteriochlorophylls*. (Springer: Dordrecht, 2006).
7. Vassiliev, S. & Bruce, D. *Photosynth. Res.* **97**, 75 (2008).
8. Balzani, V., Credi, A. & Venturi, M. *ChemSusChem* **1**, 26 (2008).
9. Adronov, A. & Frechet, J.M.J. *Chem. Commun.* 1701 (2000).
10. Balzani, V., Ceroni, P., Maestri, M. & Vicinelli, V. *Curr. Opin. Chem. Biol.* **7**, 657 (2003).

11. Cotlet, M., Gronheid, R., Habuchi, S., Stefan, A., Barbafina, A., Mullen, K., Hofkens, J., & De Schryver, F.C. *J. Am. Chem. Soc.* **125**, 13609 (2003).
12. Andrews, D.L. & Bradshaw, D.S. *J. Chem. Phys.* **121**, 2445 (2004).
13. Takahashi, M. Morimoto, H., Suzuki, Y., Odagi, T., Yamashita, M., & Kawai, H. *Tetrahedron* **60**, 11771 (2004).
14. Andrews, D.L. & Li, S. *Chem. Phys. Lett.* **433**, 239 (2006).
15. Zabala Ruiz, A., Li, H. & Calzaferri, G. *Angew. Chem.* **118**, 5408 (2006).
16. Andrews, D.L., Li, S., Rodríguez, J. & Slota, J. *J. Chem. Phys.* **127**, 134902 (2007).
17. Calzaferri, G. & Lutkouskaya, K. *Photochem. Photobiol. Sci.* **7**, 879 (2008).
18. Hepp, A., Ulrich, G., Schmechel, R., von Seggern, H. & Ziessel, R. *Synthetic Met.* **146**, 11 (2004).
19. Zhang, S., Lu, Z., Peng, Y., Liu, Y. & Yang, Y. *J. Lumin.* **128**, 1523 (2008).
20. Dos Remedios, C.G. & Moens, P.D.J. *J. Struct. Biol.* **115**, 175 (1995).
21. Dos Remedios, C.G. & Moens, P.D.J. in *Resonance energy transfer*. (Wiley: Chicester, 1999), p. 1.
22. Weiss, S. *Nat. Struct. Biol.* **7**, 724 (2000).
23. Schuler, B., Lipman, E.A. & Eaton, W.A. *Nature* **419**, 743 (2002).
24. Huebsch, N.D. & Mooney, D.J. *Biomaterials* **28**, 2424 (2007).
25. Borgia, A., Williams, P.M. & Clarke, J. *Annu. Rev. Biochem.* **77**, 101 (2008).
26. Ferreon, A.C.M. & Deniz, A.A. *BBA-Proteins Proteom.* **1814**, 1021 (2011).
27. Saini, S., Singh, H. & Bagchi, B. *J. Chem. Sci.* **118**, 23 (2006).
28. Morawetz, H. *J. Polym. Sci. A* **37**, 1725 (1999).

29. Farinha, J.P.S. & Martinho, J.M.G. *J. Phys. Chem. C* **112**, 10591 (2008).

30. Farinha, J.P.S. & Martinho, J.M.G. in *Fluorescence of Supermolecules, Polymers, and Nanosystems.* (Springer: Berlin, 2008), p. 215.

31. Zammarano, M. Maupin, P.H., Sung, L., Gilman, J.W., McCarthy, E.D., Kim, Y.S. & Fox, D.M. *ACS Nano* **5**, 3391 (2011).

32. Bastiaens, P.I.H. & Squire, A. *Trends Cell Biol.* **9**, 48 (1999).

33. des Francs, G.C., Girard, C. & Martin, O.J.F. *Phys. Rev. A* **67**, 053805 (2003).

34. des Francs, G.C., Girard, C., Juan, M. & Dereux, A. *J. Chem. Phys.* **123**, 174709 (2005).

35. Duncan, R.R. *Biochem. Soc. Trans.* **34**, 679 (2006).

36. Jares-Erijman, E.A. & Jovin, T.M. *Curr. Opin. Chem. Biol.* **10**, 409 (2006).

37. Kumar, S. Alibhai, D., Margineanu, A., Laine, R., Kennedy, G., McGinty J., Warren, S., Kelly, D., Alexandrov, Y., Munro, I., Talbot, C., Stuckey, D.W., Kimberly, C., Viellerobe, B., Lacombe, F., Lam, E.W., Taylor, H., Dallman, M.J., Stamp, G., Murray, E.J., Stuhmeier, F., Sardini, A., Katan, M., Elson, D.S., Neil, M.A.A., Dunsby, C. & French, P.M.W. *ChemPhysChem* **12**, 609 (2011).

38. Pietraszewska-Bogiel, A. & Gadella, T.W.J. *J. Microsc.* **241**, 111 (2011).

39. Andrews, D.L. & Rodríguez, J. *J. Chem. Phys.* **127**, 084509 (2007).

40. Dexter, D.L. *J. Chem. Phys.* **21**, 836 (1953).

41. Daniels, G.J., Jenkins, R.D., Bradshaw, D.S. & Andrews, D.L. *J. Chem. Phys.* **119**, 2264 (2003).

42. Förster, T. *Discuss. Faraday Soc.* **27**, 7 (1959).

Chapter 2 – Dynamics of the Dispersion Potential in an Energy Transfer System

The migration of electronic excitation between molecular units has received extensive experimental and theoretical study, in particular its spectroscopic manifestations are well characterized. However, it appears that little regard has been given to changes, intrinsic to the operation of RET, that occur in the dispersion interaction between donor and acceptor units. The dispersion interaction is itself most accurately described in terms of the Casimir-Polder potential;[1] using QED, its explicit form emerges from calculations based on intermolecular coupling through virtual photon mediators.[2-5] Recent work by Salam has determined the general formula for the dispersion potential deriving from multipolar interactions.[6-8] The relevant equations have also been secured by implementing quantum amplitude calculations using a state-sequence approach;[9] a device first proposed and developed by Jenkins *et al.*[10] Although the long-range behaviour of the leading contribution to the potential runs with the inverse *seventh* power of the inter-particle distance R, the shorter-range form that operates over distances where effects are most pronounced exhibits an R^{-6} asymptotic behaviour. The latter is well known as the attractive component of the Lennard-Jones potential. Whilst the dispersion potential is usually considered as an interaction between molecules in their ground states, a potential of similar form may readily be derived for molecules in excited states.[11-18]

Since the form of the dispersion interaction depends on the electronic states of the molecular participants, the dispersion force between neutral molecules is clearly subject to change during the course of molecular excitation, relaxation and RET. Indeed, electronic environments will first experience change upon local optical excitation of any donor, the associated modification of electromagnetic interactions between the donor and other units immediately producing modified intermolecular forces. In general, a degree of local movement can be expected as the system becomes accommodated to the new potential energy field. If the absorbed energy then transfers to a neighbouring acceptor unit of another species so that the latter acquires the excitation, *i.e.* RET occurs, the local electronic environment will suffer further change, and once again a compensating spatial accommodation can be expected to occur. In particular, in a solid-state environment where intermolecular forces are balanced in an equilibrium configuration, any changes associated with the migration of local electronic excitation should effectively act as a small perturbation to the equilibrium of intrinsic forces, producing potentially measurable displacements. As recent preliminary studies have shown, the typical magnitude of such effects falls well within the current limits of experimental detection.[13-16]

Exploiting the flexibility of the theory established in Chapter 1, the objective of the present analysis is to address a system in which various physical effects are not only mathematically, but also physically interlinked. In Section 2.1, the theory of second and fourth order interactions is developed with a particular focus on elucidating the effects of intermolecular energy transfer through RET; a succinct treatment of the

dispersion pair potential is included, in which the dependence on the electronic state of the interacting particles is explicitly delivered. Such calculations accommodating both mechanical forces and electronic processes accurate to fourth order in perturbation theory have not been attempted before. The analysis is extended to accommodate and appraise subsidiary effects due to throughput radiation, specifically additional mechanical and dynamical effects that arise on the propagation of off-resonant light through the transfer system. Since any adaptation to subtly changing force fields is most readily tested in an ensemble, rather than in individual particle pairs, Section 2.2 addresses a system in which the two units between which energy is transferred are counterpositioned on parallel one-dimensional arrays in close proximity. The theory is further extended, to elicit the dynamical behaviour, and the system response to pulsed off-resonant laser light is ascertained as a function of time. The results of the model are presented in Section 2.3, followed by concluding thoughts in Section 2.4.

2.1 Intermolecular Coupling Processes

To ensure rigorous inclusion of all processes and mechanisms to a common and consistent level, evaluation up to the fourth order of perturbative expansion is implemented, to consider all relevant couplings between physically identifiable system states. One over-riding condition is that the final state of every radiation mode is identical to its initial state, *i.e.* no net absorption or emission of radiation occurs during the course of the process under examination. For this reason, since

$H_{int}(\xi)$ from equation (1.4) can only create or destroy one photon on each operation, only even values of the power index q arise. Hence the leading non-zero terms in the series expressed by equation (1.15) can be developed, through insertion of the state completeness relation on the right-hand side of each T_0 operator:

$$M_{FI} = \sum_{R} \frac{\langle F|H_{int}(\xi)|R\rangle\langle R|H_{int}(\xi)|I\rangle}{\left(E^I - E^R\right)} + \sum_{R,S,T} \frac{\langle F|H_{int}(\xi)|T\rangle\langle T|H_{int}(\xi)|S\rangle\langle S|H_{int}(\xi)|R\rangle\langle R|H_{int}(\xi)|I\rangle}{\left(E^I - E^R\right)\left(E^I - E^S\right)\left(E^I - E^T\right)} + \ldots \,. \tag{2.1}$$

To clarify, $|R\rangle$, $|S\rangle$ and $|T\rangle$ represent intermediate states, each denominator term being the energy difference between one of these intermediates and the initial state. Additionally, the following assumptions are implied throughout. All interactions are considered to occur beyond the region of significant wavefunction overlap. The entire system is considered to be isolated and as a consequence, dynamical processes are uniquely associated with a response to the intermolecular migration of energy, and to any time-varying radiative input, such as the pulsed off-resonant laser radiation that proves to induce features of particular interest.

2.1.1 Second-order Processes

Static dipole interaction: From equation (2.1), the leading contribution represents a second-order perturbation, which in the short-range signifies the creation and annihilation of a single virtual photon. The simplest case is the static interaction of two ground-state molecules with permanent electric-dipole moments, represented as two distinct time-ordered diagrams in Figure 2.1.

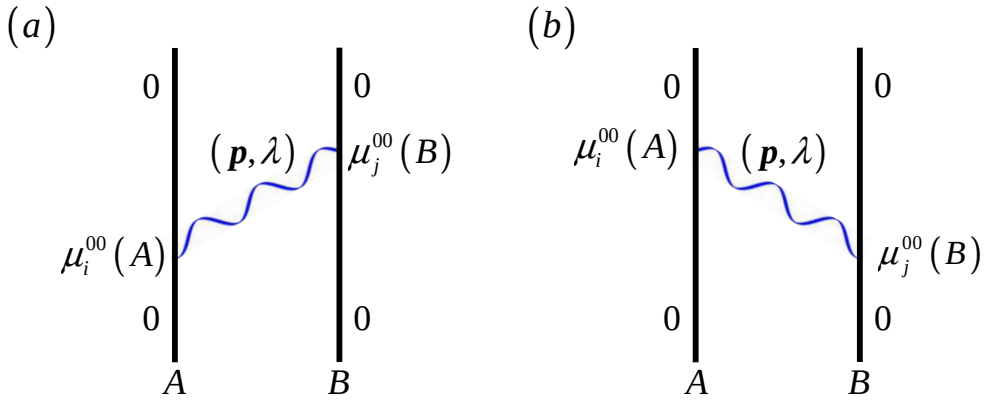

Figure 2.1 Time-ordered diagrams for static dipole-dipole coupling

These diagrams elucidate two possible contributions to the static interaction, Figure 2.1(*a*) entailing the creation of a virtual photon at molecule *A* and subsequent annihilation at *B*, and Figure 2.1(*b*) portraying the reverse. As with all subsequently described processes, a complete description requires a summation of the quantum amplitudes delivered by all such topologically distinct representations. The result emerges as follows:

$$\Delta E = \mu_i^{00}(A)\mu_j^{00}(B)V_{ij}(p,\mathbf{R}), \tag{2.2}$$

where the energy shift associated with the static coupling is represented by ΔE, and $\mu^{00}(\xi)$ signifies a ground state static electric dipole moment. The fully retarded coupling tensor of rank two, $V_{ij}(p,\boldsymbol{R})$ is exactly expressible as:

$$V_{ij}^{\pm}(p,\boldsymbol{R}) = \frac{\exp(\mp ipR)}{4\pi\varepsilon_0 R^3}\left[\left(\delta_{ij} - 3\hat{R}_i\hat{R}_j\right)(1 \pm ipR) - \left(\delta_{ij} - \hat{R}_i\hat{R}_j\right)(pR)^2\right], \tag{2.3}$$

noting that whilst both positive and negative imaginary contributions are acceptable, the latter form is more commonly cited.[19] For significantly small distances, *i.e.* where $pR \ll 1$, the coupling tensor in equation (2.3) essentially reduces to a short-range limit equivalent to the coupling of static dipoles dependent on R^{-3}, expressible as:

$$V_{ij}(0) = \frac{1}{4\pi\varepsilon_0 R^3}\left(\delta_{ij} - 3\hat{R}_i\hat{R}_j\right), \tag{2.4}$$

with $V_{ij}(0)$ being the zero-frequency result. Conventionally RET is thus described as being "radiationless" in the short-range, a process induced by electric dipole coupling.

Resonance energy transfer: In terms of an experimentally observable process, the simplest intermolecular interaction is the transfer of energy through resonance coupling between molecules, one of which is in an initially prepared excited state. As with static dipole coupling, RET is a second order interaction exhibiting two photon-matter interactions, *i.e.* the propagation of a single virtual photon, see Figure 2.2.

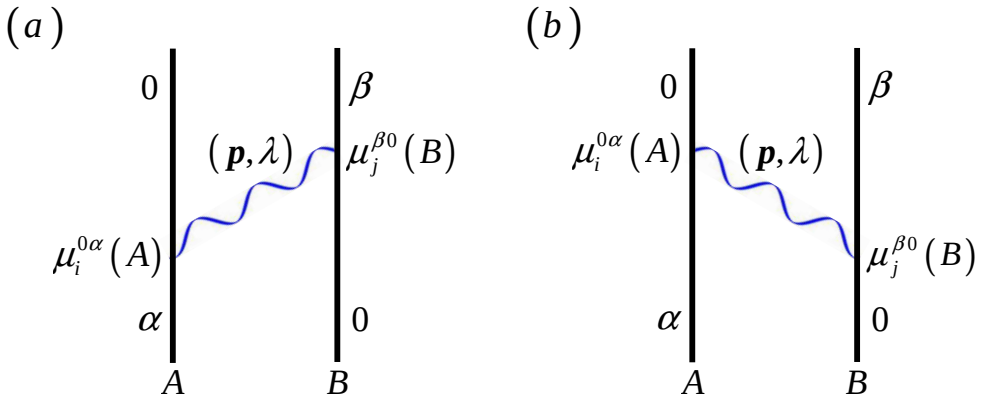

Figure 2.2 Time-ordered diagrams for RET

The matrix element for RET is again represented by the first term of equation (2.1). Using the labels 0, α and β to represent the electronic ground and corresponding excited states of the donor and acceptor respectively, the initial, final and intermediate states for RET are defined thus:

$$\begin{aligned} |I\rangle &= |A^{\alpha},B^{0};0\rangle \\ |R_1\rangle &= |A^{0},B^{0};1(\boldsymbol{p},\lambda)\rangle \\ |R_2\rangle &= |A^{\alpha},B^{\beta};1(\boldsymbol{p},\lambda)\rangle \\ |F\rangle &= |A^{0},B^{\beta};0\rangle. \end{aligned} \tag{2.5}$$

In equation (2.5), the summed intermediate states $|R\rangle$ relating to the first term of equation (2.1) have been explicitly cast in each of two permissible forms, one virtual photon being present in each. Respectively, $|R_1\rangle$ and $|R_2\rangle$ relate to conditions where both molecules, or neither, are in the electronic ground state. Detailed derivation of the second-order RET matrix element is already well documented, leading to the following result:[20-22]

$$M_{FI}^{(2)} = \mu_i^{0\alpha}(A)\mu_j^{\beta 0}(B)V_{ij}(p,\boldsymbol{R}), \tag{2.6}$$

where the superscript for $M_{FI}^{(2)}$ highlights the power order of q utilized in the matrix element derivation. Again, the short range limit of the above expression would instead employ the zero frequency coupling tensor given in equation (2.4).

2.1.2 Fourth-order Processes

Casimir-Polder (dispersion) interaction: Considered next are interactions governed by a total of four matter-radiation events. In the absence of an applied electromagnetic field, the simplest and most widely relevant example is the Casimir-Polder dispersion interaction, a process which in QED terms is mediated by the intermolecular propagation of two virtual photons.[2-5] The interaction has a matrix element associated with the second term of equation (2.1) and is illustrated by 12 distinct Feynman diagrams, see Figure 2.3.

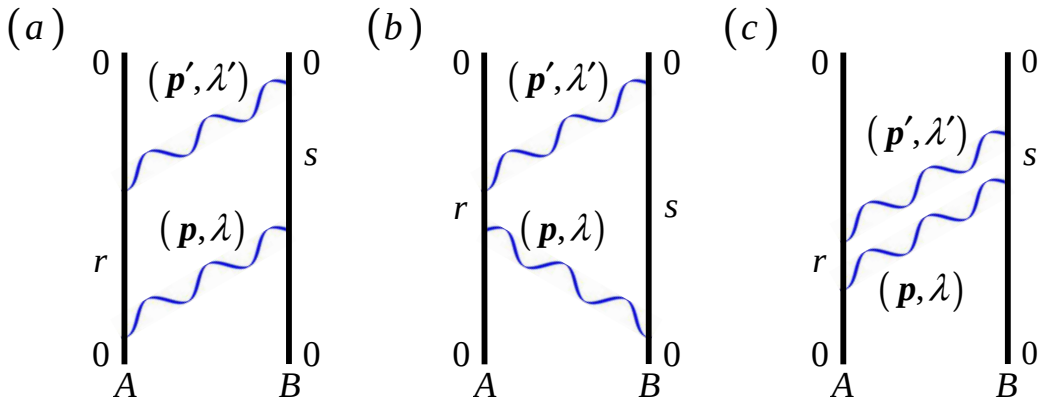

Figure 2.3 Three of twelve possible time-ordered diagrams for the Casimir-Polder dispersion interaction

As an example, for the attractive coupling between ground state molecules, the following system states define the contribution from Figure 2.3(*c*):

$$\begin{aligned}
|I\rangle &= |F\rangle = |A^0, B^0; 0\rangle \\
|R\rangle &= |A^r, B^0; 1(\boldsymbol{p},\lambda)\rangle \\
|S\rangle &= |A^0, B^0; 1(\boldsymbol{p},\lambda), 1(\boldsymbol{p}',\lambda')\rangle \\
|T\rangle &= |A^0, B^s; 1(\boldsymbol{p}',\lambda')\rangle .
\end{aligned} \tag{2.7}$$

For brevity, rather than consider all possible time-orderings, as required to define the complete potential for any distance, we instead consider two limits that exhibit strikingly different responses. In the near-zone, where intermolecular distances are small compared to the longest wavelengths of absorption or fluorescence, the coupling is essentially instantaneous. The Uncertainty Principle dictates that the short-lived virtual photons may accordingly exhibit energies that are large compared to the molecular transition energies. This acts as a constraint upon the

time-ordered contributions that contribute significantly to the dispersion interaction.[3,9] Conversely, in the far-zone limit, increasing propagation time allows the virtual photons to convey lower energies, and the calculations are dominated by contributions consistent with photon frequencies that are small with respect to the molecular absorption and emission frequencies.

For calculational simplicity, all interactions are subsequently discussed within the near-field range; the effects to be described are certainly most prominent in this region. Within this range, the key equations relating to both second-order static coupling and the fourth-order dispersion potential are more conventionally derived utilizing a dipolar coupling approximation with first- and second-order perturbation theory respectively. In the case of the former, we first consider a pairwise coupling between *A* and *B*, both having permanent electric dipoles. In a QED derivation of the coupling, it has already been established that the interaction is represented as a virtual photon transfer between *A* and *B*, for which there are two possible time-orderings (see Figure 2.1). Within the near-field range, the donor emits a photon that is almost instantly absorbed by the acceptor, and the coupling can be considered unretarded, *i.e.* the virtual photon creation and annihilation events in effect occur simultaneously. The process is now represented by just a single time-ordering (Figure 2.4). The calculation is treated by first-order perturbation theory, utilising the pairwise operator W_{AB}, which is derived by substitution of equation (2.4) into equation (2.2) and given explicitly by:

$$W_{AB} = \frac{\mu_i(A)\mu_j(B)}{4\pi\varepsilon_0 R^3}\left(\delta_{ij} - 3\hat{R}_i\hat{R}_j\right). \tag{2.8}$$

The pair interaction potential is thus determined by $\Delta E = \langle \Lambda | W_{AB} | \Lambda \rangle$, noting that W_{AB} is an operator over only molecular states. As such, $|\Lambda\rangle$ signifies the unperturbed basis state involving only the donor molecule in state *a* and the acceptor in state *b*, therefore the interaction potential emerges from equation (2.8) with the diagonal matrix elements $\mu_i^{aa}(A)$ and $\mu_j^{bb}(B)$, *i.e.* the static dipole moments substituting for the dipole operators.

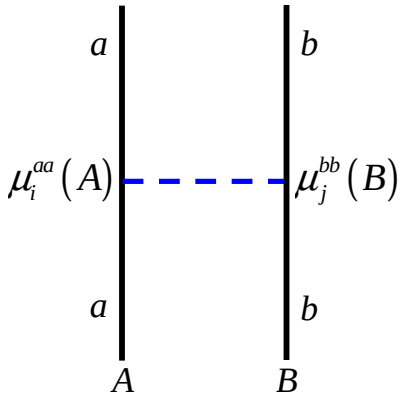

Figure 2.4 Time-ordered diagram representing near-zone static dipole-dipole coupling. The dashed line is symbolic of an almost instantaneous mediation between donor and acceptor

The dispersion interaction is an additional form of coupling which in the investigation of dynamical behavior in Section 2.2 becomes the dominant form. The assumption of a system comprising non-polar molecules means that no role is played by static dipole coupling itself. Figure 2.5 illustrates a simplified Feynman

diagram for evaluating the dispersion potential in its near-zone asymptote, where the coupling derives from two separate but instantaneous mediations between *A* and *B*.[2,5,12]

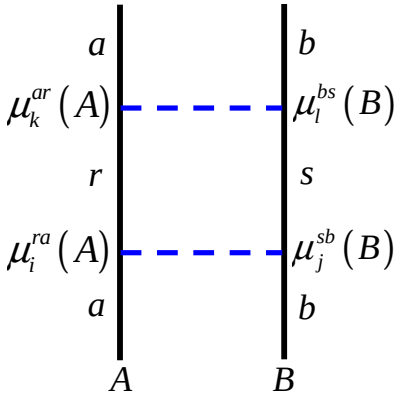

Figure 2.5 Time-ordered diagram representing near-zone dispersion potential

The coupling is treated, again through use of W_{AB}, but this time with second-order perturbation theory:

$$\Delta E = \sum_R \frac{\langle \Lambda | W_{AB} | R \rangle \langle R | W_{AB} | \Lambda \rangle}{E^\Lambda - E^R}. \tag{2.9}$$

On substitution of equation (2.8) into (2.9), with the state of each component duly specified, the following emerges:

$$\Delta E(A^aB^b) = \sum_{r,s} \frac{\left\langle A^a, B^b \left| W_{AB} \right| A^r, B^s \right\rangle \left\langle A^r, B^s \left| W_{AB} \right| A^a, B^b \right\rangle}{E^a(A) + E^b(B) - E^r(A) - E^s(B)}$$
$$= \frac{1}{16\pi^2 \varepsilon_0{}^2 R^6} \sum_{r,s} \mu_i^{ar}(A) \mu_j^{bs}(B) \mu_k^{ra}(A) \mu_l^{sb}(B) \left(\delta_{ij} - 3\hat{R}_i \hat{R}_j\right)$$
$$\times \left(\delta_{kl} - 3\hat{R}_k \hat{R}_l\right) \left(E^{ar}(A) + E^{bs}(B)\right)^{-1},$$

(2.10)

within which, $E^{ar}(A)$ and $E^{bs}(B)$ portray energy differences more generally represented by $E^{xy}(\xi) = E^x(\xi) - E^y(\xi)$, where *x* and *y* represent molecular energy levels of ξ. Whilst equation (2.10) is generally valid for rigidly oriented molecules, a key assumption throughout is that the dipole moments of both the donor and acceptor are randomly oriented, *in situ*, therefore the key features of the physics are clarified by performing an orientational average. Separate second rank averages are performed on *A* and *B*, each utilizing the general second order isotropic tensor portrayed by equation (1.26). With the isotropic average applied to the result emerging from equation (2.10) the following is ascertained:

$$\Delta E(A^aB^b) = -\frac{1}{24\pi^2 \varepsilon_0{}^2 R^6} \sum_{r,s} \frac{\left|\boldsymbol{\mu}^{ar}(A)\right|^2 \left|\boldsymbol{\mu}^{bs}(B)\right|^2}{E^{ra}(A) + E^{sb}(B)}, \tag{2.11}$$

which reduces to the well-known London formula when *a* and *b* are ground levels. In the latter case each $E^{ra}(A)$ and $E^{sb}(B)$ is positive, therefore the result of equation (2.11) is invariably a negative quantity. With due regard to the inverse

power dependence on distance, the attractive nature of the dispersion potential is thus apparent.

2.1.3 Additional Processes in the Presence of Off-resonant Laser Light

In the presence of intense off-resonant laser light, additional intermolecular effects are manifest as a result of real photon-matter interactions. For the identification of such effects, calculations are performed on a basis state for which the occupation number of at least one photon mode is non-zero. In order to determine energy shifts arising from a coupling with throughput radiation, it is necessary to identify terms that are diagonal in this basis, taking the following form:

$$|I\rangle = |F\rangle = |A^0, B^0; n(\boldsymbol{p}, l)\rangle. \tag{2.12}$$

Optically induced pair forces: The leading contribution to the interaction modified by laser input is an optically induced pair force, this fourth-order perturbation described as a real photon annihilation at the donor and stimulated re-emission from the acceptor (or vice versa), with both molecules coupled by a single virtual photon.[23,24] Possible forms of the interaction are portrayed by Figure 2.6.

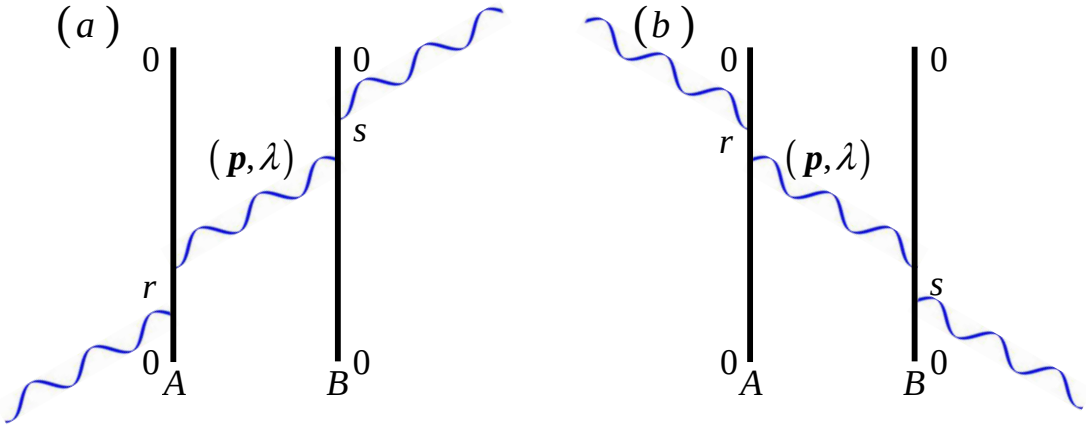

Figure 2.6 Two possible time-ordered diagrams representing the optically induced pair force

In accordance with energy conservation, the throughput radiation suffers no overall change. The analysis of an optically induced pair energy shift begins from the second contribution of equation (2.1), see for example work by Bradshaw and Andrews, leading to the following result for non-polar molecules:[25]

$$\Delta E_{ind} = \left(\frac{n\hbar cp}{\varepsilon_0 V} \right) \mathrm{Re}\left[e_i^{(l)}(\boldsymbol{p}) \alpha_{ij}(A) V_{jk}(p, \boldsymbol{R}) \alpha_{kl}(B) e_l^{(l)}(\boldsymbol{p}) \exp(-i\boldsymbol{p}.\boldsymbol{R}) \right]. \tag{2.13}$$

Here, n defines the number of real input photons, with individual energies $\hbar cp$ ($p = 2\pi / \text{laser wavelength}$). The retarded dipole-dipole coupling tensor $V_{jk}(p, \boldsymbol{R})$ takes the same form as equation (2.3). The dynamic polarizability tensors which feature in equation (2.13) are specific implementations of the formula:

$$\alpha_{ij}^{fi}(\xi)=\sum_{r}\left(\frac{\mu_i^{fr}(\xi)\mu_j^{ri}(\xi)}{E^{ri}(\xi)-\hbar cp}+\frac{\mu_j^{fr}(\xi)\mu_i^{ri}(\xi)}{E^{ri}(\xi)+\hbar cp}\right). \tag{2.14}$$

In this expression, given here in general form with a view to later calculations, omission of the state labels as in equation (2.13) signifies ground state evaluation, *i.e.* $\boldsymbol{\alpha}(\xi)=\boldsymbol{\alpha}^{00}(\xi)$.

In order to fully describe the effect of optical forces on a system, it is necessary to consider internal degrees of freedom as defined by molecular geometry. Based on equation (2.13), calculations have for example been performed for a range of cylindrical configurations including cases of tumbling, collinear and parallel donor-acceptor pairs.[24,25] In the case of isotropic molecules, the energy shift emerges as:

$$\Delta E_{ind}=\left(\frac{2I}{\varepsilon_0 c}\right)\mathrm{Re}\left[\alpha_0(A)V_{xx}(p,\boldsymbol{R})\alpha_0(B)\right], \tag{2.15}$$

where x denotes the axis of laser polarisation and accordingly, $\alpha_0(A)$ is a scalar value. The above result highlights the linear dependence on laser intensity, I. The near-field distance dependence is accommodated within the near-field tensor element $V_{xx}(p,\boldsymbol{R})$:

$$\mathrm{Re}\left[V_{xx}(p,\boldsymbol{R})\right]=-\frac{1}{2\pi\varepsilon_0 R^3}. \tag{2.16}$$

Laser-assisted resonance energy transfer: In the same way that intermolecular dispersion forces are modified by off-resonant laser light, fourth-order modifications have also been reported in connection with RET. The corresponding capacity for enhancing the rate of transfer has earned the soubriquet "laser-assisted resonance energy transfer (LARET)".[26-28] As with the optically induced pair forces, the throughput radiation once again emerges in a final state that is unchanged from the initial state, whilst in this case the material system experiences a transfer of energy from A to B. Thus, for the initial and final states of the system as a whole we have:

$$\begin{aligned} |I\rangle &= |A^{\alpha}, B^{0}; n(\boldsymbol{p}, l)\rangle \\ |F\rangle &= |A^{0}, B^{\beta}; n(\boldsymbol{p}, l)\rangle. \end{aligned} \tag{2.17}$$

It should be emphasized that the laser beam experiences no absorptive energy loss, the LARET process not to be confused with "laser-induced resonance energy transfer"; wherein laser frequencies are specifically chosen to promote energy migration by bridging a donor and acceptor frequency mismatch.[29] Depending on how the throughput radiation interacts with the donor-acceptor system, a number of possible LARET mechanisms emerge. Each entails real photon absorption and emission, coupled by a virtual photon mediator. First, consider processes where a real photon is absorbed at the donor and subsequently re-emitted from the acceptor, see Figure 2.7.

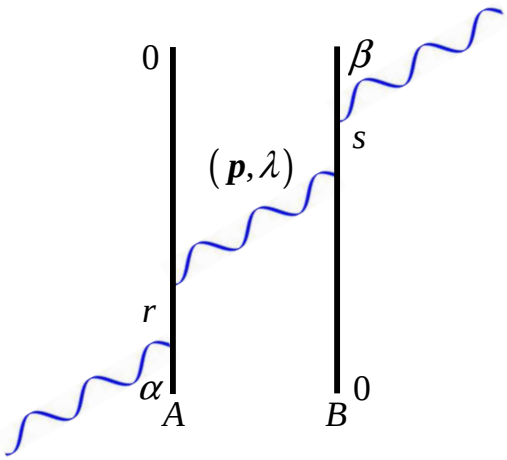

Figure 2.7 One possible time-ordered diagram representing LARET

The net matrix element, accommodating all time-orderings, takes the following form:

$$M_{FI}^{LARET(1)} = -\frac{n\hbar cp}{2\varepsilon_o V}\Big[e_i(\boldsymbol{p})\alpha_{ij}^{0\alpha}(A)V_{jk}(p,\boldsymbol{R})\alpha_{kl}^{\beta 0}(B)\bar{e}_l(\boldsymbol{p})\exp(-i\boldsymbol{p}\cdot\boldsymbol{R}) + \bar{e}_i(\boldsymbol{p})\alpha_{ij}^{0\alpha}(A)V_{jk}(p,\boldsymbol{R})\alpha_{kl}^{\beta 0}(B)e_l(\boldsymbol{p})\exp(i\boldsymbol{p}\cdot\boldsymbol{R})\Big]. \tag{2.18}$$

Terms in equation (2.18) are similar in form to those describing the optically induced pair potential as shown in equation (2.13), but here the process of energy transfer from A to B effects a differentiation between those molecules. The two parts of equation (2.18) reflect "mirrored" contributions, the first corresponding to the case where real photon absorption occurs at A with emission at B, and the second, the reverse. The full LARET matrix element is completed by the inclusion

of two further contributions associated with intermolecular interactions where the real photon absorption and emission processes both occur at the same centre:

$$M_{FI}^{LARET(2)} = \frac{n\hbar cp}{2\varepsilon_o V}\Big[\, \bar{e}_{\,i}(\boldsymbol{p}) e_l\,(\boldsymbol{p}) \beta_{ijl}^{0\alpha}(A) V_{jk}(p,\boldsymbol{R}) \mu_k^{\beta 0}(B) + \bar{e}_{\,i}(\boldsymbol{p}) e_l\,(\boldsymbol{p}) \beta_{ijl}^{\beta 0}(B) V_{jk}(p,\boldsymbol{R}) \mu_k^{0\alpha}(A) \,\Big]. \tag{2.19}$$

The hyperpolarizability tensor components $\beta_{ijl}^{fi}(\xi)$ signify the effects of three photon interactions (two real and one virtual) at a single centre, being defined in the form:

$$\begin{aligned}
&\beta_{jkl}^{fi}(\xi) = \\
&\sum_{r,s}\Bigg[\frac{\mu_l^{fs}(\xi)\mu_k^{sr}(\xi)\mu_j^{ri}(\xi)}{\left(E^{ri}(\xi)-\hbar cp_1\right)\left(E^{si}(\xi)-\hbar cp_1+\hbar cp_2\right)} \\
&+\frac{\mu_j^{fs}(\xi)\mu_k^{sr}(\xi)\mu_l^{ri}(\xi)}{\left(E^{ri}(\xi)-\hbar cp_3\right)\left(E^{si}(\xi)-\hbar cp_3+-\hbar cp_2\right)}+\frac{\mu_k^{fs}(\xi)\mu_l^{sr}(\xi)\mu_j^{ri}(\xi)}{\left(E^{ri}(\xi)-\hbar cp_1\right)\left(E^{si}(\xi)-\hbar cp_1+\hbar cp_3\right)} \\
&+\frac{\mu_k^{fs}(\xi)\mu_j^{sr}(\xi)\mu_l^{ri}(\xi)}{\left(E^{ri}(\xi)-\hbar cp_3\right)\left(E^{si}(\xi)-\hbar cp_3+\hbar cp_1\right)}+\frac{\mu_l^{fs}(\xi)\mu_j^{sr}(\xi)\mu_k^{ri}(\xi)}{\left(E^{ri}(\xi)+\hbar cp_2\right)\left(E^{si}(\xi)-\hbar cp_1\right)} \\
&+\frac{\mu_j^{fs}(\xi)\mu_l^{sr}(\xi)\mu_k^{ri}(\xi)}{\left(E^{ri}(\xi)+\hbar cp_2\right)\left(E^{si}(\xi)-\hbar cp_3\right)}\Bigg],
\end{aligned} \tag{2.20}$$

where above, the virtual photon is associated with $e_k(p)$ and energy $\hbar cp_2$, while the real photon input and output relate to $e_j(p)$, $e_l(p)$ and energies $\hbar cp_1$ and $\hbar cp_3$ respectively. It is interesting to observe that the above mechanism, involving the

occurrence of both real photon operations at a single molecular center, also has counterparts for the optically induced pair forces.[24,25,30] However in the latter case the dipole moments corresponding to those in equation (2.19) are static, which in the context of the present work, addressing isotropic molecules, are zero. In LARET, the moments are associated with transition dipoles, and such terms persist even for non-polar molecules.

2.2 Dynamic Behaviour

Intermolecular interactions are most widely understood in connection with systems in which molecules reside in their electronic ground states, a reasonable assumption when the system is in ambient conditions, and electronically excited state populations are vanishingly small. Here, however, we focus upon effects that are uniquely exhibited by systems in which additional electronic energy is present, as a result of photoexcitation for example. The nature of interactions between electrically neutral molecules certainly varies according to their electronic state, and those interactions are clearly subject to change during the course of absorption and RET.[13-16,31]

2.2.1 Effect of Electronic Excitation and Energy Transfer

Whilst the dispersion potential for a single donor-acceptor interaction is defined by equation (2.11), an ensemble of pairs incorporating donors and acceptors of any

electronic state, generates an effective system average pair potential $\overline{\Delta E}$, expressed as:

$$\overline{\Delta E} = -\frac{1}{24\pi^2 \varepsilon_0{}^2 R^6} \sum_{\substack{a=0,\alpha, \\ b=0,\beta}} N^a N^b \sum_{\substack{r=0,\alpha,\alpha^*, \\ s=0,\beta,\beta^*}} \frac{\left|\boldsymbol{\mu}^{ar}(A)\right|^2 \left|\boldsymbol{\mu}^{bs}(B)\right|^2}{E^{ra}(A) + E^{sb}(B)}. \tag{2.21}$$

In the first summation on the right-hand side of equation (2.21), N^a and N^b are the fractional populations of donors in state *a* and acceptors in state *b* respectively, whose explicit time-dependences produce dynamical effects on $\overline{\Delta E}$ as will emerge from subsequent population modeling in Section 2.2.2. The second summation in equation (2.21) is taken over donor and acceptor molecular states, each molecule being treated as a three-level system to reflect its most prominent optical features. For the generic state labels we have $r \in \{0, \alpha, \alpha^*\}$ and $s \in \{0, \beta, \beta^*\}$, perturbation theory precluding the combination $a = r$ and $b = s$. The higher energy states A^{a^*} and B^{β^*} are included as representatives of unpopulated, virtual electronic states. The physical significance of the different forms that arise for the summed interactions in equation (2.21) is that the energy denominator can, according to the pair states for which it is evaluated, yield a negative result. Bearing in mind the sign at the front of the expression and the overall dependence on an inverse power of R, it transpires that the potential in such cases no longer describes an attractive force as by contrast is always the case for neutral molecules.

2.2.2 Time-dependent System

Represented within Figure 2.8, a sequence of photophysical interactions engaging the ensemble pairs is used to evaluate the time-evolving populations N^a and N^b, subsequently to be used in determining temporal changes in the ensemble dispersion as a result of energy transfer.

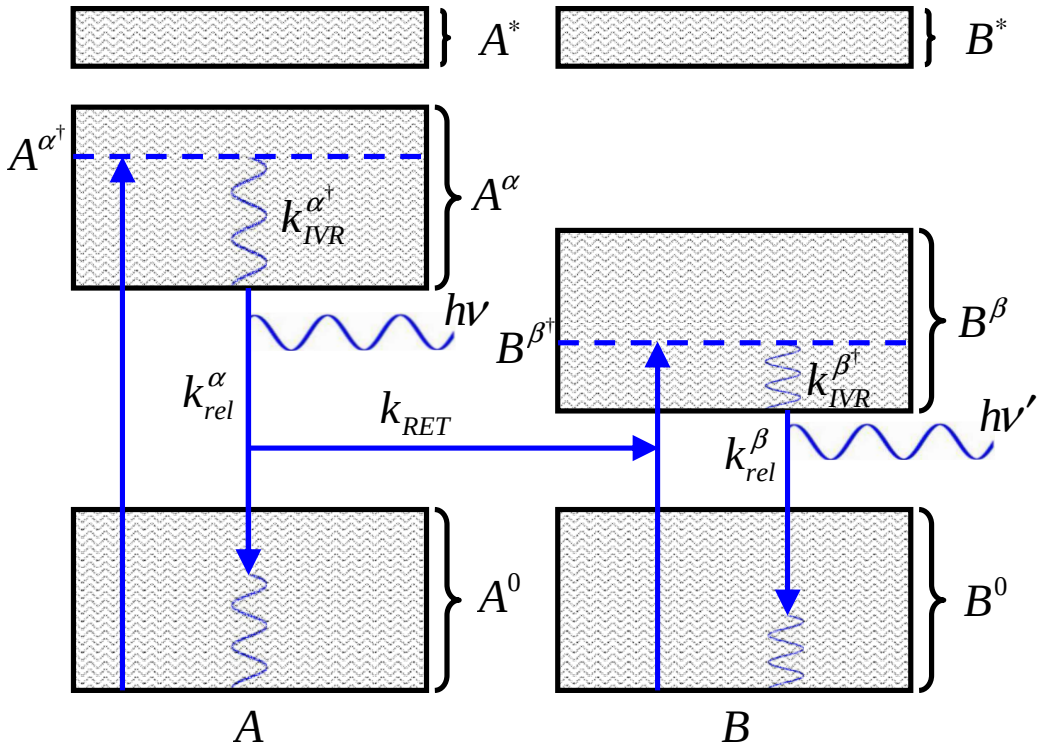

Figure 2.8 Jablonski diagram illustrating relevant photophysical processes for a dynamic system. Excitation of *A* is inferred through the diagram but the initial excitation input is deliberately withheld from the figure. After excitation of the donor, the input plays no further role in subsequent photophysical processes.

The initial state preparation is effected by an initial excitation of donor molecules through the absorption of light that is resonant with the donor but not the acceptor. The donor excitation leads to a population of excited vibrational levels, denoted by dagger superscript, of the electronic excited state A^{α}. Whilst laser excitation might result in localized movement as a result of radiation pressure, such movement can be ignored in the following calculations, such that beyond initial excitation, the input plays no further part in subsequent events. Without compromising energy conservation by the system as a whole, an immediate consequence of electronic excitation is the partial dissipation of electronic energy through coupling to nuclear vibrations, the usual process of intramolecular vibrational relaxation (IVR), assigned the rate constant k_{IVR}. In the analysis that follows, it is assumed that IVR reaches effective completion prior to relaxation to the electronic ground state, the latter proceeding through a variety of mechanisms including spontaneous emission etc. For simplicity, all such electronic relaxation processes of the donor, with the exception of RET, are included in a representative rate constant k_{rel}^{α}. The separate distinction of RET is necessary because energy migration populates the vibrational levels of B^{β}. Prior to energy transfer, the preceding IVR will generally place the donor molecule in an energy level where its decay profile has a relatively small overlap with the red end of any neighboring donor's absorption. However, in the process of RET to a nearby acceptor, a much larger spectral overlap and hence a significantly larger transfer rate will generally apply, so that energy transfer to acceptors will be the dominant process. Moreover, the spectroscopic gradient *i.e.* $E^{\alpha 0}(A) > E^{\beta 0}(B)$, commonly associated with donor-acceptor transfer will

engender a high degree of directed character, such that "backward" transfer of energy (acceptor to donor) can be ignored.[32] The final process undergone by the system is vibrational and electronic relaxation of the acceptor. Here, all relaxation processes are accommodated by the representative rate constant k_{rel}^{β}.

Time-resolved changes in the population of the initial excited state can be determined by analysis of all decay routes of A^{α}, as shown in Figure 2.8:

$$\frac{\mathrm{d}}{\mathrm{d}t} N^{\alpha} = -\left(k_{rel}^{\alpha} + k_{RET}\right) N^{\alpha}. \tag{2.22}$$

The above differential equation is solved with the initial population of A^{α}, $N^{\alpha}(0)$, assigned an arbitrary value, such that:

$$N^{\alpha}(t) = N^{\alpha}(0) \exp\left(-t\left(k_{rel}^{\alpha} + k_{RET}\right)\right). \tag{2.23}$$

Applying the physically reasonable conditions $k_{IVR}^{\beta^{\dagger}} > k_{RET}$, $N^{\alpha} > N^{\beta^{\dagger}}$ and $N^{\beta}(0) = 0$, the growth of N^{β} is dependent solely on RET from the ground vibrational state of A^{α}. Furthermore, the time-dependent variation in N^{β} is represented by the following expression:

$$\frac{\mathrm{d}}{\mathrm{d}t} N^{\beta} = k_{RET} N^{\alpha} - k_{rel}^{\beta} N^{\beta}. \tag{2.24}$$

In the presence of an auxiliary off-resonant beam, the LARET effect can significantly enhance the rate of donor-acceptor energy transfer compared to second-order RET. To represent the rate increase due to LARET an additional rate term, cast in terms of a constant k_{LARET}, is introduced to the kinetics of the donor molecule. In dealing with a laser pulse of sufficiently short duration, *i.e.* comparable to the modeled excited state lifetimes, the time-dependent behaviour of the off-resonant pulse must also be considered. To modulate the rate constant k_{LARET}, a pulse shape of the form $f(t) = \mathrm{sech}^2\left[\kappa(t-t')\right]$ is adopted with κ being proportional to the pulse width. The donor excited state decay, accounting for the effects of both RET and LARET, is now represented by:

$$\frac{\mathrm{d}}{\mathrm{d}t}N^{\alpha} = -\left(k_{rel}^{\alpha} + k_{RET} + \mathrm{sech}^2\left[\kappa(t-t')\right]k_{LARET}\right)N^{\alpha}. \tag{2.25}$$

The corresponding rate of acceptor excitation is as follows:

$$\frac{\mathrm{d}}{\mathrm{d}t}N^{\beta} = \left(k_{RET} + \mathrm{sech}^2\left[\kappa(t-t')\right]k_{LARET}\right)N^{\alpha} - k_{rel}^{\beta}N^{\beta}. \tag{2.26}$$

Finally, the optically induced pair forces must also be considered dependent on time with respect to the operation of the laser pulse. By substitution of equations (2.14) and (2.16) into equation (2.15), the temporal behavior of the corresponding optically induced pair potential is:

$$\Delta E_{ind} = -\frac{\operatorname{sech}^2\left[\kappa\left(t-t'\right)\right]I}{9\pi\varepsilon_0{}^2 cR^3}\sum_{\substack{a=0,\alpha,\\ b=0,\beta}} N^a N^b \times\sum_{r,s}\left(\left(\frac{\left|\boldsymbol{\mu}^{ar}\left(A\right)\right|^2}{E^{ra}\left(A\right)-\hbar cp}+\frac{\left|\boldsymbol{\mu}^{ar}\left(A\right)\right|^2}{E^{ra}\left(A\right)+\hbar cp}\right)\left(\frac{\left|\boldsymbol{\mu}^{bs}\left(B\right)\right|^2}{E^{sb}\left(B\right)-\hbar cp}+\frac{\left|\boldsymbol{\mu}^{bs}\left(B\right)\right|^2}{E^{sb}\left(B\right)+\hbar cp}\right)\right), \tag{2.27}$$

the factor of nine in the denominator arising as a result of isotropic averaging.

2.3 Results

It is envisaged that the donor and acceptor pairs are counterpositioned on one-dimensional arrays separated by a distance *R* across a vacuum or in air, see Figure 2.9.

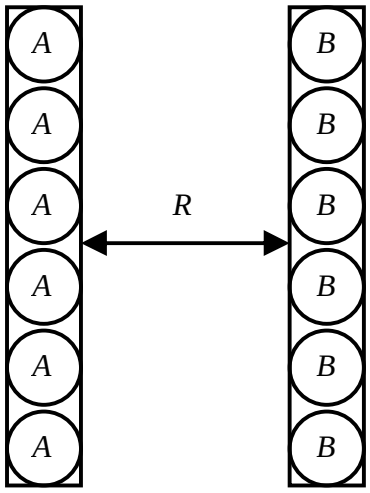

Figure 2.9 One-dimensional array configuration for ensemble donor-acceptor pairs

To quantify the dynamically evolving energy flow within an ensemble, the fractional populations N^{α} and N^{β} are first determined from equations (2.25) and (2.26). From this data, numerical results for the system energy are calculated from equation (2.21). Expected fluctuations in ensemble energy are subsequently quantified in comparison to an optically induced pair potential as represented by equation (2.27).

2.3.1 Excited State Population Analysis

Since it is only necessary to consider relative populations when addressing the temporal form of the intermolecular potentials, an arbitrary initial value of unity has been assigned to $N^{\alpha}(0)$. Importantly, this does not necessarily signify an initial fully populated electronic excited state. Three possible experimental setups are considered, the results of the excited state population analyses presented as Figures 2.10 to 2.12:

The first setup, results of which are illustrated in Figure 2.10, represents a "control" experiment whereby no energy transfer occurs between donor and acceptor arrays. The result establishes that the excited state lifetime of the donor, whose decay is attributed only to relaxation processes incorporated within k_{rel}^{α}, is set arbitrarily to approximately 3 ns. Since the excited state B^{β} is populated only through the process of RET from A, N^{β} remains zero.

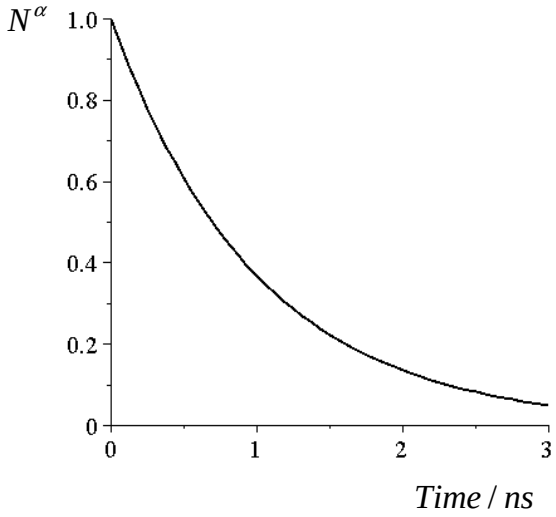

Figure 2.10 Donor excited state population for first model setup in which no RET occurs

In the second setup, it is assumed that there is a sufficiently strong short-range interaction between each donor and acceptor that the electronic state decay kinetics will be primarily determined by fast energy transfer. The dominant decay process for A^{α} is RET, as is always the case for donor-acceptor pairs within the Förster radius. Under such conditions, the excited state lifetime of the donor is, as expected, appreciably shortened; the results portrayed in Figure 2.11 indicating an approximate 60% reduction in the lifetime. In relative terms, N^{β} reaches a maximum value of roughly 50% of the initial population of A^{α} well within 1 ns of the initial donor decay, the rate of excited acceptor decay determined by k_{rel}^{β} is set equal to k_{rel}^{α}.

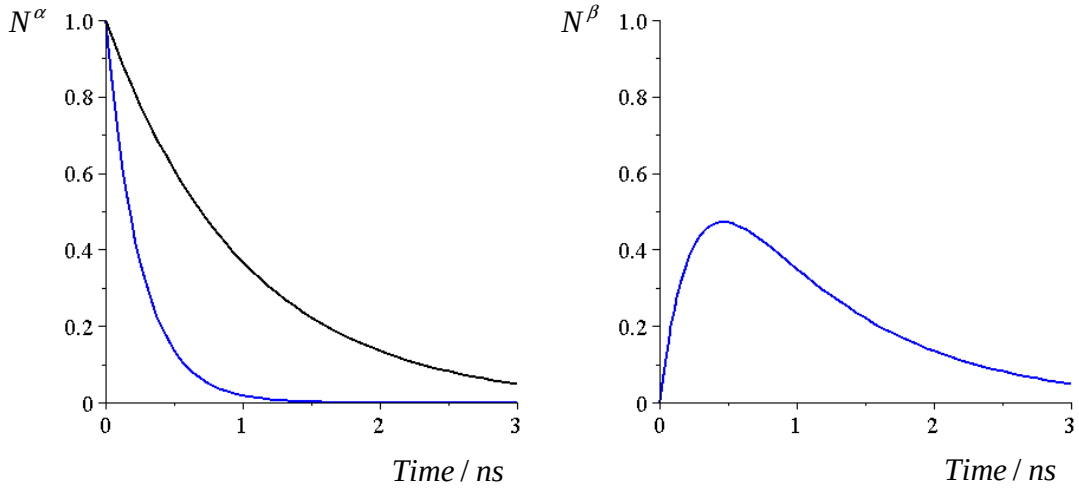

Figure 2.11 Blue data lines indicate donor and acceptor excited state populations for second model setup in which RET occurs. For comparison, black data line represents donor excited state population as presented in Figure 2.10

The final setup is identical to the second with the exception of the introduction of a pulse of off-resonant energy during the decay of the A^{α} state. The LARET input, off-resonant at a wavelength of 500 nm, is represented as having an intensity of 5×10^{16} W m^{-2} and a duration of 100 ps (full width at half maximum), delivered to the system with a delay of approximately 300 ps after initial donor excitation. Supported by recent theoretical reports on the LARET effect, an improvement in energy transfer efficiency of 50% is modeled.

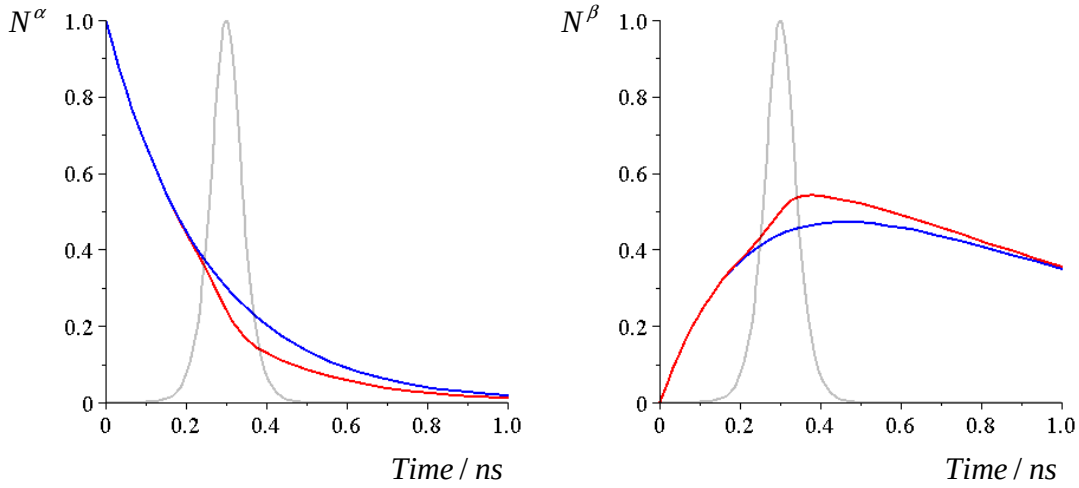

Figure 2.12 Red data lines indicate donor and acceptor excited state populations for third model setup in which RET and LARET occur. Blue data lines represent donor and acceptor excited state populations as presented in Figure 2.11 for comparison. Grey lines portray modeled off-resonant laser pulse.

2.3.2 System Energy Calculations

In the subsequent determination of numerical results for the system energy, from equations (2.21) and (2.27), the transition dipole moments $\boldsymbol{\mu}^{ar}(A)$ and $\boldsymbol{\mu}^{bs}(B)$ are set as 2 D, and the donor–acceptor intermolecular distance as 1.0 nm. The transition energies to A^{α^*} and A^{α}, from A^0 are chosen to correspond with wavelengths of 300 nm and 350 nm respectively. Lower energies are utilised for the transitions from B^0 to B^{β^*} and B^{β}, associated with wavelengths of 400 nm and 450 nm accordingly. By substitution of this data into equation (2.11), the system energy for the initial interaction between ground state donors and acceptors is calculated as being -1.2×10^{-24} J; noting that this negative value, and again the

inverse power dependence on donor-acceptor separation, determines the interaction to be attractive in nature.

The ensemble-averaged variation in the donor–acceptor pair interaction energy is now exhibited in Figures 2.13-2.15, each figure accounting for one of the model setups described in Section 2.3.1.

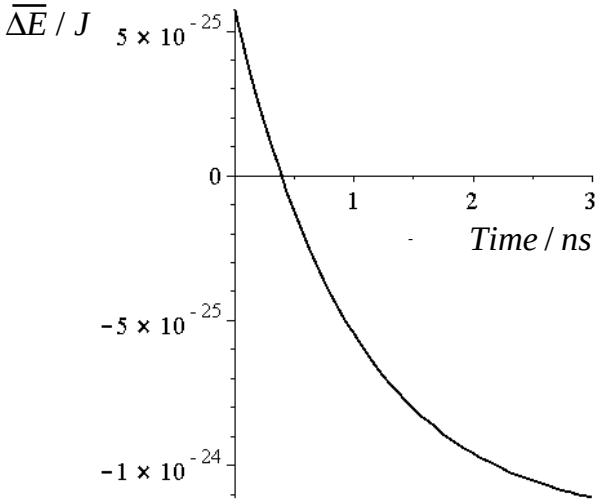

Figure 2.13 Time-resolved, ensemble pair interaction energy for first setup in which no RET occurs between donor and acceptor units.

At the outset, the interaction energy as portrayed by Figure 2.13 has been increased to a maximum of approximately 5×10^{-25} J by the preceding donor excitation. The most significant feature of this result is the sign change during the donor decay, the positive energy value duly interpreted as representing a repulsive force between both donor and acceptor arrays. As the population of the donor excited state decreases, the system returns to the equilibrium, ground state condition.

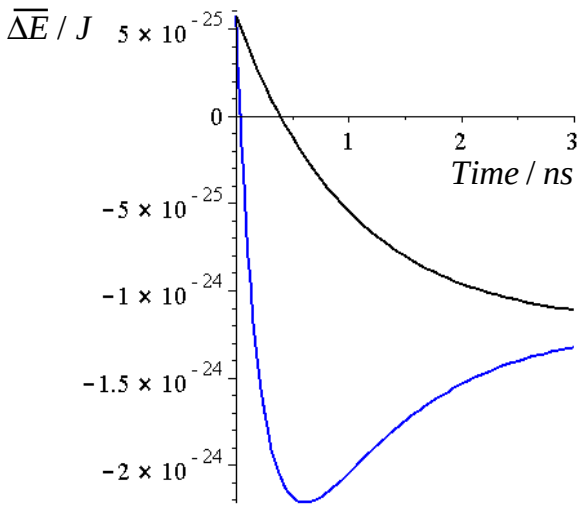

Figure 2.14 Blue data line indicates time-resolved, ensemble pair interaction energy for second setup in which RET is observed. For comparison, the black data line represents the interaction energy for the first experimental setup as presented in Figure 2.13

Exhibited in Figure 2.14, calculated results are initially similar for the second model setup, in that the initial increase in donor excited state population following laser excitation results in an increase in the interaction energy between donor and acceptor pairs. Since N^{α} decreases much more rapidly in this configuration, owing to efficient RET with the acceptor molecules, the system is expected to return to initial conditions much faster, however the increasing population of the donor excited state is observed to further modify the donor-acceptor interaction energy. As N^{β} approaches a maximum, the interaction energy reaches a minimum below that of the ground state configuration. In terms of associated forces, the donor-acceptor arrays are predicted to first separate and then draw closer to each other relative to an equilibrium position, which is then restored as both N^{α} and N^{β} reach zero.

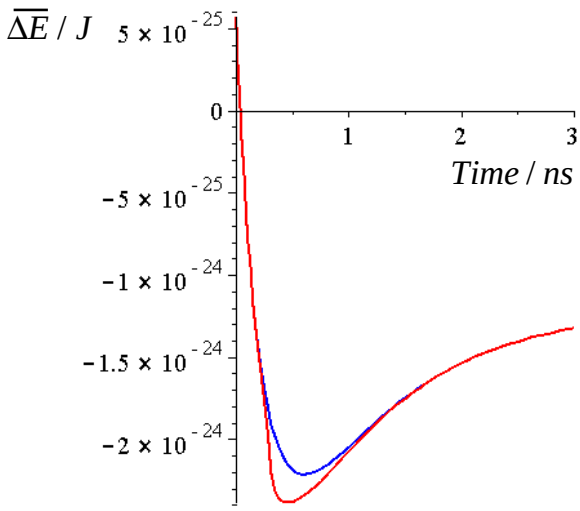

Figure 2.15 Red data line indicates time-resolved, ensemble pair interaction energy for third setup where both RET and LARET are observed. For comparison, the blue data line represents results of the second setup as presented in Figure 2.14

Figure 2.15 shows the ensemble-averaged variation in the donor–acceptor pair interaction energy as calculated for the third model setup, in which both RET and LARET feature. The results follow the pattern previously established for the second model setup up to the point where the off-resonant laser pulse infringes upon the system. Here, the increased rate of energy transfer effected by the LARET process results in a higher population of excited state acceptors, consequently lowering the interaction energy to a new minimum during this time.

As a final result, the time-resolved optical pair energy is calculated using equation (2.27) and the excited state populations determined in Section 2.3.1. For comparison, this data is plotted together with the time-resolved results presented in Figure 2.15.

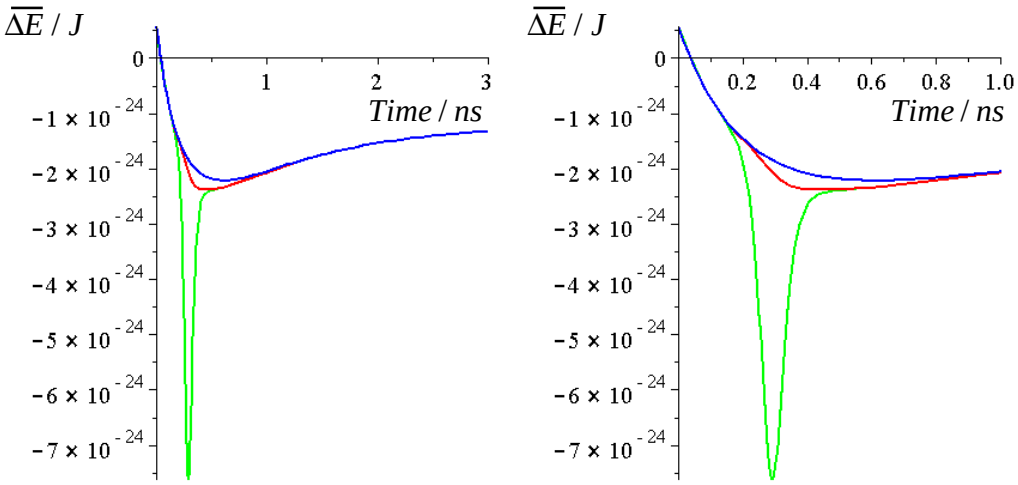

Figure 2.16 Two plots over different scale axes of all 4th order interaction energies, the green line incorporates the time-resolved optical pair energy where both RET and LARET also feature. For comparison, blue and red data lines represent results of the second and third experimental setups respectively, as presented in Figure 2.15

A striking feature of the results presented in Figure 2.16, comparing the relative significance of the fourth-order interactions, is that optically induced pair forces appear very much more significant in their effect than expected variations in the donor–acceptor pair interaction energy caused by both RET and LARET. This may prove a significant difficulty in experimentally verifying the more subtle variations in interaction energy offered by the mechanism of energy transfer. Significantly, the above results suggest in principle that the interaction energy between donor and acceptor units can be modified by a controllable, all optical input, the benefits of which may be exploited in optomechanical devices.

2.4 Discussion/Conclusion

Few areas of chemistry are not in some way linked with the underlying operation and influence of intermolecular forces. In the vast majority of these areas, where molecular matter generally resides in its electronic ground state, it is not surprising to find that the familiar forms of intermolecular potential are commonly adopted without necessary consideration of electronic state. The aim of this work, by utilizing a simple time-resolved, dynamic system has therefore been to characterise changes in intermolecular force that occur on photoexcitation, and to illustrate the practicality of measuring such shifts in energy and force in any multi-component system. Any variation in intermolecular pair potential, as determined in the present analysis, must invariably result in a localized movement that to a degree either closes or expands the distance between any donor and its counterpart acceptor.

In a system that displays typical RET behaviour, specific calculations based on an array configuration have exhibited a characteristic mechanical response and recovery, following an initial throughput of a resonant laser pulse. Whilst only a one-dimensional array system has been considered, the results of a more meaningfully scaled system involving two parallel square-based arrays, one comprising donors and the other, acceptors, has already been the focus of complementary investigations.[13-15] It is found that for a range of $\overline{\Delta E}$ values, similar in magnitude to those determined in Section 2.3, that the dispersion force for the donor-acceptor ensemble model varies in the picoNewton range. Taken as

indicators of the feasibility of measurement, these figures are highly encouraging. With the rapidly ongoing development of techniques including atomic force spectroscopy (AFM), such forces should easily fall into the range of possible measurement.[33-35] Whilst it is relatively simple to develop from the change in interaction energy a corresponding ensemble-averaged force, such results can only be regarded as indicative. The theoretical evaluation of a measurable displacement remains complex, but it is in principle achievable for any chemical system of interest, through the deployment of a suitable molecular modeling package.

One other area in which the effects described may prove of particular significance is in the development of micro- and nano-electromechanical systems (MEMS and NEMS). These devices represent a rapidly developing technology that is already being used in sensors and actuators for a variety of applications, including integrated drug delivery systems and optical scanners.[36-40] In such connections there is considerable interest in harnessing the variations in inter-atomic and intermolecular displacement that can arise as a result of quantum (Casimir force) effects, forces that become especially prominent as the size of such devices shrinks down to nanoscale dimensions.[41] The results presented above show that the engagement of energy transfer between the components in such devices can offer additional means for effecting mechanical motion. Through this and by consideration of the LARET effect, there is a distinct possibility of introducing optical force control over such nanoscale motions.

References

1. Casimir, H.B.G. & Polder, D. *Phys. Rev.* **73**, 360 (1948).
2. Power, E.A. & Thirunamachandran, T. *Phys. Rev. A* **48**, 4761 (1993).
3. Craig, D.P. & Thirunamachandran, T. *Molecular Quantum Electrodynamics*. (Dover: New York, 1998).
4. Andrews, D.L. & Allcock, P. *Optical Harmonics in Molecular Systems: Quantum Electrodynamical Theory*. (Wiley-VCH: Weinheim, 2002).
5. Salam, A. *Molecular Quantum Electrodynamics*. (Wiley: Chichester, 2009).
6. Salam, A. *Int. J. Quantum Chem.* **105**, 762 (2005).
7. Salam, A. *J. Phys. B* **39**, S651 (2006).
8. Salam, A. *J. Phys. B* **39**, S663 (2006).
9. Alligood, B.W. & Salam, A. *Mol. Phys.* **105**, 395 (2007).
10. Jenkins, R.D., Andrews, D.L. & Dávila Romero, L.C. *J. Phys. B* **35**, 445 (2002).
11. Power, E.A. & Thirunamachandran, T. *Chem. Phys.* **198**, 5 (1995).
12. Power, E.A. & Thirunamachandran, T. *Phys. Rev. A* **51**, 3660 (1995).
13. Bradshaw, D.S., Leeder, J.M., Rodriguez, J. & Andrews, D.L. *Proc. SPIE* **7034**, 703408 (2008).
14. Bradshaw, D.S., Leeder, J.M., Rodriguez, J. & Andrews, D.L. *Proc. SPIE* **6905**, 690503 (2008).
15. Andrews, D.L., Bradshaw, D.S., Leeder, J.M. & Rodríguez, J. *Phys. Chem. Chem. Phys.* **10**, 5250 (2008).

16. Andrews, D.L. & Leeder, J.M. *J. Chem. Phys.* **130**, 034504 (2009).
17. Sherkunov, Y. *Phys. Rev. A* **79**, 032101 (2009).
18. Rodriguez, J. & Salam, A. *Phys. Rev. A* **82**, 062522 (2010).
19. Daniels, G.J., Jenkins, R.D., Bradshaw, D.S. & Andrews, D.L. *J. Chem. Phys.* **119**, 2264 (2003).
20. Scholes, G.D. & Andrews, D.L. *J. Chem. Phys.* **107**, 5374 (1997).
21. Andrews, D.L. & Bradshaw, D.S. *Eur. J. Phys.* **25**, 845 (2004).
22. Salam, A. *J. Chem. Phys.* **122**, 044112 (2005).
23. Andrews, D.L., Crisp, R.G. & Bradshaw, D.S. *J. Phys. B* **39**, S637 (2006).
24. Dávila Romero, L.C. & Andrews, D.L. in *Structured Light and Its Applications: An Introduction to Phase-Structured Beams and Nanoscale Optical Forces*. (Academic Press: London, 2008), p. 79.
25. Bradshaw, D.S. & Andrews, D.L. *Phys. Rev. A* **72**, 033816 (2005).
26. Allcock, P., Jenkins, R.D. & Andrews, D.L. *Chem. Phys. Lett.* **301**, 228 (1999).
27. Allcock, P., Jenkins, R.D. & Andrews, D.L. *Phys. Rev. A* **61**, 023812 (2000).
28. Andrews, D.L. *Can. J. Chem.* **86**, 855 (2008).
29. Bambini, A. *Phys. Rev. A* **53**, 3302 (1996).
30. Salam, A. *Phys. Rev. A* **76**, 063402 (2007).
31. Cohen, A.E. & Mukamel, S. *J. Phys. Chem. A* **107**, 3633 (2003).
32. Andrews, D.L. & Rodríguez, J. *J. Chem. Phys.* **127**, 084509 (2007).
33. Baumgartner, W., Hinterdorfer, P. & Schindler, H. *Ultramicroscopy* **82**, 85 (2000).
34. Hugel, T. & Seitz, M. *Macromol. Rapid Commun.* **22**, 989 (2001).

35. Tadros, T. *Adv. Colloid Interface Sci.* **165**, 102 (2011).

36. Zara, J.M. & Smith, S.W. *Sensor. Actuat. A* **102**, 176 (2002).

37. Kim, S., Barbastathis, G. & Tuller, H.L. *J. Electroceram.* **12**, 133 (2004).

38. Tsai, N.C. & Sue, C.Y. *Sensor. Actuat. A* **134**, 555 (2007).

39. Nisar, A., Afzulpurkar, N., Mahaisavariya, B. & Tuantranont, A. *Sensor. Actuat. B* **130**, 917 (2008).

40. Liao, M. & Koide, Y. *Crit. Rev. Solid State* **36**, 66 (2011).

41. Chan, H.B., Aksyuk, V.A., Kleiman, R.N., Bishop, D.J. & Capasso, F. *Science* **291**, 1941 (2001).

Chapter 3 – Resonance Energy Transfer in a Dipole-forbidden System

In general, the RET interaction between chromophores proceeds through transition moment coupling between donor and acceptor units. By far the most commonly studied interaction is that which occurs between two electric dipoles (E1-E1 coupling), since the donor decay and acceptor excitation are usually both E1-allowed. Under such circumstances, any contributions associated with higher-order electric and magnetic multipolar coupling are comparatively very small. Specifically, in systems where E1-E1 coupling is the prominent term accounting for energy transfer, the leading magnetic dipole (M1) and electric quadrupole (E2) contributions to the observed transition rates are generally expected to be smaller by several orders of magnitude.[1-3] The theoretical and experimental study of higher-order multipole coupling nonetheless becomes relevant in instances where E1 transitions in the donor and/or acceptor are weak or entirely precluded, the nature of the coupled transition moments then being dependent on several factors including molecular geometry and symmetry.[4-7] Prior to embarking upon a detailed analysis and in order to highlight the additional factors that can influence the character of energy transfer, it is first instructive to consider real systems within which a dipole-forbidden criterion applies,

One extensively studied example of energy transfer, in which higher-order multipole coupling has proven significance, is the dynamic coupling of carotenoid and chlorophyll, or bacteriochlorophyll, pigments associated with natural light

harvesting. Carotenoids are unusual chromophores in that, in the photosynthetic systems in which they operate as donors, optically driven electronic transitions from the singlet ground state S_0 usually produce a significant population of the two lowest energy singlet excited states, S_1 and S_2. Transitions to the latter excited state result from blue/green optical absorption, whilst the former is indirectly populated by $S_2 \rightarrow S_1$ internal conversion, a feature best understood on symmetry grounds.[8-14] Carotenoids are conjugated polyene derivatives of skeletal symmetry C_{2h}, therefore the direct transition between $S_0\left(1^1A_g\right)$ and $S_1\left(2^1A_g\right)$ states is E1-forbidden by parity. On optical excitation to S_2, one obvious route for decay is through the downward, E1-allowed $S_2\left(1^1B_u\right) \rightarrow S_0\left(1^1A_g\right)$ transition, potentially leading to energy transfer to a chlorophyll acceptor. However, in many photosynthetic systems, a more significant route for decay is a highly efficient internal conversion from S_2, followed by energy transfer from S_1. In consequence, extremely high (approaching 100%) transfer efficiencies can be observed.[9,10]

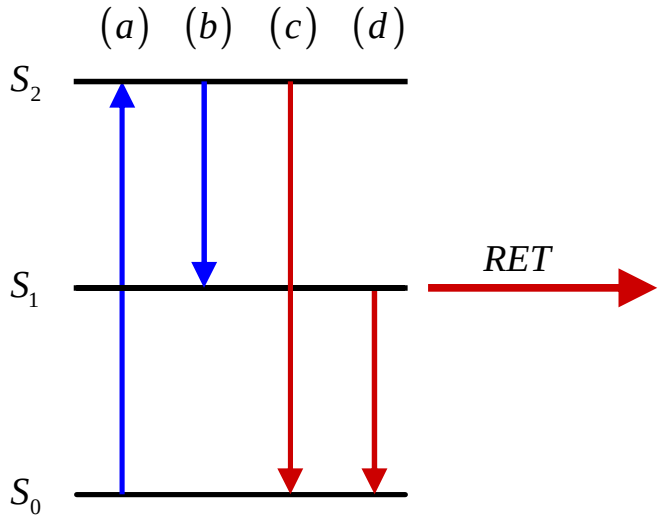

Figure 3.1 Simplified energy level diagram portraying possible electronic transitions for a carotenoid following optical excitation. For transitions (*a*) and (*b*), blue lines depict the population of both the S_2 and S_1 electronic states, the former the result of blue/green absorption and the latter, the result of efficient internal conversion from the S_2 state. Relaxational transitions necessary for RET are depicted by (*c*) and (*d*), representing the $S_2 \rightarrow S_0$ transition which is E1-allowed and the E1-forbidden $S_1 \rightarrow S_0$ transition respectively.

Whilst the involvement of electron exchange (Dexter) mechanisms cannot be ignored, given that the donor and acceptor in such photosynthetic systems are in sufficiently close proximity for wavefunction overlap to be significant, transitions from S_1 may still proceed through higher-order M1 or E2 moments, both of which are symmetry allowed.

In explaining all possible energy transfer routes portrayed in Figure 3.1, including the E1-allowed $S_2\left(1^1B_u\right) \rightarrow S_0\left(1^1A_g\right)$ transition, further complications need to be addressed. For any separation of the donor and acceptor chromophores that is

comparable to their physical sizes, the ideal dipole approximation breaks down and the shape of the molecular charge distributions becomes significant. Recent reports on carotenoid-chlorophyll energy transfer have exploited extended-dipole models such as the transition density cube method, in which the total interaction is treated as a sum of all local interactions observed between regions of donor and acceptor transition density.[7,9,12,15] Only in cases where the chromophores are sufficiently far apart, that the distributed interactions between their component transition densities occur over similar distances, can the total interaction between multipole moments be considered with regard to an averaged donor-acceptor separation. Such caveats are much less important in the case of smaller molecules.

Moving beyond the context of light absorbing pigments in plants, another type of system in which E1-forbidden donor-acceptor coupling is significant is afforded by crystals (or glasses) doped with lanthanide ions. Exploiting the unique optical properties associated with the *f*-orbitals of these rare-earth materials, energy transfer between di- and tri-valent ions features in a number of applications such as frequency up- and down-conversion, and in an enhanced methodology for the RET spectroscopic ruler.[16-18] Whilst a large number of optical transitions in rare-earth ions are E1-forbidden on parity grounds, the local structure of the solid in doped crystalline materials can play a decisive role in determining viable pathways for energy migration. It is widely held that ions located at crystal sites without inversion symmetry permit mixing between the energy levels of the 4*f*- and 5*d*-orbitals. As a result, “forced” E1-allowed transitions are permitted, which generally

dominate the contribution of higher-order electric and magnetic moments. However, when the lanthanide ions are located at sites with inversion symmetry, forced E1 transitions are typically precluded, and additional forms of multipolar interaction are often presumed to occur.[19-21]

The aim of the present research is to provide a basis to assess the relative mechanistic significance of different contributions to the rate of energy transfer, within a donor-acceptor pair evaluated under the following conditions. The system of study utilizes chromophores that are small in size with respect to donor-acceptor separation, hence the ideal dipole approximation holds and the need to develop an extended multipole model is obviated. Secondly, the molecular system is of sufficiently high symmetry that the donor decay and acceptor excitation transitions are rigorously E1-forbidden, but E2-allowed (and potentially M1-allowed). To be concise in the analysis that follows, such a system will be referred to as E1-E1 forbidden, the label signifying that, for example, E1-M1 and M1-E1 coupling are also both forbidden. Since any transition that is E2-allowed is also permitted by two successive E1 couplings, it is also necessary to entertain another, seldom considered energy transfer mechanism based on a second order $E1^2$-$E1^2$ coupling. Such a coupling clearly has the potential to feature in small molecules and lanthanide-based energy transfer systems. Specifically, we shall focus on the interaction between a pair of centrosymmetric molecules, or a pair of ions located in centrosymmetric sites within a crystal lattice, the implications of which will become apparent during the following analysis.

After extending the theory of RET in Section 3.1 to accommodate higher-order multipole coupling, the study will focus upon a generalized donor-acceptor interaction that accommodates both E2-E2 and $E1^2$-$E1^2$ couplings, allowing comparisons to be drawn between the two mechanisms. The former, addressed in Section 3.1.1, is chosen as a representative of multipolar couplings of similar order, such as E2-M1, M1-E2 and M1-M1. For present purposes the couplings that entail M1 transitions will be disregarded for lucidity of explanation and in recognition that in systems of sufficiently high local symmetry, certain optical transitions will be E2-allowed and yet rigorously M1-forbidden. Here, and in Section 3.1.2 – where the theory of $E1^2$-$E1^2$ coupling is presented – the ensuing rate contributions for each form of coupling are derived and represented in an experimentally relevant form by appropriate use of orientational averaging. Results are subsequently summarised and discussed in Sections 3.2 and 3.3.

3.1 Resonance Energy Transfer in E1-forbidden Systems

In the following comparison between different forms of donor-acceptor interaction, the results of calculations are reported in the near-zone limit for a number of reasons. First, it is a significant feature that any system's dependence on chromophore separation changes markedly according to the order of intermolecular coupling involved. Whilst generally smaller in magnitude than E1-E1 coupling at all separations, higher-order multipole interactions also diminish much more rapidly with donor-acceptor distance, being dependent on higher inverse powers.[1-3]

Secondly, energy transfer is usually studied in systems that satisfy the near-zone conditions that favor RET; it is within this regime that radiationless energy transfer is preferred over all other possible modes of relaxation, including fluorescence decay. Finally, focusing on the near-zone limit again considerably reduces the complexity of the results, since donor-acceptor distances are small enough that retardation features can be suppressed, *i.e.* the coupling can be viewed as essentially instantaneous. In the near-zone analysis that follows, however, it may be remarked that the assumption does not compromise the rigor of analysis. On retaining the fully retarded form of the resonance coupling tensors, precisely the same methods are deployed.

Having already established the theoretical foundation for near-zone, E1-E1 coupled, RET interactions in Section 2.1.1, the theory is now expanded to incorporate higher-order electric multipole coupling. As previously discussed, the leading term with regard to perturbation theory, contributing to the rate of energy migration is second-order with respect to $H_{int}(\xi)$. The corresponding matrix element is exactly expressible as the first term of equation (2.1) and is now represented as an expanded sum over all orders of electric multipole coupling:

$$M_{FI} = \sum_{l,m} M_{FI}^{l-m}, \tag{3.1}$$

where for example, M_{FI}^{1-1} and M_{FI}^{1-2} respectively represent the matrix elements associated with E1-E1 and E1-E2 coupling. As remarked earlier, whilst magnetic

counterparts are amenable to the following method of analysis and the corresponding calculation is straightforward, their inclusion considerably increases the complexity of the ensuing equations. The physical principles that we shall establish are perfectly well exhibited by the electric terms. Continuing by substitution of equation (1.8) into the first term of equation (2.1), followed by a series of well-documented calculational steps, including a summation over all virtual photon polarisations and wave-vectors, each term in equation (3.1) is developed into a form concisely expressible as follows:[22-25]

$$M_{FI}^{l-m} = E_{i_1 i_2 \ldots i_l}^{(l)0\alpha}(A)\, E_{j_1 j_2 \ldots j_l}^{(m)\beta 0}(B)\, V_{i_1 j_1 i_2 \ldots i_l j_2 \ldots j_m}(p, \boldsymbol{R}). \tag{3.2}$$

The electromagnetic interaction between A and B is described by the retarded resonance coupling tensor $V(p, \boldsymbol{R})$, whose rank is determined by a sum of the electric multipole orders of the transitions at A and B, noting that when both l and m represent transition dipoles, the above matrix element represents an E1-E1 coupling with $V(p, \boldsymbol{R})$ expressible exactly as equation (2.3). The exact form of the coupling tensor has previously been developed from a general formula for a number of transition moment interactions including E1-E1, E1-E2 and E2-E2, with relevant explicit results exploited later.[22,24]

For the development that follows, higher-order perturbation correction terms should also be considered. Since each such term has to accommodate paired virtual photon creation and annihilation events, in order to satisfy the condition of overall energy

conservation, these corrections are all of even order, the fourth rank being the most significant. The full RET matrix element is accordingly identical to equation (2.1) and is presented again for convenience:

$$M_{FI} = \sum_{R} \frac{\langle F | H_{int}(\xi) | R \rangle \langle R | H_{int}(\xi) | I \rangle}{\left(E^I - E^R\right)}, \\ + \sum_{R,S,T} \frac{\langle F | H_{int}(\xi) | T \rangle \langle T | H_{int}(\xi) | S \rangle \langle S | H_{int}(\xi) | R \rangle \langle R | H_{int}(\xi) | I \rangle}{\left(E^I - E^R\right)\left(E^I - E^S\right)\left(E^I - E^T\right)} + \ldots,$$

(3.3)

As previously proposed, E1 transitions associated with single-quantum energy transfer between *A* and *B* are considered either vanishingly small or entirely precluded, thus the single-photon terms in equation (3.1) including M_{FI}^{1-1}, M_{FI}^{1-2} and M_{FI}^{2-1} are disregarded. The leading one-photon process is therefore treated as E2-E2 coupling described by M_{FI}^{2-2}. The dominant contribution associated with two-quantum RET, described by the second term in equation (3.3), entails two E1-allowed transitions at both the donor and acceptor, namely $E1^2$-$E1^2$ coupling described by $M_{FI}^{1^2-1^2}$. Notably, symmetry selection rules impose the same conditions for both E2 and $E1^2$ transitions. Assuming all higher-order couplings are of negligible magnitude, the overall matrix element becomes a sum of the first- and second-order contributions:

$$M_{FI} = M_{FI}^{2-2} + M_{FI}^{1^2-1^2}. \tag{3.4}$$

The rate of energy transfer between the system states $|I\rangle$ and $|F\rangle$ is determinable through Fermi's Golden Rule by substitution of equation (3.4) into equation (1.12), the RET rate presented as:

$$\Gamma = \frac{2\pi\rho}{\hbar}\left(\left|M_{FI}^{2-2}\right|^2 + 2\,\mathrm{Re}\,M_{FI}^{2-2}\bar{M}_{FI}^{1^2-1^2} + \left|M_{FI}^{1^2-1^2}\right|^2\right), \tag{3.5}$$

where a quantum interaction cross term evolves in the form $M_{FI}^{2-2}M_{FI}^{1^2-1^2}$. Each of the contributions in equation (3.5) are now separately evaluated.

3.1.1 First-order Quadrupole-quadrupole (E2-E2) Coupling

As discussed, first-order energy transfer effected by E2-E2 coupling proceeds by mediation of a single virtual photon between *A* and *B*. The donor decay and acceptor excitation engage E2 transition moments which are now cast specifically as $Q_{ij}^{0\alpha}(A)$ and $Q_{kl}^{\beta 0}(B)$. The coupling is illustrated completely by two time-ordered diagrams, Figures 3.2(*a*) and 3.2(*b*), each portraying one of two possible time-orderings for the interaction. In the case of near-zone coupling, the interaction is treated as unretarded, the corresponding static limit duly illustrated by Figure 3.2(*c*).

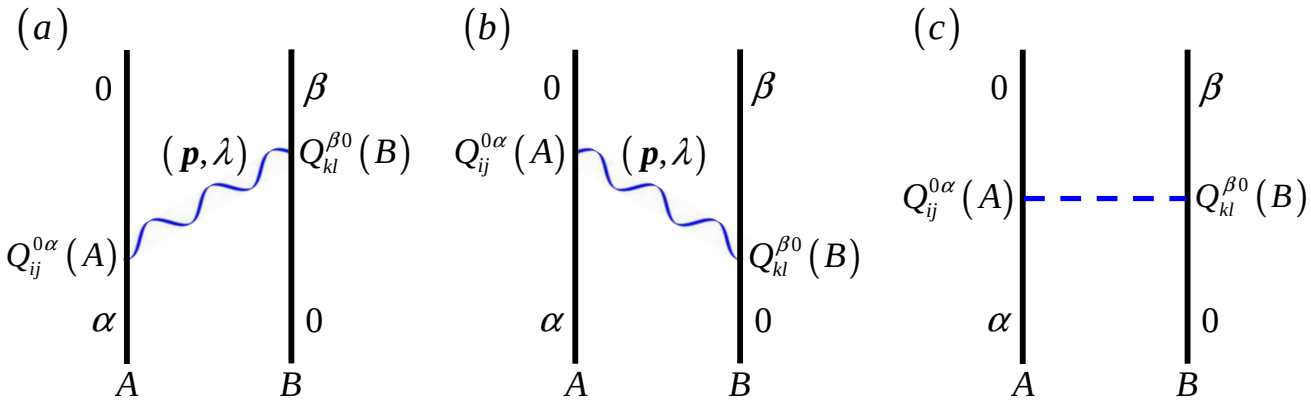

Figure 3.2 All possible time-ordered diagrams for E2-E2 energy transfer. The two retarded time orderings are represented by (*a*) and (*b*), whilst the near zone, unretarded coupling is portrayed by (*c*)

The matrix element determined from equation (3.2) is exactly expressible as:

$$M_{FI}^{2-2} = Q_{ij}^{0\alpha}(A)\,Q_{kl}^{\beta 0}(B)\,V_{ikjl}(p,\boldsymbol{R}), \tag{3.6}$$

featuring a first-order engagement with the near-zone, fully index symmetric fourth rank interaction tensor, $V_{ikjl}(p,\boldsymbol{R})$:

$$V_{ikjl}(p,\boldsymbol{R}) = \frac{3}{4\pi\varepsilon_0 R^5}\Big[\left(\delta_{ik}\delta_{jl}+\delta_{ij}\delta_{kl}+\delta_{il}\delta_{jk}\right)-5\left(\delta_{ik}\hat{R}_j\hat{R}_l+\delta_{ij}\hat{R}_k\hat{R}_l+\delta_{il}\hat{R}_j\hat{R}_k\right.$$
$$\left.+\delta_{jk}\hat{R}_i\hat{R}_l+\delta_{kl}\hat{R}_i\hat{R}_j+\delta_{jl}\hat{R}_i\hat{R}_k\right)+35\hat{R}_i\hat{R}_k\hat{R}_j\hat{R}_l\Big]. \tag{3.7}$$

The contribution to the rate of energy transfer as required by equation (3.5), invokes the modulus square of equation (3.6), and to represent conditions in which

transition moments are randomly oriented, the result is expressed following an isotropic average:

$$\left\langle \left| M_{FI}^{2-2} \right|^2 \right\rangle = \left\langle Q_{ij}^{0\alpha}(A)\bar{Q}_{i'j'}^{0\alpha}(A) \right\rangle \left\langle Q_{kl}^{\beta 0}(B)\bar{Q}_{k'l'}^{\beta 0}(B) \right\rangle V_{ikjl}(p,\boldsymbol{R})\bar{V}_{i'k'j'l'}(p,\boldsymbol{R}), \quad (3.8)$$

where $\bar{Q}_{i'j'}^{0\alpha}(A)$, $\bar{Q}_{k'l'}^{\beta 0}(B)$ and $\bar{V}_{i'k'j'l'}(p,\boldsymbol{R})$ signify the complex conjugates of the parameters featured in equation (3.6). The orientational averages in equation (3.8) involve freely rotating the transition moments of both *A* and *B* independently of each other. The two fourth-rank averages utilize the general isotropic tensor presented previously as equation (1.26) and are evaluated separately, first for A:

$$\begin{aligned} \left\langle Q_{ij}^{0\alpha}(A)\bar{Q}_{i'j'}^{0\alpha}(A) \right\rangle = \frac{Q_{\lambda\mu}^{0\alpha}(A)\bar{Q}_{\lambda'\mu'}^{0\alpha}(A)}{30} \Big[& \delta_{ij}\delta_{i'j'}\left(4\delta_{\lambda\mu}\delta_{\lambda'\mu'} - \delta_{\lambda\lambda'}\delta_{\mu\mu'} - \delta_{\lambda\mu'}\delta_{\mu\lambda'}\right) \\ & + \delta_{ii'}\delta_{jj'}\left(-\delta_{\lambda\mu}\delta_{\lambda'\mu'} + 4\delta_{\lambda\lambda'}\delta_{\mu\mu'} - \delta_{\lambda\mu'}\delta_{\mu\lambda'}\right) \\ & + \delta_{ij'}\delta_{i'j}\left(-\delta_{\lambda\mu}\delta_{\lambda'\mu'} - \delta_{\lambda\lambda'}\delta_{\mu\mu'} + 4\delta_{\lambda\mu'}\delta_{\mu\lambda'}\right)\Big], \end{aligned} \quad (3.9)$$

which rotationally decouples the donor by referring its quadrupole tensor components to a donor-fixed frame denoted by Greek subscripts. Exploiting the traceless and index-symmetric properties of electric quadrupole moments, equation (3.9) can be recast in the following simplified form:

$$\left\langle Q_{ij}^{0\alpha}(A)\bar{Q}_{i'j'}^{0\alpha}(A) \right\rangle = \frac{\left|Q^{0\alpha}(A)\right|^2}{30}\left(-2\delta_{ij}\delta_{i'j'} + 3\delta_{ii'}\delta_{jj'} + 3\delta_{ij'}\delta_{i'j}\right). \quad (3.10)$$

The same method is applied to resolve the rotational average of B. The ensuing, fully averaged result is therefore:

$$\left\langle \left| M_{FI}^{2-2} \right|^2 \right\rangle = \frac{\left|Q^{0\alpha}(A)\right|^2 \left|Q^{\beta 0}(B)\right|^2}{900} \left(-2\delta_{ij}\delta_{i'j'} + 3\delta_{ii'}\delta_{jj'} + 3\delta_{ij'}\delta_{i'j}\right) \times \left(-2\delta_{kl}\delta_{k'l'} + 3\delta_{kk'}\delta_{ll'} + 3\delta_{kl'}\delta_{k'l}\right) V_{ikjl}(p,\boldsymbol{R}) \bar{V}_{i'k'j'l'}(p,\boldsymbol{R}). \tag{3.11}$$

We observe in passing that the above representation of E2-E2 rotational averaging differs from the form displayed in equation (A12) of reference [24], in that additional terms appear in equation (3.11), specifically the delta products $-2\delta_{ij}\delta_{i'j'}$ and $-2\delta_{kl}\delta_{k'l'}$. However, in the contraction of equation (3.11) with the E2-E2 interaction tensor and its conjugate, inclusion of these additional delta products yield vanishing terms. Both approaches therefore lead to identical expressions for the measurable, rotationally averaged rate of energy transfer between two electric quadrupoles, succinctly written as:

$$\Gamma^{2-2} = \frac{63\rho \left|Q^{0\alpha}(A)\right|^2 \left|Q^{\beta 0}(B)\right|^2}{5\hbar\pi\varepsilon_0{}^2 R^{10}}. \tag{3.12}$$

3.1.2 Second-order Dipole-dipole ($E1^2$-$E1^2$) Coupling

When considering the interaction over all donor-acceptor separations, $E1^2$-$E1^2$ coupling is properly considered a two-quantum process, *i.e.* one in which two

virtual photons mediate the energy exchange. The coupling is represented by 12 distinct time-ordered diagrams, an example of which is presented as Figure 3.3(*a*). However, within the near-zone, $E1^2$-$E1^2$ coupling can be described as two separately occurring, essentially instantaneous interactions between donor and acceptor. The previously stated 12 contributions to the energy transfer now contract to a single representation as in Figure 3.3(*b*).

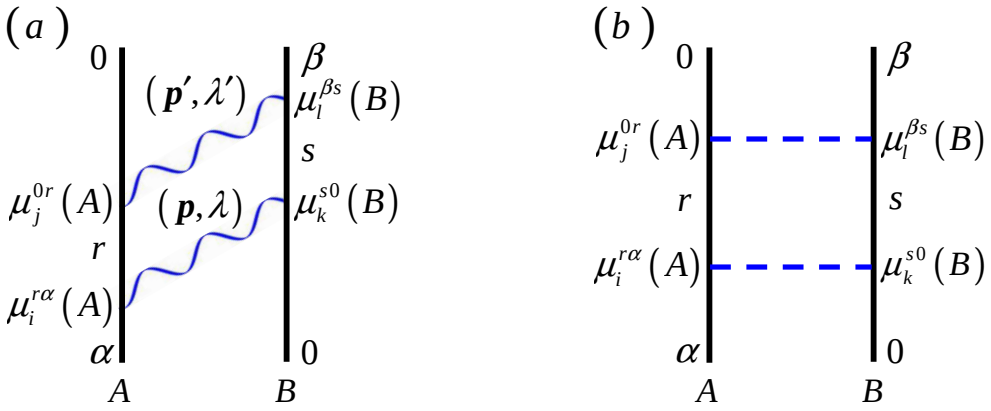

Figure 3.3 Time-ordered diagrams of $E1^2$-$E1^2$ energy transfer. Figure (*a*) portrays one of twelve possible representations of the full, retarded interaction. Figure (*b*) depicts the near zone, unretarded coupling.

Similar to previous developments discussed in Chapter 2, both the donor and acceptor transitions progress through a time interval in which each exists in a superposition of intermediate states. With reference back to equation (3.3) such intermediate states are addressed through a summation over both sets of molecular eigenstates, *r* and *s* respectively, these state superpositions being weighted by inverse energies that represent the offset from exact energy conservation during the time interval. It emerges that the matrix element of $E1^2$-$E1^2$ is expressible as:

$$M_{FI}^{1^2-1^2} = \sum_{\substack{r\neq 0,\alpha \\ s\neq 0,\beta}} \frac{\mu_i^{r\alpha}(A)\mu_j^{0r}(A)\mu_k^{s0}(B)\mu_l^{\beta s}(B)V_{ik}(p,\boldsymbol{R})V_{jl}(p,\boldsymbol{R})}{E^{\alpha r}(A)+E^{0s}(B)}, \tag{3.13}$$

To explain the above restrictions in the sums over *r* and *s*, reference is made to figure 3.3(*b*). If for example the intermediate state *r* were allowed to be identical to the donor excited state configuration, *i.e.* $r=\alpha$, the first photon interaction at *A* would engage an E1 transition moment $\mu_i^{\alpha\alpha}(A)$, which is in fact the static moment of the excited state. Such static moments vanish for centrosymmetric molecules and consequently, only transition moments in which the molecular state changes can be entertained. The inclusion of a single static dipole coupling in *A* would also require that the molecular decay transition proceeds via the other E1-interaction. The overall mechanism would therefore invalidate the E1-forbidden property of the system under consideration.

The matrix element, equation (3.13) is clearly second-order in the E1-E1 interaction tensor, the general near-zone limit of which has already been presented as equation (2.4). As previously established by equation (3.5), the isotropically averaged modulus square of equation (3.13) is required to determine the transition rate for a randomly oriented ensemble:

$$\left\langle \left| M_{FI}^{1^2-1^2} \right|^2 \right\rangle = \sum_{\substack{r\neq 0,\alpha \\ s\neq 0,\beta}} \left\langle \mu_i^{r\alpha}(A)\bar{\mu}_{i'}^{r\alpha}(A)\mu_j^{0r}(A)\bar{\mu}_{j'}^{0r}(A)\right\rangle$$
$$\times\left\langle \mu_k^{s0}(B)\bar{\mu}_{k'}^{s0}(B)\mu_l^{\beta s}(B)\bar{\mu}_{l'}^{\beta s}(B)\right\rangle V_{ik}(p,\boldsymbol{R})\bar{V}_{i'k'}(p,\boldsymbol{R}) \qquad (3.14)$$
$$\times V_{jl}(p,\boldsymbol{R})\bar{V}_{j'l'}(p,\boldsymbol{R})\left(E^{\alpha r}(A)+E^{0s}(B)\right)^{-2}.$$

Separate fourth order rotational averages of both A and B are again utilized, the result of the former being:

$$\sum_{r\neq 0,\alpha}\left\langle \mu_i^{r\alpha}(A)\bar{\mu}_{i'}^{r\alpha}(A)\mu_j^{0r}(A)\bar{\mu}_{j'}^{0r}(A)\right\rangle = \frac{1}{30}\left(\delta_{ij}\delta_{i'j'}\Pi_1(A)\right.$$
$$\left.+\delta_{ii'}\delta_{jj'}\Pi_2(A)+\delta_{ij'}\delta_{i'j}\Pi_3(A)\right), \qquad (3.15)$$

with the parameters $\Pi_1(A)$, $\Pi_2(A)$ and $\Pi_3(A)$ representing the following functions of molecular transition moments in A:

$$\Pi_1(A)=\sum_{r\neq 0,\alpha} 4\left|\mu^{r\alpha}\right|^2\left|\mu^{0r}\right|^2-\left|\mu^{r\alpha}\cdot\mu^{0r}\right|^2-\left|\mu^{r\alpha}\cdot\bar{\mu}^{0r}\right|^2$$
$$\Pi_2(A)=\sum_{r\neq 0,\alpha} -\left|\mu^{r\alpha}\right|^2\left|\mu^{0r}\right|^2+4\left|\mu^{r\alpha}\cdot\mu^{0r}\right|^2-\left|\mu^{r\alpha}\cdot\bar{\mu}^{0r}\right|^2 \qquad (3.16)$$
$$\Pi_3(A)=\sum_{r\neq 0,\alpha} -\left|\mu^{r\alpha}\right|^2\left|\mu^{0r}\right|^2-\left|\mu^{r\alpha}\cdot\mu^{0r}\right|^2+4\left|\mu^{r\alpha}\cdot\bar{\mu}^{0r}\right|^2.$$

Repeating the method for B conveys the result of fully averaging over both *A* and *B*, and consequently equation (3.14) can be re-expressed:

$$\left\langle \left| M_{FI}^{1^2-1^2} \right|^2 \right\rangle = \frac{1}{900} \sum_{\substack{r\neq 0,\alpha \\ s\neq 0,\beta}} \left(\delta_{ii'}\delta_{jj'}\delta_{kk'}\delta_{ll'}\Pi_1(A)\Pi_1(B) + \delta_{ii'}\delta_{jj'}\delta_{kl}\delta_{k'l'}\Pi_1(A)\Pi_2(B) \right.$$
$$+\delta_{ii'}\delta_{jj'}\delta_{kl'}\delta_{k'l}\Pi_1(A)\Pi_3(B) + \delta_{ij}\delta_{i'j'}\delta_{kk'}\delta_{ll'}\Pi_2(A)\Pi_1(B)$$
$$+\delta_{ij}\delta_{i'j'}\delta_{kl}\delta_{k'l'}\Pi_2(A)\Pi_2(B) + \delta_{ij}\delta_{i'j'}\delta_{kl'}\delta_{k'l}\Pi_2(A)\Pi_3(B)$$
$$+\delta_{ij'}\delta_{i'j}\delta_{kk'}\delta_{ll'}\Pi_3(A)\Pi_1(B) + \delta_{ij'}\delta_{i'j}\delta_{kl}\delta_{k'l'}\Pi_3(A)\Pi_2(B)$$
$$\left. +\delta_{ij'}\delta_{i'j}\delta_{kl'}\delta_{k'l}\Pi_3(A)\Pi_3(B) \right) V_{ik}(p,\boldsymbol{R})V_{jl}(p,\boldsymbol{R})V_{i'k'}(p,\boldsymbol{R})V_{j'l'}(p,\boldsymbol{R})$$
$$\times \left(E^{\alpha r}(A) + E^{0s}(B) \right)^{-2},$$

(3.17)

where $\Pi_1(B)$, $\Pi_2(B)$ and $\Pi_3(B)$ are analogous to the results in equation (3.16):

$$\Pi_1(B) = \sum_{s\neq 0,\beta} 4\left|\mu^{s0}\right|^2 \left|\mu^{\beta s}\right|^2 - \left|\mu^{s0}\cdot\mu^{\beta s}\right|^2 - \left|\mu^{s0}\cdot\bar{\mu}^{\beta s}\right|^2$$
$$\Pi_2(B) = \sum_{s\neq 0,\beta} -\left|\mu^{s0}\right|^2 \left|\mu^{\beta s}\right|^2 + 4\left|\mu^{s0}\cdot\mu^{\beta s}\right|^2 - \left|\mu^{s0}\cdot\bar{\mu}^{\beta s}\right|^2 \qquad (3.18)$$
$$\Pi_3(B) = \sum_{s\neq 0,\beta} -\left|\mu^{s0}\right|^2 \left|\mu^{\beta s}\right|^2 - \left|\mu^{s0}\cdot\mu^{\beta s}\right|^2 + 4\left|\mu^{s0}\cdot\bar{\mu}^{\beta s}\right|^2.$$

Finally, full contraction of the interaction tensors in equation (3.17), followed by substitution of this result into equation (3.5), reveals the transition rate due to near-zone $E1^2$-$E1^2$ coupling as:

$$\Gamma^{1^2-1^2} = \frac{\rho}{6400\hbar\pi^3\varepsilon_0{}^4R^{12}} \sum_{\substack{r\neq 0,\alpha \\ s\neq 0,\beta}} \big(2\Pi_1(A)\Pi_1(B)+\Pi_1(A)\Pi_2(B)+\Pi_1(A)\Pi_3(B)+$$
$$\Pi_2(A)\Pi_1(B)+2\Pi_2(A)\Pi_2(B)+\Pi_2(A)\Pi_3(B)+\Pi_3(A)\Pi_1(B)$$
$$+\Pi_3(A)\Pi_2(B)+2\Pi_3(A)\Pi_3(B)\big(E_{\alpha r}(A)+E_{0s}(B)\big)^{-2}. \tag{3.19}$$

3.1.3 Contribution of Quantum Interference

Derivation of the overall energy transfer rate presented in equation (3.5) is concluded by assessing the contribution of the cross-term, a quantum interference of the E2-E2 and $E1^2$-$E1^2$ couplings. The cross term $M_{FI}^{2-2}M_{FI}^{1^2-1^2}$ evolves as a product of the matrix elements for $E1^2$ and E2 coupling as represented by equations (3.6) and (3.13) respectively, such that:

$$\left\langle M_{FI}^{2-2}\bar{M}_{FI}^{1^2-1^2}\right\rangle = \sum_{\substack{r\neq 0,\alpha \\ s\neq 0,\beta}} \left\langle \bar{\mu}_{i'}^{r\alpha}(A)\bar{\mu}_{j'}^{0r}(A)Q_{ij}^{0\alpha}(A)\right\rangle\left\langle \bar{\mu}_{k'}^{s0}(B)\bar{\mu}_{l'}^{\beta s}(B)Q_{kl}^{\beta 0}(B)\right\rangle$$
$$\times\bar{V}_{i'k'}(p,\boldsymbol{R})\bar{V}_{j'l'}(p,\boldsymbol{R})V_{ikjl}(p,\boldsymbol{R})\big(E^{\alpha r}(A)+E^{0s}(B)\big)^{-1}. \tag{3.20}$$

The rotational average of both A and B is again fourth order in the Cartesian indices and the former is expressible as:

$$\sum_{r\neq 0,\alpha}\left\langle \bar{\mu}_{i'}^{r\alpha}(A)\bar{\mu}_{j'}^{0r}(A)Q_{ij}^{0\alpha}(A)\right\rangle = \sum_{r\neq 0,\alpha}\frac{\bar{\mu}_{\lambda'}^{r\alpha}(A)\bar{\mu}_{\mu'}^{0r}(A)Q_{\lambda\mu}^{0\alpha}(A)}{30}\left(-2\delta_{ij}\delta_{i'j'}+3\delta_{ii'}\delta_{jj'}+3\delta_{ij'}\delta_{i'j}\right), \tag{3.21}$$

once more exploiting the traceless property of the quadrupole transition moment. Following the equivalent average of B, and contraction of the interaction tensor terms, the following quantum interference rate contribution emerges:

$$\Gamma^{2-1^2} = \frac{27\rho}{50\hbar\pi^2\varepsilon_0{}^3R^{11}}\sum_{\substack{r\neq 0,\alpha\\ s\neq 0,\beta}}\bar{\mu}_{\lambda'}^{r\alpha}(A)\bar{\mu}_{\mu'}^{0r}(A)Q_{\lambda\mu}^{0\alpha}(A)\bar{\mu}_{\pi'}^{s0}(B)\bar{\mu}_{\nu'}^{\beta s}(B)Q_{\pi\nu}^{\beta 0}(B) \times\left(E^{\alpha r}(A)+E^{0s}(B)\right)^{-1}. \tag{3.22}$$

Both for the donor and the acceptor, this coupling therefore depends on an inner tensor product of transition quadrupole and paired transition dipole components. The total donor-acceptor energy transfer rate is the sum of equations (3.12), (3.19) and (3.22).

3.2 Discussion

Whilst E2-E2 coupling has already been determined within a QED framework, the $E1^2$-$E1^2$ mechanism has seldom been considered, perhaps owing to the mechanisms' relatively small contribution for the majority of E1-allowed systems.

As discussed in the introduction prior to Section 3.1, certain criteria need to be satisfied if such mechanisms are not to be over-ridden by other means of energy transfer; small molecules of reasonably high symmetry, held in close proximity, offer one likely arrangement. However, in the context of RET in lanthanide-doped media, specific realizations can already be identified. Insightful work by Chua and Tanner[19] has highlighted a small number of specific examples in which $E1^2$-$E1^2$ energy migration from the ${}^5D_0$ states of rare earth dopants might prove significant; one presented case features Sm^{2+} as the donor within SrF_2 crystals. The magnitude of an exchange interaction contribution could not be ascertained, but the results suggested that the lead contribution for Sm^{2+} energy transfer is a second-order $E1^2$-$E1^2$ coupling; the lead first-order interaction is believed to be a comparatively weak hexadecapole-hexadecapole (E4-E4) coupling. It was further proposed that $E1^2$-$E1^2$ coupling in Sm^{2+} doped crystals should be favored by the low-lying configuration of the $4f^{n-1}5d$ orbital relative to $4f^n$, conducive to the two-step mechanism by which $4f^{n-1}5d$ acts as a populated intermediate. It is notable that, whereas "intermediate" states within the presented QED analysis are a consequence of virtual photon propagation, and they need not represent physically populated configurations, the positioning of such energy levels does have a significant bearing on transition rates, warranting further discussion.

Whilst difficult to directly measure without designed experimentation, the relative significance of energy transfer via E2-E2 and $E1^2$-$E1^2$ coupling can be assessed by comparison of equations (3.12) and (3.19). A key difference between the two

mechanisms is that the higher-order perturbation result is shown to be dependent on the energy difference between ground and intermediate states of both the donor and acceptor. From equation (3.19), the inverse square dependence on $E^{\alpha r}(A)+E^{0s}(B)$ shows that the rate of transition due to $\mathrm{E1}^2$-$\mathrm{E1}^2$ is highest when either there are states *r* and *s* whose energies are close to E^{α} and E^{0} respectively, or alternatively when they are close to E^{0} and E^{β} respectively, the latter condition established by application of overall energy conservation, *i.e.* $E^{\alpha 0}(A)=E^{\beta 0}(B)$ such that $E^{\alpha r}(A)+E^{0s}(B)=E^{0r}(A)+E^{\beta s}(B)$. More generally, since the acceptor intermediate state will have a higher energy level than the ground state, $E^{0s}(B)$ will always yield a negative result and the rate of $\mathrm{E1}^2$-$\mathrm{E1}^2$ energy transfer will therefore be high if $E^{\alpha r}(A)\approx E^{s0}(B)$, with the further condition that $E^{\alpha r}(A)>E^{s0}(B)$. The present analysis concludes that the $\mathrm{E1}^2$-$\mathrm{E1}^2$ mechanism is most effective when both intermediate states *r* and *s* have energy levels between the ground and excited states of the donor and acceptor respectively, so that the donor and acceptor levels directly involved in energy transfer, *i.e.* A^{α} and B^{β}, are not the lowest unoccupied states.

3.3 Conclusion

Working within the near-zone limit, the above analysis highlights the contributions of both E2-E2 coupling and the seldom considered second-order $\mathrm{E1}^2$-$\mathrm{E1}^2$ coupling. For both forms of interaction, experimentally meaningful rate equations are secured

by the use of orientational averaging and the mechanisms analyzed with reference to systems in which E1-forbidden transitions are commonly reported. The total system energy transfer rate also entails a quantum interference term. Following a complete QED analysis, the contribution of each form of coupling is evaluated in terms of its dependence on chromophore separation, the latter generally proving the factor most readily amenable to verification by experimental means. The energy transfer rate for E2-E2 and $E1^2$-$E1^2$ interactions are confirmed to decay with R^{-10} and R^{-12} dependences, respectively. Because of their different power law indices, there is a short-range regime, whose extent is ultimately determined by the magnitudes of the transition moments, in which both mechanisms will have similar levels of significance and in this case the cross-term with an R^{-11} dependence will also come into play. It has also been demonstrated that the second-order $E1^2$-$E1^2$ coupling will contribute most significantly within systems that possess suitably disposed virtual state configurations.

Moving beyond a single donor-acceptor pair interaction, an extension of this general theory is envisaged in which ensembles of chromophores are considered. Ensemble modeling methods can be applied to quantify the total interaction of a single donor with a number of acceptors within a given coordination shell, these methods being more representative of practical experimental application.[26,27] As discussed in Chapter 2, the effects of mounting both donors and acceptors as surface substrates on juxtaposed 1- or 2D lattices could also be considered.[28-31] All directly opposing as well as diagonal chromophore interactions between donor and

acceptor plates could then be determined. As both E2-E2 and $E1^2$-$E1^2$ transitions can be significant in lanthanide ions doped in crystal structures, an analysis in which donor and acceptor chromophores are constructed within 3D lattices may prove insightful.[32,33] Such a system may necessarily require additional factors to be entertained, such as phonon-assisted or spin-forbidden triplet state energy transfer. Depending on the structure of the lattice environment and the proximity of neighboring donor or acceptor chromophores, the possible involvement of third-body interactions might also need to be accounted for.[34-36] Current results and the framework in which they presented are robust enough to support any such modification.

References

1. Daniels, G.J., Jenkins, R.D., Bradshaw, D.S. & Andrews, D.L. *J. Chem. Phys.* **119**, 2264 (2003).
2. Andrews, D.L. *Can. J. Chem.* **86**, 855 (2008).
3. Baer, R. & Rabani, E. *J. Chem. Phys.* **128**, 184710 (2008).
4. Craig, D.P. & Thirunamachandran, T. *Theor. Chem. Acc.* **102**, 112 (1999).
5. Andrews, D.L. & Bradshaw, D.S. *Eur. J. Phys.* **25**, 845-858 (2004).
6. Andrews, D.L. & Leeder, J.M. *J. Chem. Phys.* **130**, 184504 (2009).
7. Langhals, H., Esterbauer, A.J., Walter, A., Riedle, E. & Puglies, I. *J. Am. Chem. Soc.* **132**, 16777 (2010).

8. Scholes, G.D., Harcourt, R.D. & Fleming, G.R. *J. Phys. Chem. B* **101**, 7302 (1997).
9. Ritz, T., Damjanovic, A., Schulten, K., Zhang, J.P. & Koyama, Y. *Photosynth. Res.* **66**, 125 (2000).
10. Macpherson, A.N., Arellano, J.B., Fraser, N.J., Cogdell, R.J. & Gillbro, T. *Biophys. J.* **80**, 923 (2001).
11. Ritz, T., Damjanovic, A. & Schulten, K. *ChemPhysChem* **3**, 243 (2002).
12. Vaswani, H.M., Holt, N.E. & Fleming, G.R. *Pure Appl. Chem.* **77**, 925 (2005).
13. Polivka, T., Hiller, R.G. & Frank, H.A. *Arch. Biochem. Biophys.* **458**, 111 (2007).
14. Polívka, T. & Frank, H.A. *Accounts Chem. Res.* **43**, 1125 (2010).
15. Krueger, B.P., Scholes, G.D. & Fleming, G.R. *J. Phys. Chem. B* **102**, 5378 (1998).
16. Selvin, P.R. *Annu. Rev. Biophys. Biomol. Struct.* **31**, 275 (2002).
17. Chen, D., Wang, Y., Yu, Y., Huang, P. & Weng, F. *J. Solid State Chem.* **181**, 2763 (2008).
18. Sun, C.Y., Zheng, X.J., Chen, X.B., Li, L.C. & Jin, L.P. *Inorg. Chim. Acta*. **362**, 325 (2009).
19. Chua, M. & Tanner, P.A. *Chem. Phys.* **250**, 267 (1999).
20. Henderson, B. & Imbusch, G.F. *Optical Spectroscopy of Inorganic Solids*. (Oxford University Press: Oxford, 2006).
21. Wybourne, B.G. & Smentek, L. *Optical Spectroscopy of Lanthanides: Magnetic and Hyperfine Interactions*. (CRC: Boca Raton, 2007).

22. Scholes, G.D. & Andrews, D.L. *J. Chem. Phys.* **107**, 5374 (1997).
23. Jenkins, R.D., Daniels, G.J. & Andrews, D.L. *J. Chem. Phys.* **120**, 11442 (2004).
24. Salam, A. *J. Chem. Phys.* **122**, 044112 (2005).
25. Salam, A. *Molecular Quantum Electrodynamics*. (Wiley: Chichester, 2009).
26. Bar-Haim, A., Klafter, J. & Kopelman, R. *J. Am. Chem. Soc.* **119**, 6197 (1997).
27. Andrews, D.L., Li, S., Rodríguez, J. & Slota, J. *J. Chem. Phys.* **127**, 134902 (2007).
28. Bradshaw, D.S., Leeder, J.M., Rodriguez, J. & Andrews, D.L. *Proc. SPIE* **7034**, 703408 (2008).
29. Bradshaw, D.S., Leeder, J.M., Rodriguez, J. & Andrews, D.L. *Proc. SPIE* **6905**, 690503 (2008).
30. Andrews, D.L., Bradshaw, D.S., Leeder, J.M. & Rodríguez, J. *Phys. Chem. Chem. Phys.* **10**, 5250 (2008).
31. Andrews, D.L. & Leeder, J.M. *J. Chem. Phys.* **130**, 034504 (2009).
32. Vásquez, S.O. *Phys. Rev. B* **60**, 8575 (1999).
33. Andrews, D.L. & Jenkins, R.D. *J. Chem. Phys.* **114**, 1089 (2001).
34. Xia, S. & Tanner, P.A. *Phys. Rev. B* **66**, 214305 (2002).
35. Rozbicki, E. & Machnikowski, P. *Phys. Rev. Lett.* **100**, 027401 (2008).
36. May, V. *J. Chem. Phys.* **129**, 114109 (2008).

SECTION 2 – Quantum Electrodynamical Development of Radiation Induced Fluorescence

The following section, consisting of two chapters, introduces novel theory and results relating to radiation induced fluorescence. In laser-based studies of fluorescence, it is well known that polarisation features of the emission convey rich information on structural details of the sample, particularly in condensed phase molecular media. The character of emission from fluorescent species owes its origin to both the properties of the input light and the internal configuration of transitions and molecular energy levels. Consequently, the findings of each chapter are drawn from theoretically determined electric polarisation properties of the output signal.

Chapter 4 develops the theory of multiphoton, *i.e.* two- and three-photon, induced fluorescence, the application of which is particularly prevalent in modern research owing primarily to the technique's unparalleled ability to deliver high-resolution, three dimensional imaging of heterogeneous samples. In general terms, the capture of high quality images aids the investigation of chemically specific information, since fluorescence intensity distributions allow the determination of the relative location, concentration and structure of specific molecular species *in situ*. However, the attendant advantages offered by multiphoton methods include further features that have as yet received relatively little attention. For example, detailed information can be secured on the degree of chromophore orientational order through polarisation-resolved measurements. Note that throughout this section, the term "chromophore" is used to signify a

molecular component or label that can both absorb light and fluoresce, however, the term “fluorophore” is equally valid. This chapter reports the equations that are required for any such investigation. The general analysis, addressing a system of chromophores oriented in three dimensions, determines the fluorescence signal produced by the linear and nonlinear polarisations that are induced by one-, two- and three-photon absorptions, allowing for any rotational relaxation. The results indicate that multiphoton imaging can be further developed as a diagnostic tool, to selectively discriminate micro-domains within a sample that exhibit a degree of orientational correlation. Any such technique could equally monitor dynamical changes in this localised order, perhaps resulting from a chemical interaction or acting in response to an externally applied stimulus.

The final chapter of this thesis explores a novel development in radiation induced fluorescence, namely “laser-controlled fluorescence”, a process whereby the character of fluorescent emission is modified by a laser controlled, optically nonlinear input. In operation, a pulse of off-resonant probe laser beam of sufficient intensity is applied to a system exhibiting fluorescence during the interval of excited state decay following the initial excitation. The result is a rate of decay that can be controllably modified, the associated changes in fluorescence behaviour affording new, chemically-specific information and novel technological application via all optical switching. Chapter 5 investigates a two-level emission model in the further analysis of this process. The results prove especially relevant in the imaging of physical systems employing fluorescent markers, these ranging from quantum dots to green fluorescence

protein. Expressions are presented for the laser-controlled fluorescence anisotropy exhibited by samples in which the fluorophores are randomly oriented. It is also shown that, in systems with suitably configured electronic levels and symmetry properties, fluorescence emission can be produced from energy levels that would normally decay non-radiatively.

Chapter 4 – Insight into Chromophore Orientation through Multiphoton Fluorescence

Polarisation-resolved measurements afford key information on molecular structure, and the degree or extent of local orientational order.[1,2] The elucidation of such information is widely exploited in fluorescence imaging, where the objective to secure quality, three-dimensionally resolved images is supplemented by a scope to accurately distinguish the location, concentration and structure of specific chromophores.[3-5] In connection with conventional (single-photon) fluorescence, such principles are well known and widely applied across a diverse range of physical systems. Numerous studies have focused on confined, highly ordered materials where chromophores are held in crystalline structures, or samples such as cell membranes, molecular films or fiber, where they are less rigidly bound to a physical matrix.[6-10] In such instances, the rotational freedom of the targeted species is commonly restricted, enforcing a degree of orientational order relative to the external structure. Whereas polarisation-derived information is often restricted to two spatial dimensions, the determination of three-dimensional orientation can also be explored.[11] Numerous investigations have extended the scope of such studies into the single-molecule regime, to elucidate information that is obscured in ensemble studies.[12-14]

An ever-increasing number of studies now exploit the advantages inherent in multiphoton excitation. Experimental applications are particularly prevalent in

biological studies, where they afford a capability for imaging to sub-cellular resolution, with limited photodamage, and without any need to suppress light scattering.[15-21] One of the most appealing features of multiphoton-induced imaging is its adaptability, and the fact that the associated instrumentation is also often well suited to additional means of sample interrogation. Commonly used, complementary modes of measurement include second-harmonic generation, sum-frequency generation, coherent anti-Stokes Raman scattering, and Raman spectroscopy, all of which are frequently combined with two-photon fluorescence.[22-24] Whilst three-photon microscopy in particular has been less commonly studied than its two-photon counterpart, it is recognized that image contrast can be enhanced as the number of concerted photon interactions increases.[25,26] The incorporation of additional techniques can permit the visual sectioning of specific molecular domains within bulk material, expanding the potential for applying multiphoton imaging as a tool in structural diagnostics. Nonetheless, securing all of the orientational information that is latent in multiphoton fluorescence is technically demanding, and at present it is compromised by the lack of a complete understanding – certainly in the case of three-photon excitation studies – of how the polarisation response from a fully disordered system relates to the detailed electronic properties of the constituent chromophores.

This chapter presents the results of an investigation aiming to secure a robust, thorough and comprehensive representation of the fluorescence polarisation

properties generated in response to one-, two- and three-photon excitation of molecular chromophores. The single-photon case is included both as a means of introducing the theoretical formalism, and to help elicit patterns of response between the different orders, established subsequently. Although two-photon studies are more common, the selection rules for three-photon excitation offer the possibility of access to states that are not amenable to one- or two-photon excitation.[27-31] Results established by means of an isotropic orientational average determine the induced fluorescence response generated within a fully disordered molecular environment, meaning a complete system, or micro-domains within a complete system, in which all chromophores are randomly oriented in three dimensions. It can be anticipated that the averaged results will prove their value in determining the random orientation limit of a dynamic spectrum, providing a means by which multiphoton imaging can be further developed to monitor and quantify variations in chromophore orientation. In a system with some orientational order, for example one that is undergoing a chemical or biological function, or responding to a controlled external stimulus, the extent of deviation in the fluorescence response, compared to that expected from an isotropic sample, will quantifiably register the degree of order.

In Section 4.1, essential details relating to the theoretical representation of one-, two- and three-photon induced fluorescence are established, casting the output signals in terms of their associated electric polarisation and molecular transition moment properties through standard methods of QED. Whilst the general methods

have already been established, orientational averaging procedures are detailed in Section 4.2, the results of which define the fully disordered limits of both the single and multiphoton fluorescence processes. The analysis requires implementation of fourth-, sixth- and eighth-rank tensor averages.[32,33] The complexity of the averaging procedure escalates rapidly with the tensor rank, and it is not surprising that eighth rank averaging has rarely been utilized, having only recently been deployed in the context of laser-controlled fluorescence.[34] The significance, patterns and applications of these results are discussed in Section 4.3.

4.1 Multiphoton Fluorescence

To approach the key polarisation issues, it is appropriate to begin with a representation of the optical process in its entirety, subsuming the single- or multi-photon absorption of laser input, and the emission of fluorescent radiation. Each stage occurs with an efficiency that is determined by the strength of coupling between the ground and relevant excited electronic levels. As implemented in previous chapters, the coupling is described through matrix elements that feature component values of the relevant transition dipoles and multiphoton tensors. The process efficiency, once more determined by Fermi's rule, is in each case proportional to the modulus square of such matrix elements, noting that the excitation and emission events will be treated as mutually independent, since in practice they occur in a step-wise fashion. For our purposes we shall assume the validity of a Born-Oppenheimer separation of wavefunctions and focus upon

electronic transitions; the corresponding vibrational energies are generally small compared to the electronic state energy differences. Also we assume a development through molecular states that is typically associated with electric dipole transitions; the contribution from both magnetic and higher order electric contributions throughout this chapter is deemed insignificant. The theory that follows will provide a means for interrogating the extent of correlation between the transition moments associated with absorption and emission. Specific attention will be given to the extent to which fluorescence retains a directionality of polarisation from the initial excitation.

To achieve fluorescence intensity results amenable to experimental application, the output fluorescence signal, $I_{flu}^{(n)}(\phi)$, is defined as a function of the experimentally controllable angle between the polarisation vector of the incident light and the resolved polarisation of the emission, ϕ, and it can be cast in general terms of the separate matrix elements for n^{th} order multiphoton absorption and single-photon emission, namely $M_{\nu 0}^{(n)}(\xi)$ and $M_{0\alpha}(\xi)$ respectively. Our representation allows the possibility for excited state processes such as internal conversion, hindered rotation, rotational diffusion, intramolecular energy transfer etc. to intervene between the excitation and radiative decay. Adopting labels 0 and ν to denote the molecular ground and initially excited energy levels, and α for the level from which emission occurs, the intensity of fluorescence can be cast as follows:

$$I_{flu}^{(n)}(\phi) = K^{(n)} \sum_{\xi} \left\langle \left| M_{\nu 0}^{(n)}(\xi) \right|^2 \left| M_{0\alpha}(\xi) \right|^2 \right\rangle. \tag{4.1}$$

The fluorescence signal in equation (4.1) is thus portrayed in terms of the physically separable efficiencies of the absorption and emission processes; the constant of proportionality $K^{(n)}$ is itself dependent on experimental parameters including the n^{th} power of the mean laser irradiance, and the degree of n^{th} order coherence.[35] To assess the relationship between $I_{flu}^{(n)}$ and ϕ for a fully disordered system in which molecular chromophores, or more specifically the transition moments associated with multiphoton absorption and single photon emission, are randomly oriented relative to the input propagation, the angular brackets in equation (4.1) are again implemented in terms of an orientational average. First, to determine the results for one-, two- and three-photon induced fluorescence, it is necessary to define the form of all associated matrix elements. Each is derived by standard methods, with the underlying principles introduced in a detailed description of single-photon induced fluorescence that follows.

4.1.1 One-photon Induced Fluorescence

It is expedient to concisely review the simplest, familiar case of one-photon induced fluorescence, as it establishes the methods to be used for the more intricate multiphoton cases that follow. Theory for the process of single-photon induced fluorescence is characterized by the development of two distinct matter-radiation

interactions. The first describes the optical excitation of a chromophore by single-photon absorption, inducing an electronic transition from the ground to an accessible excited state configuration. The second interaction entails molecular relaxation and photon emission, usually returning the chromophore to its ground electronic state. For the complete process of one-photon induced fluorescence, the initial, intermediate and final system states are thus described as:

$$\left.\begin{aligned} |I\rangle &= |\xi^0; m(\boldsymbol{p},\lambda)\rangle, \\ |A\rangle &= |\xi^\nu; (m-1)(\boldsymbol{p},\lambda)\rangle, \\ |A'\rangle &= |\xi^\alpha; 0(\boldsymbol{p}',\lambda')\rangle, \\ |F\rangle &= |\xi^0; 1(\boldsymbol{p}',\lambda')\rangle, \end{aligned}\right\} \tag{4.2}$$

Noting that the transition between $|I\rangle$ and $|F\rangle$ progresses through two real, physically identifiable intermediate states, $|A\rangle$ and $|A'\rangle$ – the latter allowed to differ by accommodating any ultrafast intramolecular redistribution processes that might precede emission, such relaxation typically manifest in a Stokes shift. To clarify, $\boldsymbol{p}$ and λ respectively represent the wave-vectors and polarisations of the input beam, distinct from $\boldsymbol{p}'$ and λ' which serve as properties of the output fluorescence. The input mode conveys *m* photons within a quantization volume that encloses the absorbing chromophore. For simplicity the state of the optical output mode is omitted from the state descriptions of $|I\rangle$ and $|A\rangle$ because that mode suffers no change in the intervening (absorption) transition; equally the state of the

input beam, thereafter unchanged, is omitted from the designations of $|A'\rangle$ and $|F\rangle$ as their coupling only concerns the fluorescence output.

Initial Absorption: The initial photon absorption drives evolution between the system states $|I\rangle$ and $|A\rangle$ of equation (4.2), the photon promoting an electronic transition between molecular states ξ^0 and ξ^ν. The required matrix element utilizes first-order perturbation theory and is derived following substitution of equation (1.9) into equation (1.15), where $q=1$. The substitution deploys the photon annihilation operator within the interaction Hamiltonian, the resulting matrix element for one-photon absorption following as:

$$M_{\nu 0}^{(1)}(\xi) = -i\sum_{\boldsymbol{p},\lambda}\left(\frac{m\hbar cp}{2\varepsilon_0 V}\right)^{\frac{1}{2}} e_i^{(\lambda)}(\boldsymbol{p})\,\mu_i^{\nu 0}(\xi)\exp\left(i\boldsymbol{p}\cdot\boldsymbol{R}_\xi\right). \tag{4.3}$$

Single-Photon Emission: The emission engages electronic decay of the excited chromophore and creation of a single photon into the vacuum radiation field, the process expressed by equation (4.2) as a transition between system states $|A'\rangle$ and $|F\rangle$. The matrix element now engages the photon creation operator in equation (1.5), giving:

$$M_{0\alpha}(\xi) = i\sum_{\boldsymbol{p}',\lambda'}\left(\frac{\hbar cp'}{2\varepsilon_0 V}\right)^{\frac{1}{2}} \overline{e}_i^{(\lambda')}(\boldsymbol{p}')\,\mu_i^{0\alpha}(\xi)\exp\left(-i\boldsymbol{p}'\cdot\boldsymbol{R}_\xi\right). \tag{4.4}$$

On substitution of the derived matrix elements for both absorption and emission into equation (4.1), a complete expression for the signal output following single photon excitation emerges:

$$I_{flu}^{(1)}(\phi) = K^{(1)} \sum_{\xi} \sum_{\boldsymbol{p},\boldsymbol{p}',\lambda,\lambda'} \left\langle \left(e_i^{(\lambda)} \overline{e}_j^{(\lambda')} \overline{e}_k^{(\lambda)} e_l^{(\lambda')} \mu_i^{\nu 0} \mu_j^{0\alpha} \overline{\mu}_k^{\nu 0} \overline{\mu}_l^{0\alpha} \right) \right\rangle, \tag{4.5}$$

where the modulus squares of equations (4.3) and (4.4) have been employed and the product of parameters within the parentheses of each matrix element is incorporated into the proportionality constant $K^{(1)}$. Starting above and continuing for all relevant expressions to follow, a number of labels including the wave-vectors $(\boldsymbol{p})$ and $(\boldsymbol{p}')$ of the electric polarisation terms, as well as the molecule identity (ξ) associated with the dipole transition moments, have been suppressed for clarity. For additional convenience, in the orientational averaging procedure to be utilized in Section 4.2, a new notation is now introduced in which the products of the unit electric polarisation vectors, and those of the molecular transition moments, are each incorporated into second rank tensors as follows:

$$I_{flu}^{(1)}(\phi) = K^{(1)} \sum_{\xi} \sum_{\boldsymbol{p},\boldsymbol{p}',\lambda,\lambda'} \left\langle S_{ij} \overline{S}_{kl} T_{ij} \overline{T}_{kl} \right\rangle, \tag{4.6}$$

where specifically S_{ij} and $\overline{S}_{ij}$ denote $e_i^{(\lambda)}(\boldsymbol{p})\overline{e}_j^{(\lambda')}(\boldsymbol{p}')$ and $\overline{e}_i^{(\lambda)}(\boldsymbol{p})e_j^{(\lambda')}(\boldsymbol{p}')$. Likewise, the molecular transition moment products described by T_{ij} and $\overline{T}_{ij}$ correspond to $\mu_i^{\nu 0}(\xi)\mu_j^{0\alpha}(\xi)$ and $\overline{\mu}_i^{\nu 0}(\xi)\overline{\mu}_j^{0\alpha}(\xi)$. In these examples, and in all subsequent applications of this notation presented in this chapter, the last index in the electric polarisation and molecular transition tensors relates to photon emission. Equation (4.6) thus expresses a result that embraces, in the term within angular brackets, the angular disposition of the chromophore transition moments with respect to the input and output polarisation vectors. In a rigidly oriented system, by forgoing the orientational average the result would thus exhibit a dependence on $\cos^2\eta\cos^2\gamma$, where η is the angle between the absorption moment and the input polarisation, γ that between the emission moment and the fluorescence polarisation.

4.1.2 Two-photon Induced Fluorescence

Two-photon induced fluorescence is characterized by the development of three distinct matter-radiation interactions, specifically the concerted absorption of two photons followed by one-photon emission. The initial, intermediate and final system states are defined as:

$$\left.\begin{aligned} |I\rangle &= |\xi^0; m(\boldsymbol{p},\lambda)\rangle, \\ |B\rangle &= |\xi^\nu; (m-2)(\boldsymbol{p},\lambda)\rangle, \\ |B'\rangle &= |\xi^\alpha; 0(\boldsymbol{p}',\lambda')\rangle, \\ |F\rangle &= |\xi^0; 1(\boldsymbol{p}',\lambda')\rangle, \end{aligned}\right\} \tag{4.7}$$

First, we focus on the matrix element for the two-photon transition between $|I\rangle$ and $|B\rangle$.

Two-Photon Absorption: The acquisition of two photon energies by the chromophore in its excitation to level ξ^ν, leads to a system state $|B\rangle$. The associated matrix element entails a progression through a virtual intermediate system state $|R\rangle$, in which one photon has been annihilated and the chromophore, lacking a resonant level to match the photon energy, is accordingly in a superposition of virtual molecular states ξ^r:

$$\left.\begin{aligned} |I\rangle &= |\xi^0; m(\boldsymbol{p},\lambda)\rangle, \\ |R\rangle &= |\xi^r; (m-1)(\boldsymbol{p},\lambda)\rangle, \\ |B\rangle &= |\xi^\nu; (m-2)(\boldsymbol{p},\lambda)\rangle. \end{aligned}\right\} \tag{4.8}$$

Any energy non-conserving state $|R\rangle$ can be sustained as long as it is allowed by the time-energy uncertainty principle and this will again be reflected in a weighting factor, varying with the inverse of the mismatch energy. The necessary second-

order matrix element describing the transition between $|I\rangle$ and $|B\rangle$ through $|R\rangle$ is derived by substitution of equation (1.9) into equation (1.15), where $q=2$, noting that the initial and evolved intermediate system energies are $E^0+m\hbar cp$ and $E^r+(m-1)\hbar cp$ respectively:

$$M_{\nu 0}^{(2)}(\xi)=m_2^{1/2}\sum_{\boldsymbol{p},\lambda}\left(\frac{\hbar cp}{2\varepsilon_0 V}\right)e_i^{(\lambda)}e_j^{(\lambda)}\frac{1}{2}\sum_r\left(E^{0r}+\hbar cp\right)^{-1}\left(\mu_i^{\nu r}\mu_j^{r0}+\mu_j^{\nu r}\mu_i^{r0}\right). \qquad (4.9)$$

Here, the quantization volume initially contains the chromophore and two photons of the incident radiation, the factor of $m_2^{1/2}\equiv\left[m(m-1)\right]^{1/2}$ correspondingly arises from the successive operations of the photon annihilation operator. The above expression exploits the symmetry of the electric polarisation terms $e_i^{(\lambda)}(\boldsymbol{p})e_j^{(\lambda)}(\boldsymbol{p})$ with respect to exchange of the indices *i* and *j*. Similar to theory presented in Chapter 2, the two dipole product contributions in equation (4.9) relate to each of the possible time-orderings in which the two, indistinguishable input photons can be annihilated, noting that the factor of $\frac{1}{2}$ is introduced to preclude over-counting. The above two-photon absorption matrix element can thus be presented as:

$$M_{\nu 0}^{(2)}(\xi)=\sum_{\boldsymbol{p},\lambda}\left(\frac{m_2^{1/2}\hbar cp}{2\varepsilon_0 V}\right)e_i^{(\lambda)}e_j^{(\lambda)}\alpha_{(ij)}^{\nu 0}, \qquad (4.10)$$

where, in the above expression, bracketed subscripts denote symmetry in the enclosed indices. The second rank molecular response tensor $\alpha_{(ij)}^{\nu 0}$ is defined as:

$$\alpha_{(ij)}^{\nu 0} = \frac{1}{2}\sum_{r}\left(E^{0r} + \hbar cp\right)^{-1}\left(\mu_i^{\nu r}\mu_j^{r0} + \mu_j^{\nu r}\mu_i^{r0}\right), \tag{4.11}$$

being a specific implementation of a more general formula presented earlier as equation (2.14).

Full process: Returning to equation (4.4), the matrix element for one-photon emission is now deployed, and substitution of this and equation (4.10) into equation (4.1) determines the two-photon induced fluorescence signal. In the following expression the proportionality constant $K^{(2)}$ contains a factor m_2, which in general conveys a quadratic dependence on the intensity, and which is also a function of the photon statistics of the input beam.[35] Thus, the following expression is derived:

$$I_{flu}^{(2)}(\phi) = K^{(2)}\sum_{\xi}\sum_{\boldsymbol{p},\boldsymbol{p}',\lambda,\lambda'}\left\langle S_{(ij)k}\bar{S}_{(lm)n}T_{(ij)k}\bar{T}_{(lm)n}\right\rangle, \tag{4.12}$$

here expressing the electric vector and molecular transition moment products as third rank tensors such that $S_{(ij)k}$ and $\bar{S}_{(ij)k}$ correspond to $e_i^{(\lambda)}(\boldsymbol{p})e_j^{(\lambda)}(\boldsymbol{p})\bar{e}_k^{(\lambda')}(\boldsymbol{p}')$ and $\bar{e}_i^{(\lambda)}(\boldsymbol{p})\bar{e}_j^{(\lambda)}(\boldsymbol{p})e_k^{(\lambda')}(\boldsymbol{p}')$, whilst $T_{(ij)k}$ and $\bar{T}_{(ij)k}$ signify $\alpha_{(ij)}^{\nu 0}(\xi)\mu_k^{0\alpha}(\xi)$ and $\bar{\alpha}_{(ij)}^{\nu 0}(\xi)\bar{\mu}_k^{0\alpha}(\xi)$ respectively. In this case, for an oriented sample, the dependence

on emission angle is again $\cos^2\gamma$. However the dependence on input polarisation is considerably more intricate, being determined by a weighted combination of $\cos^2$ functions for each angle between the input polarisation vector and one of a selection of transition moments, *i.e.* $\boldsymbol{\mu}^{vr}$, $\boldsymbol{\mu}^{r0}$, for each level *r*.

4.1.3 Three-photon Induced Fluorescence

For three-photon induced fluorescence, the initial, intermediate excited and final system states are:

$$\left.\begin{aligned} |I\rangle &= |\xi^0; m(\boldsymbol{p},\lambda)\rangle, \\ |C\rangle &= |\xi^v; (m-3)(\boldsymbol{p},\lambda)\rangle, \\ |C'\rangle &= |\xi^\alpha; 0(\boldsymbol{p}',\lambda')\rangle, \\ |F\rangle &= |\xi^0; 1(\boldsymbol{p}',\lambda')\rangle. \end{aligned}\right\} \tag{4.13}$$

There are four photon-matter interactions, one of which is one-photon emission, again characterized by equation (4.4).

Three-Photon Absorption: For the three-photon transition between $|I\rangle$ and $|C\rangle$ there are two distinct virtual intermediate system states, $|R\rangle$ and $|S\rangle$ as follows:

$$\left.\begin{aligned}
|I\rangle &= \left|\xi^0; m(\boldsymbol{p},\lambda)\right\rangle, \\
|R\rangle &= \left|\xi^r; (m-1)(\boldsymbol{p},\lambda)\right\rangle, \\
|S\rangle &= \left|\xi^s; (m-2)(\boldsymbol{p},\lambda)\right\rangle, \\
|C\rangle &= \left|\xi^v; (m-3)(\boldsymbol{p},\lambda)\right\rangle.
\end{aligned}\right\} \tag{4.14}$$

Utilising the above conditions, the three-photon matrix element emerges following substitution of equation (1.9) into equation (1.15) where $q=3$, such that:

$$\begin{aligned}
M_{v0}^{(3)}(\xi) = -m_3^{1/2} i \sum_{\boldsymbol{p},\lambda} \left(\frac{\hbar c p}{2\varepsilon_0 V}\right)^{\frac{3}{2}} e_i^{(\lambda)} e_j^{(\lambda)} e_k^{(\lambda)} \frac{1}{6} \sum_{r,s} \left(\left(E^{0r} + \hbar c p\right)\left(E^{0s} + 2\hbar c p\right)\right)^{-1} \\
\times \left(\mu_i^{vs}\mu_j^{sr}\mu_k^{r0} + \mu_i^{vs}\mu_k^{sr}\mu_j^{r0} + \mu_j^{vs}\mu_i^{sr}\mu_k^{r0} + \mu_j^{vs}\mu_k^{sr}\mu_i^{r0} \right. \\
\left. + \mu_k^{vs}\mu_i^{sr}\mu_j^{r0} + \mu_k^{vs}\mu_j^{sr}\mu_i^{r0}\right),
\end{aligned} \tag{4.15}$$

the factor of $\frac{1}{6}$ again to offset over-counting. In terms of radiation quanta, *V* initially contains three photons of the input light, therefore $m_3^{1/2} \equiv \left[m(m-1)(m-2)\right]^{1/2}$ as a result of the three successive operations of the photon annihilation operator. The above result can be recast in terms of a third rank molecular response tensor $\beta_{(ijk)}^{v0}$, being a specific implementation of equation (2.20), the former defined as:

$$\begin{aligned}
\beta_{(ijk)}^{v0} = \frac{1}{6} \sum_{r,s} \left[\left(E^{0r} + \hbar c p\right)\left(E^{0s} + 2\hbar c p\right)\right]^{-1} \left(\mu_i^{vs}\mu_j^{sr}\mu_k^{r0} + \mu_i^{vs}\mu_k^{sr}\mu_j^{r0} \right. \\
\left. + \mu_j^{vs}\mu_i^{sr}\mu_k^{r0} + \mu_j^{vs}\mu_k^{sr}\mu_i^{r0} + \mu_k^{vs}\mu_i^{sr}\mu_j^{r0} + \mu_k^{vs}\mu_j^{sr}\mu_i^{r0}\right).
\end{aligned} \tag{4.16}$$

Full process: The fluorescence due to three-photon excitation can now be presented as:

$$I_{flu}^{(3)}(\phi) = K^{(3)} \sum_{\xi} \sum_{\boldsymbol{p},\boldsymbol{p}',\lambda,\lambda'} \left\langle S_{(ijk)l} \bar{S}_{(mno)p} T_{(ijk)l} \bar{T}_{(mno)p} \right\rangle, \tag{4.17}$$

where $K^{(3)}$ subsumes a factor $m_3 \Rightarrow g^{(3)} \bar{m}^3$, conveying a cubic dependence on the input beam intensity and a linear dependence on its degree of third order coherence.[35] In equation (4.17), the electric polarisation and molecular transition moments are described in terms of fourth rank tensors, where $S_{(ijk)l}$ and $\bar{S}_{(ijk)l}$ respectively represent $e_i^{(\lambda)}(\boldsymbol{p}) e_j^{(\lambda)}(\boldsymbol{p}) e_k^{(\lambda)}(\boldsymbol{p}) \bar{e}_l^{(\lambda')}(\boldsymbol{p}')$ and $\bar{e}_i^{(\lambda)}(\boldsymbol{p}) \bar{e}_j^{(\lambda)}(\boldsymbol{p}) \bar{e}_k^{(\lambda)}(\boldsymbol{p}) e_l^{(\lambda')}(\boldsymbol{p}')$, whilst $T_{(ijk)l}$ and $\bar{T}_{(ijk)l}$ correspond to $\beta_{(ijk)}^{\nu 0}(\xi) \mu_l^{0\alpha}(\xi)$ and $\bar{\beta}_{(ijk)}^{\nu 0}(\xi) \bar{\mu}_l^{0\alpha}(\xi)$, the final index of each again being associated with the one-photon emission. While the index *l* and *p* contractions in equation (4.17) associated with the molecular invariants $T_{(ijk)l}$ and $\bar{T}_{(mno)p}$ would again deliver the $\cos^2\gamma$ factor for a rigid sample, the orientation relative to the input polarisation depends on a multitude of angles, corresponding to the orientations of the transition moments $\boldsymbol{\mu}^{\nu s}$, $\boldsymbol{\mu}^{sr}$, $\boldsymbol{\mu}^{r0}$, summed over states *r* and *s*.

4.2 Rotational Averaging of Single- and Multiphoton Fluorescence Signals

Before the implementation of a rotational average, the general results for the fluorescence output in one-, two- and three-photon induced systems, represented by equations (4.6), (4.12) and (4.17) respectively, are applicable to systems in which the responsible chromophores have arbitrary orientations with respect to experimentally determined input and detection configurations. As such, these results are directly applicable to all ordered samples in which individual chromophores are held in a fixed orientation, or others comprising domains with significant local orientational correlations. To address substantially less ordered systems it is expedient to secure corresponding results for an opposite extreme, namely systems of completely random orientation. To this end, the above results are now subjected to an orientational averaging protocol. One-photon induced fluorescence is addressed first, highlighting procedures within the method in detail, although the simplicity of this case belies the significantly greater technical complexity in securing results for the higher-order interactions. The latter calculations are extremely complex, and in the case of three-photon fluorescence they are only viable by the use of the specialized, not widely familiar techniques, as reported below.

4.2.1 Orientational Average for One-photon Induced Fluorescence

From equation (4.6), the one-photon induced fluorescence signal exhibits an implicit sum over four separate Cartesian indices, each of which are known to assume *x*, *y* or *z* values with respect to a chosen frame. The results are resolved through fourth-rank orientational averaging. Summarising the procedure first outlined in Chapter 1, the molecular and radiation components of the system are first uncoupled by assigning to the latter a laboratory-fixed frame of reference, denoted by Latin indices. The molecular transition moments within T_{ij} and $\overline{T}_{kl}$ are similarly referred to a molecule-fixed frame, labeled by Greek indices, and the output signal is re-expressed:

$$\begin{aligned} I_{flu}^{(1)}(\phi) &= K^{(1)} \sum_{\xi} \sum_{\boldsymbol{p},\boldsymbol{p}',\lambda,\lambda'} \left\langle S_{ij} \overline{S}_{kl} T_{ij} \overline{T}_{kl} \right\rangle \\ &= K^{(1)} \sum_{\xi} \sum_{\boldsymbol{p},\boldsymbol{p}',\lambda,\lambda'} S_{ij} \overline{S}_{kl} T_{\lambda\mu} \overline{T}_{\nu\sigma} \left\langle \ell_{i\lambda} \ell_{j\mu} \ell_{k\nu} \ell_{l\sigma} \right\rangle, \end{aligned} \tag{4.18}$$

where the molecular and radiation reference frames are linked through the product of direction cosines between the frame axes, represented within the angular brackets. As the only parameters of equation (4.18) that are now dependent on molecular orientation, the orientational average is implemented over $\left\langle \ell_{i\lambda} \ell_{j\mu} \ell_{k\nu} \ell_{l\sigma} \right\rangle$, the general result for which is presented as equation (1.26). The inherent Kronecker delta functions operate on the molecular and radiation tensors featured in equation (4.18), for example $\delta_{ij}\delta_{kl}$ effects tensor contractions in the radiation frame, with

$S_{ij}\overline{S}_{kl}$ yielding $S_{ii}\overline{S}_{kk}$. All of the ensuing results are then expressible in terms of scalar products between input and output polarisation components. In the commonly utilized deployment of plane-polarised input laser light, the polarisation vectors are real and the scalar product of two polarisation vectors is concisely summarized by:

$$\overset{(-)(\lambda)}{\boldsymbol{e}} \cdot \overset{(-)(\lambda')}{\boldsymbol{e}} = \delta_{\lambda\lambda'} + \left(1-\delta_{\lambda\lambda'}\right)\cos\phi\,, \tag{4.19}$$

the angle ϕ having already been established as that between the input and output polarisation vectors. The final result for the orientationally averaged single-photon induced fluorescence output emerges in terms of ϕ as:

$$\begin{aligned} I_{flu}^{(1)}(\phi) = \frac{K^{(1)}}{30}\sum_{\xi}\sum_{\boldsymbol{p},\boldsymbol{p}',\lambda,\lambda'}\Big[&\left(T_{\lambda\lambda}\overline{T}_{\mu\mu} + T_{\lambda\mu}\overline{T}_{\mu\lambda}\right)\left(3\cos^2\phi - 1\right) - \left(2T_{\lambda\mu}\overline{T}_{\lambda\mu}\right) \\ &\times\left(\cos^2\phi - 2\right)\Big], \end{aligned} \tag{4.20}$$

incorporating three molecular invariants, $T_{\lambda\lambda}\overline{T}_{\mu\mu}$, $T_{\lambda\mu}\overline{T}_{\mu\lambda}$ and $T_{\lambda\mu}\overline{T}_{\lambda\mu}$. For this case of one-photon induced fluorescence, it is further possible to express the molecular tensors in equation (4.20) relative to the magnitude of the molecular transition moments $\boldsymbol{\mu}^{\nu 0}$ and $\boldsymbol{\mu}^{0\alpha}$, and the angle between them, β, such that:

$$I_{flu}^{(1)}\left([\phi],[\beta]\right)=\frac{K^{(1)}}{30}\sum_{\xi}\sum_{\boldsymbol{p},\boldsymbol{p}',\lambda,\lambda'}\left|\boldsymbol{\mu}^{\nu 0}\right|^2\left|\boldsymbol{\mu}^{0\alpha}\right|^2 \times\left[\left(3\cos^2\phi-1\right)\left(2\cos^2\beta\right)-2\left(\cos^2\phi-2\right)\right], \tag{4.21}$$

where the identities $T_{\lambda\lambda}\bar{T}_{\mu\mu}=T_{\lambda\mu}\bar{T}_{\mu\lambda}=\left|\boldsymbol{\mu}^{\nu 0}\right|^2\left|\boldsymbol{\mu}^{0\alpha}\right|^2\cos^2\beta$, and $T_{\lambda\mu}\bar{T}_{\lambda\mu}=\left|\boldsymbol{\mu}^{\nu 0}\right|^2\left|\boldsymbol{\mu}^{0\alpha}\right|^2$ apply. Resolving equation (4.21) for fluorescence components parallel or perpendicular to the input polarisation leads to the familiar degree of fluorescence anisotropy for a randomly oriented sample, specifically $r=\left(I_{\parallel}-I_{\perp}\right)/\left(I_{\parallel}+2I_{\perp}\right)=\frac{1}{5}\left(3\cos^2\beta-1\right)$.[1,2] The equivalent, general results for two- and three-photon induced fluorescence, derived in the following, have not been determined before.

4.2.2 Orientational Average for Two-photon Induced Fluorescence

The established averaging methods are now applied to equation (4.12) for the two-photon induced fluorescence output, decoupling the molecular and radiation frames as before:

$$I_{flu}^{(2)}\left(\phi\right)=K^{(2)}\sum_{\xi}\sum_{\boldsymbol{p},\boldsymbol{p}',\lambda,\lambda'}S_{(ij)k}\bar{S}_{(lm)n}T_{(\lambda\mu)\nu}\bar{T}_{(\sigma\tau)\rho}\left\langle\ell_{i\lambda}\ell_{j\mu}\ell_{k\nu}\ell_{l\sigma}\ell_{m\tau}\ell_{n\rho}\right\rangle. \tag{4.22}$$

Delivery of the result now requires the implementation of a sixth-rank orientational average, the general form of which is presented as equation (1.27). It transpires that

the fluorescence signal is now generally expressible in terms of fifteen molecular invariants (terms contracting T and $\overline{T}$ tensors) which are distinct, though generally they are not all linearly independent:

$$\begin{aligned} I_{flu}^{(2)}(\phi) = \frac{K^{(2)}}{210} \sum_{\xi} \sum_{\mathbf{p},\mathbf{p}',\lambda,\lambda'} \Big[\Big(& T_{(\lambda\lambda)\mu}\overline{T}_{(\mu\nu)\nu} + T_{(\lambda\lambda)\mu}\overline{T}_{(\nu\mu)\nu} + T_{(\lambda\mu)\lambda}\overline{T}_{(\mu\nu)\nu} \\ & + T_{(\lambda\mu)\lambda}\overline{T}_{(\nu\mu)\nu} + T_{(\lambda\mu)\lambda}\overline{T}_{(\nu\nu)\mu} + T_{(\lambda\mu)\mu}\overline{T}_{(\lambda\nu)\nu} + T_{(\lambda\mu)\nu}\overline{T}_{(\lambda\nu)\mu} + T_{(\lambda\mu)\mu}\overline{T}_{(\nu\lambda)\nu} \\ & + T_{(\lambda\mu)\nu}\overline{T}_{(\nu\lambda)\mu} + T_{(\lambda\mu)\mu}\overline{T}_{(\nu\nu)\lambda} + T_{(\lambda\mu)\nu}\overline{T}_{(\mu\nu)\lambda} + T_{(\lambda\mu)\nu}\overline{T}_{(\nu\mu)\lambda} \Big) \left(3\cos^2\phi - 1\right) \\ & - 2\left(T_{(\lambda\lambda)\mu}\overline{T}_{(\nu\nu)\mu} + T_{(\lambda\mu)\nu}\overline{T}_{(\lambda\mu)\nu} + T_{(\lambda\mu)\nu}\overline{T}_{(\mu\lambda)\nu} \right) \left(2\cos^2\phi - 3\right) \Big]. \end{aligned} \tag{4.23}$$

Each of the above molecular invariants is a scalar, expressing one particular aspect of the overall propensity of the chromophore to generate two-photon fluorescence. Each is expressible as a sum of four separate terms entailing specific transition moments, for example:

$$\begin{aligned} T_{(\lambda\mu)\nu}\overline{T}_{(\lambda\mu)\nu} &= \alpha_{(\lambda\mu)}^{\nu 0}\mu_{\nu}^{0\alpha}\overline{\alpha}_{(\lambda\mu)}^{\nu 0}\overline{\mu}_{\nu}^{0\alpha} \\ &= \frac{1}{4}\sum_{r,\tilde{r}} \left[\left(E^{0r} + \hbar cp \right) \left(E^{0\tilde{r}} + \hbar cp \right) \right]^{-1} \left(\mu_{\lambda}^{\nu r}\mu_{\mu}^{r0}\overline{\mu}_{\lambda}^{\nu\tilde{r}}\overline{\mu}_{\mu}^{\tilde{r}0} \right. \\ &\quad \left. + \mu_{\lambda}^{\nu r}\mu_{\mu}^{r0}\overline{\mu}_{\mu}^{\nu\tilde{r}}\overline{\mu}_{\lambda}^{\tilde{r}0} + \mu_{\mu}^{\nu r}\mu_{\lambda}^{r0}\overline{\mu}_{\lambda}^{\nu\tilde{r}}\overline{\mu}_{\mu}^{\tilde{r}0} + \mu_{\mu}^{\nu r}\mu_{\lambda}^{r0}\overline{\mu}_{\mu}^{\nu\tilde{r}}\overline{\mu}_{\lambda}^{\tilde{r}0} \right) \mu_{\nu}^{0\alpha}\overline{\mu}_{\nu}^{0\alpha}. \end{aligned} \tag{4.24}$$

in which the state labels r and $\tilde{r}$ identify two virtual states which must be allowed to be different, since each appears in a separate sum. These summations preclude factorizing out the absorption and emission transition moments, without further assumptions that would compromise the generality of the result. It is, however,

possible to re-define equation (4.23) in a more concise form by considering index symmetry properties, since a number of the invariants are equal, for example $T_{(\lambda\lambda)\mu}\overline{T}_{(\mu\nu)\nu} + T_{(\lambda\lambda)\mu}\overline{T}_{(\nu\mu)\nu} + T_{(\lambda\mu)\lambda}\overline{T}_{(\nu\nu)\mu} + T_{(\lambda\mu)\mu}\overline{T}_{(\nu\nu)\lambda} \equiv 4T_{(\lambda\lambda)\mu}\overline{T}_{(\mu\nu)\nu}$. In consequence, the 15 molecular invariants in equation (4.23) reduce to just 4 distinct terms:

$$I_{flu}^{(2)}(\phi) = \frac{K^{(2)}}{105}\sum_{\xi}\sum_{\mathbf{p},\mathbf{p}',\lambda,\lambda'}\Big[\Big(2T_{(\lambda\lambda)\mu}\overline{T}_{(\mu\nu)\nu} + 4T_{(\lambda\mu)\lambda}\overline{T}_{(\mu\nu)\nu}\Big)\big(3\cos^2\phi - 1\big) - \Big(T_{(\lambda\lambda)\mu}\overline{T}_{(\nu\nu)\mu} + 2T_{(\lambda\mu)\nu}\overline{T}_{(\lambda\mu)\nu}\Big)\big(2\cos^2\phi - 3\big)\Big]. \tag{4.25}$$

Despite the simple form of equation (4.25), it should be remembered that each invariant is in fact a sum of distinct products of components of the tensor *T*, since in each case the Cartesian indices λ, μ and ν can each take *x, y* or *z* values. Moreover, each of those tensor components is in general determined by combinations of transition moments that involve a tier of intermediate levels *r*, that tier being in principle of unlimited extent. The experimental determination of these individual parameters is impossible, because the above result provides for no more than two linearly independent polarisation measurements. Moreover, calculational methods cannot assist, since even the most sophisticated molecular software cannot usually secure the necessary convergence in the sums over states, even for relatively small molecules. However, there is sufficient information in the result of equation (4.25) to yield physically meaningful interpretations, as will be shown in the discussion in Section 4.3. The value of the present method is still more evident in the following three-photon case. Although the procedure for securing the following result is

significantly more complex, it does in fact produce concisely expressible and tractable results.

4.2.3 Orientational Average for Three-photon Induced Fluorescence

The orientationally averaged output signal for three-photon induced fluorescence is now considered, beginning with a re-expression of equation (4.17) as:

$$I_{flu}^{(3)}(\phi) = K^{(3)} \sum_{\xi} \sum_{\boldsymbol{p},\boldsymbol{p}',\lambda,\lambda'} S_{(ijk)l} \overline{S}_{(mno)p} T_{(\lambda\mu\nu)\sigma} \overline{T}_{(\tau\rho\pi)\eta} \left\langle \ell_{i\lambda} \ell_{j\mu} \ell_{k\nu} \ell_{l\sigma} \ell_{m\tau} \ell_{n\rho} \ell_{o\pi} \ell_{p\eta} \right\rangle, \tag{4.26}$$

requiring an eighth-rank average. In contrast to the fourth and sixth rank orientational averages already utilized, the general form of the eighth-rank expression, specifically applied as $\left\langle \ell_{i\lambda} \ell_{j\mu} \ell_{k\nu} \ell_{l\sigma} \ell_{m\tau} \ell_{n\rho} \ell_{o\pi} \ell_{p\eta} \right\rangle$, is rarely reported owing to the extreme complexity in presenting and resolving the matrix result. However, following the same methodology, a general result has now been determined in which the three-photon induced fluorescence signal is described in terms of 105 molecular invariants. In order to present a more manageable result, it is necessary to again exploit the index-symmetrized form of the molecular tensors, allowing the output signal then to be expressed much more simply in terms of just 5 unique molecular invariants:

$$I_{flu}^{(3)}(\phi)=\frac{K^{(3)}}{315}\sum_{\xi}\sum_{\boldsymbol{p},\boldsymbol{p}',\lambda,\lambda'}\Big[\Big(3T_{(\lambda\lambda\mu)\mu}\overline{T}_{(\nu\nu\sigma)\sigma}+6T_{(\lambda\lambda\mu)\nu}\overline{T}_{(\mu\nu\sigma)\sigma}+6T_{(\lambda\mu\nu)\lambda}\overline{T}_{(\mu\nu\sigma)\sigma}\Big)$$
$$\times\Big(3\cos^2\phi-1\Big)-\Big(3T_{(\lambda\lambda\mu)\nu}\overline{T}_{(\mu\sigma\sigma)\nu}+2T_{(\lambda\mu\nu)\sigma}\overline{T}_{(\lambda\mu\nu)\sigma}\Big)\Big(3\cos^2\phi-4\Big)\Big].$$

(4.27)

Each invariant, again comprises a sum of tensor component products. As with two-photon induced fluorescence, the inherent summation over accessible intermediate states, in this case r, $\tilde{r}$, s and $\tilde{s}$, precludes further simplification of equation (4.27).

4.3 Discussion

A striking feature of the equations determining both single- and multiphoton fluorescence response, namely equations (4.20), (4.25) and (4.27), is that they all prove to be expressible in a relatively simple, generic form. In fact, the multiphoton fluorescence output associated with randomly disposed chromophores can be described through the following formula:

$$I_{flu}^{(n)}(\phi)=K^{(n)}\sum_{\xi}\sum_{\boldsymbol{p},\boldsymbol{p}',\lambda,\lambda'}\Big[\Lambda^{(n)}\Big(3\cos^2\phi-1\Big)-\Upsilon^{(n)}\Big(n\cos^2\phi-\big(n+1\big)\Big)\Big],\qquad(4.28)$$

with both $\Lambda^{(n)}$ and $\Upsilon^{(n)}$ representable as a sum of distinct molecular invariants, the former featuring as a coefficient of the second Legendre polynomial $\left(3\cos^2\phi-1\right)$,

characteristic of time-resolved fluorescence anisotropy. There is no angle at which the $\Upsilon^{(n)}$ term can be made to vanish. However, under "magic angle" conditions where ϕ is 54.7º, the $\Lambda^{(n)}$ terms do disappear, so that the corresponding measurement should enable the identification, at least in relative terms, of $\Upsilon^{(n)}$.

To proceed with the more general case, it is helpful to cast the above expression in the form:

$$I_{flu}^{(n)}(\phi) = K'^{(n)} \sum_{\xi} \sum_{\boldsymbol{p},\boldsymbol{p}',\lambda,\lambda'} \left[n+1-y+(3y-n)\cos^2\phi \right], \tag{4.29}$$

where $K'^{(n)} = K^{(n)}\Upsilon^{(n)}$, $y = \Lambda^{(n)}/\Upsilon^{(n)}$. The latter parameter is a scalar that characterises the relative values of the molecular invariant groupings in equations (4.20), (4.25) and (4.27). Although the precise value of *y* will depend on the component values of the transition tensors, it can be shown that *y* is positive and limited to an upper bound of $(n+1)$. The graphs of Figures 4.1-4.3 exhibit the functional form of the fluorescence polarisation, for one-, two- and three-photon induced fluorescence, over the range $(0 \le \phi \le \pi/2)$, the behavior over the next quadrant being a mirror image in the ordinate axis in each case.

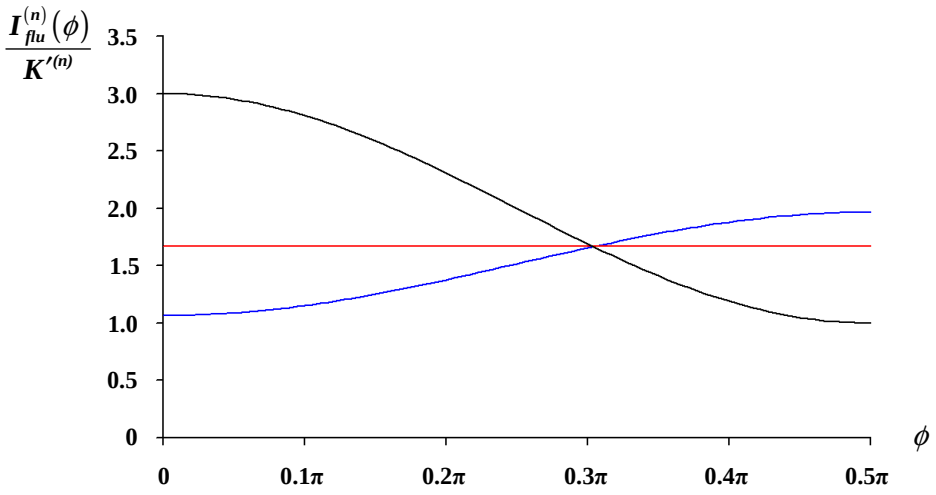

Figure 4.1 The relative angular disposition of polarisation in fluorescence produced by single-photon absorption $(n=1)$. The blue, red and black curves correspond to $3y/n$ = 0.1, $3y/n$ = 1 and $3y/n$ = 3 respectively.

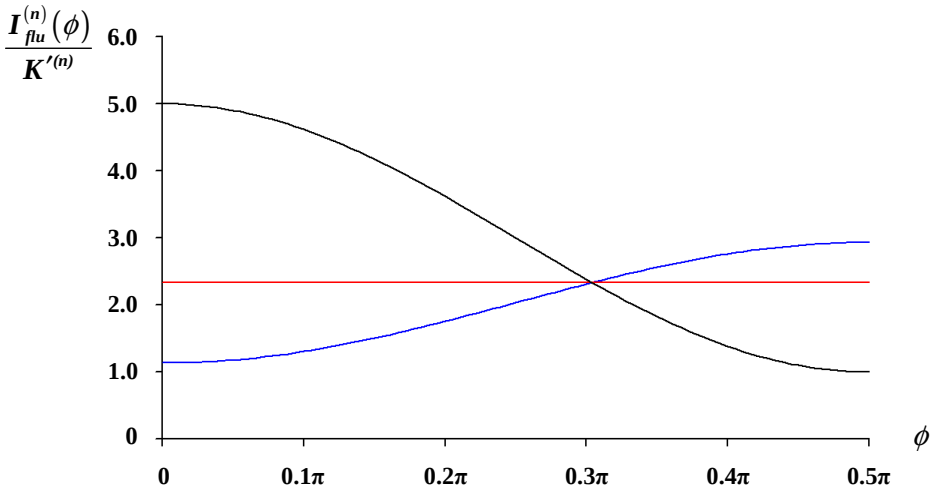

Figure 4.2 The relative angular disposition of polarisation in fluorescence produced by two-photon absorption $(n=2)$. The blue, red and black curves correspond to $3y/n$ = 0.1, $3y/n$ = 1 and $3y/n$ = 3 respectively

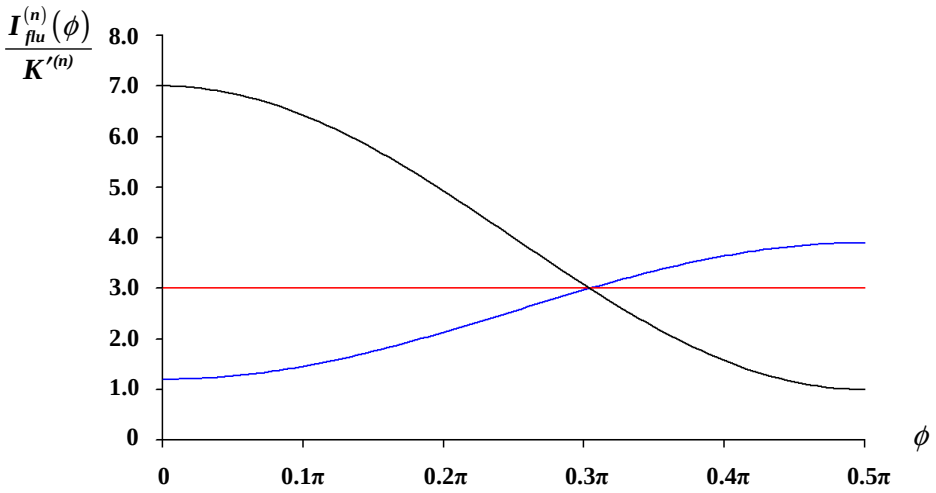

Figure 4.3 The relative angular disposition of polarisation in fluorescence produced by three-photon absorption $(n=3)$. The blue, red and black curves correspond to $3y/n$ = 0.1, $3y/n$ = 1 and $3y/n$ = 3 respectively.

The graphs all show the behavior for different values of *y* and each clearly portrays the magic angle condition cited above as the point at which the curves for all different values of *y* intersect. For each type of excitation, curves are shown for $3y/n$ = 0.1, 1.0 and 3.0. The curves corresponding to the case, $3y/n$ = 0.1, represent an extreme condition, $\Lambda^{(n)} \ll \Upsilon^{(n)}$, characterized by strongly depolarised emission. The curves drawn for $3y/n$ = 1.0 are of special interest because the fluorescence proves in each case to be independent of the resolving polarisation, a general feature that has not to our knowledge been discovered before. This is a condition under which the fluorescence produced through the concerted absorption of any number of photons becomes completely unpolarised. The results for $3y/n$ = 3.0 are perhaps the most interesting, being indicative of the statistically most likely outcome. This condition arises within each of the relevant general equations,

(4.20), (4.25) and (4.27), when the featured molecular invariants are of approximately equal value, for example in the two-photon case where $T_{(\lambda\lambda)\mu}\overline{T}_{(\mu\nu)\nu} = T_{(\lambda\mu)\lambda}\overline{T}_{(\mu\nu)\nu} = T_{(\lambda\lambda)\mu}\overline{T}_{(\nu\nu)\mu} = T_{(\lambda\mu)\nu}\overline{T}_{(\lambda\mu)\nu}$. Here there is a strong retention of polarisation and it is remarkable that this condition leads in every case to $\Lambda^{(n)}/\Upsilon^{(n)} = y = n$, a further, previously unreported result.

Emission anisotropies are determined by $r = \left(\left\langle I_{\parallel}\right\rangle - \left\langle I_{\perp}\right\rangle\right)\Big/\left(\left\langle I_{\parallel}\right\rangle + 2\left\langle I_{\perp}\right\rangle\right)$, where $\left\langle I_{\parallel}\right\rangle$ and $\left\langle I_{\perp}\right\rangle$ are the components of the rotationally averaged fluorescence intensity polarised parallel and perpendicular, respectively, to the electric vector of the input. The result conforms to the simple formula $r = 2n/(2n+3)$ and yields the following specific values: (i) $n = 1;\ r = 2/5 = 0.4$, the familiar result; also (ii) $n = 2;\ r = 4/7 = 0.57$; and (iii) $n = 3;\ r = 6/9 = 0.67$. These limiting case results are in precise agreement with values that arise specifically when all transition moments are considered parallel, a special case previously reported by Lakowicz *et al.*[36] The correlation serves to verify a limiting case of the present, more general results, but it is also notable that the conditions under which such behavior arises are not only associated with parallel transition moments. The same observations will result, for example if all of the molecular transition tensor elements have similar magnitudes. Although fluorescence anisotropies can be determined in principle even from fully oriented domains, samples of the latter kind may readily be distinguished on the basis of an anisotropy that varies with rotation of the sample itself.

4.4 Conclusion

The results of the above theory represent tools that can be applied in the analysis of polarisation-determined features in two- and three-photon fluorescence from samples of considerable molecular complexity. By determining how either type of multiphoton-induced fluorescence signal responds to the orientation of a polarizer, it is in principle possible to distinguish and quantify any departure from local orientational order or disorder within a bulk sample. Key to this discrimination is the difference in angular disposition of the fluorescence polarisation.

In samples whose chromophores are rigidly oriented, the fluorescence signal from an ensemble with common orientation takes the form of a $\cos^2\phi$ distribution with respect to the angle ϕ between the emission moment and the resolved polarisation. On rotation of the polarizer through 180° there will be an angle at which the signal is extinguished, both for single- and multi-photon induced fluorescence, although the angular positions for the minimum and maximum fluorescence intensities, $I_{\min}^{(n)}$ and $I_{\max}^{(n)}$ respectively, may of course not necessarily correspond to $\phi = 0$ and 90°. However, as shown, the behavior from a randomly oriented sample is in general distinctively different. In the cases considered above, all satisfy the condition that the ratio $I_{\min}^{(n)} / I_{\max}^{(n)}$ lies in the interval $\left(1, 1/(2n+1)\right)$. This suggests that in a general case the measured value of $I_{\min}^{(n)} / I_{\max}^{(n)}$ registered against the scale $\left(1, 1/(2n+1)\right)$

should represent a robust, easily determined single-value indicator of the degree of disorder in fluorescence produced by *n*-photon excitation.

References

1. Lakowicz, J.R. *Principles of Fluorescence Spectroscopy*. (Kluwer Academic/Plenum Publishers: New York, 1999).
2. Valeur, B. *Molecular Fluorescence*. (Wiley-VCH: Weinheim, 2002).
3. Festy, F., Ameer-Beg, S.M., Ng, T. & Suhling, K. *Mol. BioSyst.* **3**, 381 (2007).
4. Levitt, J.A., Matthews, D.R., Ameer-Beg, S.M. & Suhling, K. *Curr. Opin. Biotech.* **20**, 28 (2009).
5. Gradinaru, C.C., Marushchak, D.O., Samim, M. & Krull, U.J. *Analyst* **135**, 452 (2010).
6. Inoué, S., Shimomura, O., Goda, M., Shribak, M. & Tran, P.T. *P. Natl. Acad. Sci. USA* **99**, 4272 (2002).
7. Brasselet, S., Le Floc'h, V., Treussart, F., Roch, J.-F., Zyss, J., Botzung-Appert, E., & Ibanez, A. *Phys. Rev. Lett.* **92**, 207401 (2004).
8. Corry, B., Jayatilaka, D., Martinac, B. & Rigby, P. *Biophys. J.* **91**, 1032 (2006).
9. Gasecka, A., Han, T.-J., Favard, C., Cho, B.R. & Brasselet, S. *Biophys. J.* **97**, 2854 (2009).
10. Gasecka, A., Dieu, L.-Q., Brühwiler, D. & Brasselet, S. *J. Phys. Chem. B* **114**, 4192 (2010).
11. Empedocles, S.A., Neuhauser, R. & Bawendi, M.G. *Nature* **399**, 126 (1999).

12. Weiss, S. *Nat. Struct. Biol.* **7**, 724 (2000).

13. Weston, K.D. & Goldner, L.S. *J. Phys. Chem. B* **105**, 3453 (2001).

14. Vacha, M. & Kotani, M. *J. Chem. Phys.* **118**, 5279 (2003).

15. Williams, R.M., Zipfel, W.R. & Webb, W.W. *Curr. Opin. Chem. Biol.* **5**, 603 (2001).

16. Helmchen, F. & Denk, W. *Curr. Opin. Neurobiol.* **12**, 593 (2002).

17. Rubart, M. *Circ. Res.* **95**, 1154 (2004).

18. Diaspro, A., Chirico, A.D.G. & Collini, M. *Q. Rev. Biophys.* **38**, 97 (2005).

19. Oheim, M., Michael, D.J., Geisbauer, M., Madsen, D. & Chow, R.H. *Adv. Drug Deliver. Rev.* **58**, 788 (2006).

20. Diaspro, A., Bianchini, P., Vicidomini, G., Faretta, M., Ramoino, P. & Usai, C. *Biomed. Eng. Online* **5**, 36 (2006).

21. Wang, B.-G., König, K. & Halbhuber, K.-J. *J. Microsc.* **238**, 1 (2010).

22. Jhan, J., Chang, W., Chen, H., Lee, Y., Wu, M., Chen, C. & Liau, I. *Opt. Express* **16**, 16431 (2008).

23. Provenzano, P.P., Eliceiri, K.W. & Keely, P.J. *Clin. Exp. Metastasis* **26**, 357 (2009).

24. Yue, S., Slipchenko, M.N. & Cheng, J. *Laser and Photonics Reviews* **5**, 496 (2011).

25. Balaji, J., Desai, R. & Maiti, S. *Microsc. Res. Techniq.* **63**, 67 (2004).

26. Chu, S.W., Tai, S.P., Ho, C.L., Lin, C.H. & Sun, C.K. *Microsc. Res. Techniq.* **66**, 193 (2005).

27. Andrews, D.L. & Ghoul, W.A. *J. Chem. Phys.* **75**, 530 (1981).

28. Galasso, V. *J. Chem. Phys.* **92**, 2495 (1990).

29. Pasquarello, A. & Quattropani, A. *Phys. Rev. B* **43**, 3837 (1991).

30. Galasso, V. *Chem. Phys.* **161**, 189 (1992).

31. Jagatap, B.N. & Meath, W.J. *J. Opt. Soc. B* **19**, 2673 (2002).

32. Andrews, D.L. & Thirunamachandran, T. *J. Chem. Phys.* **67**, 5026 (1977).

33. Andrews, D.L. & Ghoul, W.A. *J. Phys. A* **14**, 1281 (1981).

34. Leeder, J.M., Bradshaw, D.S. & Andrews, D.L. *J. Phys. Chem. B* **115**, 5227 (2011).

35. Loudon, R. *The Quantum Theory of Light*. (Oxford University Press: Oxford, 2000).

36. Lakowicz, J.R., Gryczynski, I., Malak, H., Schrader, M., Engelhardt, P., Kano, H. & Hell, S.W. *Biophys. J.* **72**, 567 (1997).

Chapter 5 – Laser-modified and Laser-controlled Fluorescence in Two-level Systems

In any molecular system that exhibits fluorescence, the primary result of ultraviolet/visible absorption is the electronic excitation of individual chromophores. Typically, ultrafast intramolecular vibrational redistribution processes produce a degree of immediate relaxation and partial degradation of the acquired energy, with subsequent fluorescence typically occurring from the lowest vibrational level of the electronic excited state. Consequently, the characteristics of emission in "conventional" molecular fluorescence are relatively insensitive to the optical frequency of any monochromatic source used to create the initial electronic excitation. Whilst the input has to be encompassed by an absorption band of the target chromophore, the rapid relaxation processes that occur prior to fluorescence mean that the decay usually occurs from around the energy threshold of the electronically excited state, irrespective of the precise input frequency. There is therefore limited scope to explore dispersion properties of the material beyond the simple line-shape of the emission itself. In technical terms, the transition dipole moment for fluorescence emission is considered a frequency independent property.

As is well known, the throughput of a laser beam in such photo-activated systems can produce stimulated emission when the optical frequency matches the fluorescence, a phenomenon that has found analytical applications in stimulated emission depletion spectroscopy.[1-6] However, in the newly discovered process of laser-controlled fluorescence, innovated by Bradshaw and Andrews, a passive,

completely off-resonant laser beam of moderate intensity interacts with the emission. Under such conditions the probe engages with the fluorescent emission through a third-order response tensor that is indeed strongly dependent on optical frequency. In this sense, the transition moment for the emission acquires a frequency dependence and in consequence each excited-state lifetime, τ, is appreciably modified.[7-10]

The essence of the effect can be captured in a very simple general formula, $\tau^{-1} = \tau_{flu}^{-1} + \tau_{nr}^{-1} + KI$, where the first two terms on the right correspond to inverses of the excited-state lifetimes for fluorescence and competing non-radiative decay respectively. The effect of the probe emerges in the form of the additional term proportional to *I*, the irradiance of the off-resonant probe. In a heterogeneous sample the above constant of proportionality, K, which is determined by detailed molecular nonlinearity, will generally take a different value for each chemically distinct component. Initial estimates suggest that fluorescence lifetimes, under specified conditions, can be reduced by 10% or more, for an input laser irradiance of 10^{11} W cm^{-2}, with typical values of 16×10^{-30} C m for the magnitude of the transition dipole moment and a photonic energy as 10^{-19} J, so that the effect should be readily amenable to measurement with modulation-based instrumentation.[7] One can draw some analogy with the well-known enhancement of emission, which can occur through coupling with strong electric fields.[11-13] However, the mechanism of laser-controlled fluorescence proceeds through direct interaction with the oscillating

electric field of throughput electromagnetic radiation, as opposed to a nearby surface or static field.

In the limiting case, where the probe-induced term dominates the expression for inverse lifetime, laser-controlled fluorescence represents more than just a mechanism to modify the rate of emission. Such a system would possess weak or entirely forbidden "conventional" transition pathways between the ground and lowest excited electronic states, *i.e.* both τ_{flu}^{-1} and τ_{nr}^{-1} are small or equal to zero. Fluorescence would subsequently occur only as a result of the mutual interaction between excited state chromophores and the off-resonant throughput, the latter conferring optical nonlinearity on the system, providing an alternative allowed pathway. Due to the pulsed nature of the input, there is a significant capacity for the probe light to act as a switch for the fluorescence in such cases. Numerous examples of such systems containing E1-forbidden relaxation transitions are cited in the introduction to Chapter 3.

The following chapter details how in systems of randomly oriented chromophores, the effects of laser-controlled fluorescence will manifest as changes to the emission anisotropy. The theoretical foundations of laser-controlled fluorescence are presented in Section 5.1. In Section 5.2, it is shown how a two-level formulation of theory can be implemented using an expedient, entirely rigorous procedural algorithm that highlights the twin dependence on static and transition dipole moments. Using this method, tractable expressions are secured whose broad

validity extends to any material whose emission spectrum is dominated by one excited electronic state.[14-17] As a topical example, the present analysis focuses particular attention on quantum dots, where there is additional scope to exploit a well-characterized size-dependence in the dispersion properties.[18,19] In section 5.3, rotational averages are implemented and precise expressions are duly presented for the modified fluorescence anisotropy, characterizing and quantifying the probe control mechanism. The analysis is concluded in Section 5.4.

5.1. Laser-modified Fluorescence

As previously discussed in Chapter 1, fluorescence that occurs through spontaneous emission, as further depicted by Figure 5.1, generally involves a single matter-radiation interaction, and its representation in theory is cast in terms of first-order time-dependent perturbation theory.

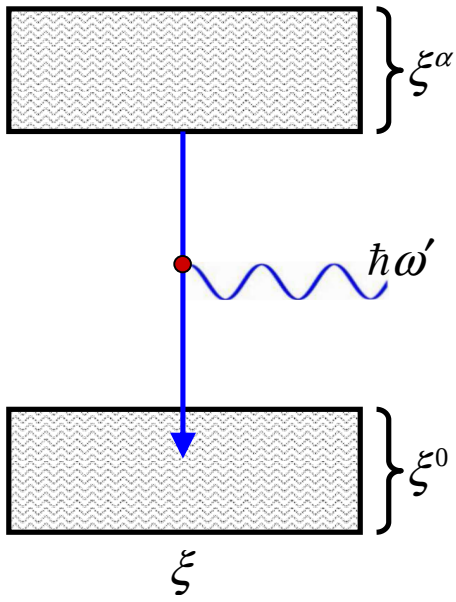

Figure 5.1 Energy level representation for spontaneous one-photon fluorescence. Electronic states and their vibrational manifolds are signified by the boxes. The vertical arrow represents the "downward" electronic transition instigating the emission of a photon of energy $\hbar\omega'$. The ground and excited molecular states are again labeled as ξ^{0} and ξ^{α} respectively, and the filled dot symbolizes a single matter-radiation interaction.

Once the radiation responsible for the initial electronic excitation has passed out of the system, and assuming that no other light is present, the higher order, odd-rank perturbation terms that may in principle contribute, are instead deemed insignificant, only denoting self-energy corrections. However, these higher-order interactions will also arise on application of an off-resonant probe laser, namely where a laser wavelength is chosen at which the chromophores are optically transparent. There is no net absorption or stimulated emission of such a beam, yet elastic forward-scattering events do occur as the photons are annihilated and created into the same radiation mode. Such events can engage by nonlinear coupling with

the fluorescence emission, resulting in three concerted matter-radiation interactions, see Figure 5.2. The quantum amplitude of such a process is now determined by third-order perturbation theory, *i.e.* the form of the required matrix element is determined from substitution of $q=3$ into equation (1.15). Similar effects are observed in connection with RET.[20-27]

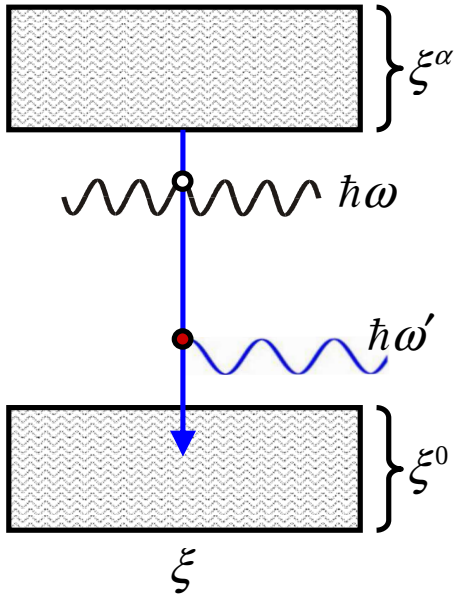

Figure 5.2 Energy level representation for the nonlinear coupling mechanism. The off-resonant laser beam with photon energy $\hbar\omega$ is included and the un-filled dot represents two concerted matter-radiation interactions (*i.e.* elastic forward-scattering).

The intensity of fluorescence, $I'_{flu}\left(\Omega'\right)$, or power per unit solid angle, Ω', is derived from equation (1.12), where the associated rate determined from Fermi's Golden Rule is multiplied by the energy of a fluorescence photon, $\hbar cp' = \hbar\omega'$. The result represents the signal that is produced by a single molecule initially in the

relevant excited state. By inclusion of the mechanism under present scrutiny, the net intensity is hence determined from $I'_{flu}(\Omega')d\Omega' = 2\pi\rho\omega'\sum_{\xi}\left|M_{0\alpha}^{(1)}(\xi)+M_{0\alpha}^{(3)}(\xi)\right|^2$, where $M_{0\alpha}^{(1)}(\xi)$ and $M_{0a}^{(3)}(\xi)$ are the quantum amplitudes for the first- and third-order interaction processes, respectively, and the density of radiation states is $\rho = \left(p'^2V/8\pi^3hc\right)d\Omega'$.[10] Assuming all laser sources and fluorescence outputs are plane polarised, a general representation for the intensity of laser-modified fluorescence follows:

$$I'_{flu}(\Omega') = \left(\frac{cp'^4}{8\pi^2\varepsilon_0}\right)\Big[e'_ie'_j\mu_i^{0\alpha}\mu_j^{0\alpha} + (I/c\varepsilon_0)e_ie_je'_ke'_l\chi_{ijk}^{0\alpha}\mu_l^{0\alpha} + \left(I^2/4c^2\varepsilon_0^2\right)e_ie_je'_ke_le_me'_n\chi_{ijk}^{0\alpha}\chi_{lmn}^{0\alpha}\Big], \tag{5.1}$$

where again, the usual labels associated with the polarisation vectors of the fluorescence and probe photons, $e'(\boldsymbol{p}')$ and $e(\boldsymbol{p})$ respectively, have been suppressed for clarity. The irradiance of the laser probe is denoted as *I* and the nonlinear transition susceptibility $\chi_{ijk}^{0\alpha}(\xi)$ represents a specific implementation of the general third-rank response tensor defined earlier as equation (2.20). Explicitly exhibiting the frequency dispersion, $\chi_{ijk}^{0\alpha}(\xi)$ is represented as:

$$\chi_{ijk}^{0\alpha}(\xi)=\sum_{r}\sum_{s\neq\alpha}\left(\frac{\mu_k^{0s}(\xi)\mu_j^{sr}(\xi)\mu_i^{r\alpha}(\xi)}{E^{s\alpha}\left(E^{r\alpha}-\hbar\omega\right)}+\frac{\mu_k^{0s}(\xi)\mu_i^{sr}(\xi)\mu_j^{r\alpha}(\xi)}{E^{s\alpha}\left(E^{r\alpha}+\hbar\omega\right)}\right)$$
$$+\sum_{r}\sum_{s}\left(\frac{\mu_j^{0s}(\xi)\mu_k^{sr}(\xi)\mu_i^{r\alpha}(\xi)}{\left(E^{s\alpha}-\hbar\omega+\hbar\omega'\right)\left(E^{r\alpha}-\hbar\omega\right)}+\frac{\mu_i^{0s}(\xi)\mu_k^{sr}(\xi)\mu_j^{r\alpha}(\xi)}{\left(E^{s\alpha}+\hbar\omega+\hbar\omega'\right)\left(E^{r\alpha}+\hbar\omega\right)}\right)$$
$$+\sum_{r\neq 0}\sum_{s}\left(\frac{\mu_j^{0s}(\xi)\mu_i^{sr}(\xi)\mu_k^{r\alpha}(\xi)}{\left(E^{s\alpha}-\hbar\omega+\hbar\omega'\right)\left(E^{r\alpha}+\hbar\omega'\right)}+\frac{\mu_i^{0s}(\xi)\mu_j^{sr}(\xi)\mu_k^{r\alpha}(\xi)}{\left(E^{s\alpha}+\hbar\omega+\hbar\omega'\right)\left(E^{r\alpha}+\hbar\omega'\right)}\right),$$

(5.2)

With reference to later comments, it is worth noting here that there is no assumption of Kleinman symmetry at this stage, this being a simplifying device commonly made for calculational expediency that would impose complete index symmetry for the above tensor.[28]

The initial term on the right-hand side of equation (5.1) corresponds to spontaneous emission, intrinsic to the system and independent of the probe laser beam. The last term signifies a coupling of the elastically forward-scattered probe beam with the fluorescence emission. The middle term, linear in *I*, signifies a quantum interference of these two concurrent processes. The overall multiplier of *I* in this term can be identified with $\hbar\omega'$ times the *K* that appeared in the equation for excited state lifetime discussed prior to Section 5.1. In principle, measuring the effect of the passive beam at varying levels of intensity should enable the value of *K* to be experimentally determined. In general, it may be assumed that the leading term in equation (5.1) is non-zero and the middle one is the leading correction, although a configuration is possible in which the third term exists on its own, *i.e.*

when the first and second terms are null. This concept forms the basis of a proposed optical switch mechanism to be discussed in detail in Section 5.3.

5.2 Theory Pertaining to Two-level Systems

Considering the dependence of the fluorescence signal on the optical frequency of the probe, it is evident that the denominators within the third-rank tensor of equation (5.2) are primarily responsible for determining any degree of enhancement or suppression of the optical emission. These factors are ultimately determined by the relative positioning of the chromophore energy levels, relative to the magnitude of the probe photon energy. To discover more, it is convenient to assume that the probe light is delivered in the form of a tunable beam with optical frequency $\omega < \omega'$, a condition that specifically precludes single-photon excitation of ground-state molecules. It will also be assumed that the chosen range of probe frequencies cannot produce multiphoton excitation. The main challenge in evaluating the nonlinear response characterized by the transition tensors within equation (5.2) now lies with implementing the required sum over intermediate states. There is a potentially infinite number of energy levels associated with *r* and *s*, and to ease calculational complexity it is common to reduce such sets to a small, finite number by approximation. In the present context, it is defensible to consider only the states through which the majority of the optical transitions occur, which in the case of many fluorescent systems limits the selection to just the ground and lowest energy excited states, *i.e.* a two-state model may be applied. To be clear, the assumption is

that the character of the fluorescence emission process, including the effect of the probe radiation, is dominated by two electronic levels. It is not to be presumed that the state from which the fluorescence decay occurs is necessarily the same as the state initially populated by photoexcitation.

Restricting both intermediate states featured within equation (5.2) to just $\left|\xi^0\right\rangle$ and $\left|\xi^\alpha\right\rangle$, only four unique routes can describe virtual transition sequences from the excited to ground molecular states progressing through both *r* and *s*, the $\xi^\alpha \to \xi^r \to \xi^s \to \xi^0$ sequences specifically expressible as $\xi^\alpha \to \xi^0 \to \xi^0 \to \xi^0$, $\xi^\alpha \to \xi^\alpha \to \xi^0 \to \xi^0$, $\xi^\alpha \to \xi^0 \to \xi^\alpha \to \xi^0$ and $\xi^\alpha \to \xi^\alpha \to \xi^\alpha \to \xi^0$. Each sequence generates a combination of $\xi^0 \leftrightarrow \xi^\alpha$ transition dipole moments, $\boldsymbol{\mu}^{0\alpha}(\xi)$ and $\boldsymbol{\mu}^{\alpha 0}(\xi)$, in combination with the static dipole moments of the ground and excited energy levels, $\boldsymbol{\mu}^{00}(\xi)$ and $\boldsymbol{\mu}^{\alpha\alpha}(\xi)$ respectively. It can be assumed that the former transition electric moments $\boldsymbol{\mu}^{0\alpha}(\xi)$ and $\boldsymbol{\mu}^{\alpha 0}(\xi)$ are real and also equal. Detailed analysis reveals that the dependence on static moments emerges only in terms of their vector difference, $\boldsymbol{d}(\xi) = \boldsymbol{\mu}^{\alpha\alpha}(\xi) - \boldsymbol{\mu}^{00}(\xi)$, *i.e.* the shift in dipole moment that accompanies the transition. This feature applies to all nonlinear optical susceptibilities, treated by a two-level model. With the benefit of an algorithmic method, the following prescription can be adopted:[29-31]

$$\boldsymbol{\mu}^{\alpha\alpha}(\xi) \to \boldsymbol{\mu}^{\alpha\alpha}(\xi) - \boldsymbol{\mu}^{00}(\xi) = \boldsymbol{d}(\xi)\,;\ \boldsymbol{\mu}^{00}(\xi) \to 0. \tag{5.3}$$

Applying this protocol requires application of an associated rule, that any transitional mechanism that connects the initial and final system states (here, for the emission process) through a ground state static dipole is to be discarded, and hence only two of the originally proposed four sequences, namely $\xi^{\alpha} \to \xi^{0} \to \xi^{\alpha} \to \xi^{0}$ and $\xi^{\alpha} \to \xi^{\alpha} \to \xi^{\alpha} \to \xi^{0}$ persist. Applied to the six terms within equation (5.2), the two-level third-rank response tensor is generally expressible as a sum of 12 separate contributions. Further simplification ensues because a number of these terms, when $r = 0$ and/or $s = \alpha$, are precluded by the conditions of perturbation theory. The two-state form of $\chi_{ijk}^{0\alpha}(\xi)$ thus re-emerges as:

$$\chi_{ijk}^{0\alpha}(\xi) = \frac{2}{\hbar^2} \frac{\mu_i^{0\alpha}(\xi)\mu_j^{0\alpha}(\xi)\mu_k^{0\alpha}(\xi)}{\left(\omega^2 - \omega'^2\right)} + \frac{\mu_i^{0\alpha}(\xi) d_j d_k}{\hbar^2 \omega\omega'} - \frac{\mu_j^{0\alpha}(\xi) d_i d_k}{\hbar^2 \omega\omega'} \ . \tag{5.4}$$

It may be observed that the second and third terms on the right in equation (5.4) exhibit an antisymmetry with respect to interchange of the indices *i* and *j*. However, in the physical observable delivered by equation (5.1), this tensor is index-contracted with a *i*,*j*-symmetric product of polarisation vectors. Consequently, since only the *i*,*j*-symmetric part of equation (5.4) can contribute to the fluorescence signal, it is expedient to replace $\chi_{ijk}^{0\alpha}(\xi)$, without further approximation, by an index-symmetrised form, $\chi_{(ij)k}^{0\alpha}(\xi)$, that is defined as follows:

$$\chi^{0\alpha}_{(ij)k}(\xi) \equiv \frac{1}{2}\left(\chi^{0\alpha}_{ijk}(\xi) + \chi^{0\alpha}_{jik}(\xi)\right) = \frac{2}{\hbar^2}\frac{\mu^{0\alpha}_i(\xi)\mu^{0\alpha}_j(\xi)\mu^{0\alpha}_k(\xi)}{\left(\omega^2 - \omega'^2\right)}. \tag{5.5}$$

It is notable that the result of the above expression is in fact fully index-symmetric, meaning symmetric with respect to interchange of any pair of indices. It is therefore noted that the two-level model delivers a result that is consistent with the adoption of Kleinman symmetry, even though the latter condition has not been artificially imposed. Furthermore, there is a significant physical consequence, as it emerges that the physical mechanism for the laser-controlled emission depends only on transition dipoles, and not on the static moments. In passing it should be observed that a low-frequency, $\omega \to 0$, limit of the above analysis requires caution, because in this limit some of the intermediate system states, allowed for a finite ω, become identifiable with the initial or final state of the process, and are necessarily removed from the sum over states. However, the ensuing result is of little interest since it represents only a correction to the more prominent response, which arises in second order perturbation theory, as noted earlier.

5.2.1 Two-level Quantum Dot Systems

Applicable to a diverse range of applications, quantum dots are exploited as highly efficient chromophores, typically possessing excellent quantum yields and photostability as well as size-tunable and therefore highly selectable optical properties.[32-34] The ease with which such systems can now be manufactured,

chemically manipulated and structurally ordered, as well as their relative simplicity, also makes quantum dots the ideal prototype media in which to observe new nonlinear optical processes. Amongst the wide-ranging investigations into such materials, a number of recent studies have focused on RET, nonlinear optical response and all-optical switching.[35-41] Addressing quantum dots within the established theory requires further assessment of the fully symmetric, third-rank response tensor presented as equation (5.5). This expression can be re-defined relative to the energy difference between the ground and excited states through the relationship $E^{\alpha 0} \equiv \hbar\omega'$, such that:

$$\chi^{0\alpha}_{(ij)k}\left(\xi_{QD}\right)=2\frac{\mu_i^{0\alpha}\left(\xi_{QD}\right)\mu_j^{0\alpha}\left(\xi_{QD}\right)\mu_k^{0\alpha}\left(\xi_{QD}\right)}{\hbar^2\omega^2-\left(E^{\alpha 0}\right)^2}, \tag{5.6}$$

where ξ_{QD} represents the molecular label for any fluorescent, two-level quantum dot media. Exploiting a unique property of quantum dots, the same energy difference is itself dependent on particle size through the following expression:[42]

$$E^{\alpha 0} = E_0^{\alpha 0} + K'\left(R^{-2}\right), \tag{5.7}$$

where $E_0^{\alpha 0}$ represents the difference in energy between excited and ground states of the bulk semi-conductor material *i.e.* on scales outside the quantum size regime, where the energy gap becomes insensitive to particle size. The second term in equation (5.7) represents a correction term highlighting the well-known blue-shift in

emission wavelength with decreasing quantum dot radius, *R*. By substitution of equation (5.7) into the right hand side of equation (5.6):

$$\chi_{i(jk)}^{0\alpha}\left(\xi_{QD}\right)=2\mu_{i}^{0\alpha}\left(\xi_{QD}\right)\mu_{j}^{0\alpha}\left(\xi_{QD}\right)\mu_{k}^{0\alpha}\left(\xi_{QD}\right) \times\left[\left(\hbar\omega\right)^{2}-\left(E_{0}^{\alpha 0}\right)^{2}-2K'E_{0}^{\alpha 0}\left(R^{-2}\right)-K'^{2}\left(R^{-4}\right)\right]^{-1}. \tag{5.8}$$

As a correction term, it can generally be assumed that $K'\left(R^{-2}\right)$ is small in comparison to both $\left(\hbar\omega+E_{0}^{\alpha 0}\right)$ and $\left(\hbar\omega-E_{0}^{\alpha 0}\right)$, and therefore by extension, the $K'^{2}\left(R^{-4}\right)$ term within equation (5.8) represents an insignificant contribution that is subsequently discarded. Moreover, following a Taylor series expansion, the two-level, third-rank response tensor can be presented in a final form as:

$$\chi_{i(jk)}^{0\alpha}\left(\xi_{QD}\right)=2\mu_{i}^{0\alpha}\left(\xi_{QD}\right)\mu_{j}^{0\alpha}\left(\xi_{QD}\right)\mu_{k}^{0\alpha}\left(\xi_{QD}\right)\left[\left(\left(\hbar\omega\right)^{2}-\left(E_{0}^{\alpha 0}\right)^{2}\right)^{-1} +2K'E_{0}^{\alpha 0}\left(R^{-2}\right)\left(\left(\hbar\omega\right)^{2}-\left(E_{0}^{\alpha 0}\right)^{2}\right)^{-2}\right]. \tag{5.9}$$

Essentially, the first term in equation (5.9) is equal to equation (5.5) and represents the nonlinear response to any bulk material undergoing fluorescence decay, whilst subject to an input of non-resonant light. Unique to quantum dots, the second term represents a lead correction displaying a dependence on R^{-2}.

5.3 Fluorescence Anisotropy

As is well established, there is a great deal of important information, highly relevant to speciation and structure determination, which can be derived from fluorescence anisotropy. Specifically, the anisotropy parameters signify the degree to which fluorescence retains a directionality of polarisation from the initial excitation.[43] The associated experimental measurements can also inform on excited state photophysical processes such as internal conversion, rotational diffusion and intramolecular energy transfer etc. Each of these processes represents one of the means by which the character of fluorescent emission can differ from that of the preceding absorption, quite apart from the Stokes shift in wavelength that is normally apparent. The former processes all provide situations in which the emission dipole moment need not be parallel to the absorption moment. To accommodate such features in the present theory, the initial absorption must now be incorporated into our analysis. Since the probe beam is only delivered to the system after the initial excitation, we have:

$$\left\langle I'_{flu}\left(\Omega'\right)\right\rangle \sim \left\langle \left|M_{abs}\left(\xi\right)\right|^2 \left|M^{(1)}_{flu}\left(\xi\right)+M^{(3)}_{flu}\left(\xi\right)\right|^2 \right\rangle, \tag{5.10}$$

where the subscript *abs* denotes the single-photon absorption mechanism. As before, the angular brackets denote an orientational average accounting for the molecular transition moments associated with absorption and emission (the latter duly modified by the probe), that although correlated within the molecular frame,

are together randomly oriented relative to the input propagation. The structure of equation (5.10) provides for the excitation and emission processes to be separable in time. In more detail, the quantum amplitude $M_{abs}(\xi)$ corresponding to the initial absorption is proportional to $\boldsymbol{e}_0(\boldsymbol{p}_0)\cdot\boldsymbol{\mu}^{\nu 0}(\xi)$, where $\boldsymbol{e}_0(\boldsymbol{p}_0)$ represents the input polarisation vector aligned in the *z*-direction by definition, and $\left|\xi^{\nu}\right\rangle$ designates the state initially populated by the excitation. As indicated above, the latter may or may not be the same as the electronic state from which subsequently emission occurs, depending on factors such as the possibility of intervening relaxation or intramolecular energy transfer.

Identical to the method utilized in Chapter 4, the fluorescence anisotropy is now determined from the general expression $r' = \left(\left\langle I'_{\parallel}\right\rangle - \left\langle I'_{\perp}\right\rangle\right)\Big/\left(\left\langle I'_{\parallel}\right\rangle + 2\left\langle I'_{\perp}\right\rangle\right)$. In the present context, this requires the detailed examination of the tensor contractions within equation (5.1) following the inclusion of the initial excitation parameters and the performance of necessary orientational averages.

5.3.1 First-order Correction

After the inclusion of $\boldsymbol{e}_0(\boldsymbol{p}_0)$ and $\boldsymbol{\mu}^{\nu 0}(\xi)$ factors into equation (5.1), the first term represents single-photon induced fluorescence, the last term corresponds to the process modified by the off-resonant laser throughput and the second term, the lead correction, signifies a quantum interference of these two processes. For present

purposes it is assumed that the third term under these conditions represents a comparatively small contribution to be considered later. The most computationally effective procedure for implementing the necessary orientational averages is now well established. The leading term associated with conventional fluorescence requires only a fourth-rank tensor average, whilst the lead correction requires a sixth-rank average. On completion, the following result emerges:

$$\begin{aligned}\left\langle I'_{flu}\left(\Omega'\right)\right\rangle = \frac{\Xi\left(I_0,\omega_0\right)}{15}\Big[& T_{ii}\overline{T}_{jj}\left(3\cos^2\phi-1\right)-T_{ij}\overline{T}_{ij}\left(\cos^2\phi-2\right)\\ & +\frac{I}{7c\varepsilon_0}\Big(2T_{i(ij)j}\overline{T}_{kk}\left(9\cos\theta\cos\varphi\cos\phi-3\cos^2\theta-3\cos^2\varphi-3\cos^2\phi+2\right)\\ & +T_{i(ij)k}\overline{T}_{jk}\left(-12\cos\theta\cos\varphi\cos\phi+11\cos^2\theta+4\cos^2\varphi+4\cos^2\phi-5\right)\\ & +2T_{i(ij)k}\overline{T}_{kj}\left(9\cos\theta\cos\varphi\cos\phi-3\cos^2\theta-3\cos^2\varphi-3\cos^2\phi+2\right)\\ & +T_{i(jj)i}\overline{T}_{kk}\left(-12\cos\theta\cos\varphi\cos\phi+4\cos^2\theta+4\cos^2\varphi+11\cos^2\phi-5\right)\\ & +T_{i(jj)k}\overline{T}_{ik}\left(8\cos\theta\cos\varphi\cos\phi-5\cos^2\theta-5\cos^2\varphi-5\cos^2\phi+8\right)\\ & +T_{i(jk)j}\overline{T}_{ik}\left(-12\cos\theta\cos\varphi\cos\phi+4\cos^2\theta+11\cos^2\varphi+4\cos^2\phi-5\right)\Big)\Big],\end{aligned}$$

(5.11)

where $\Xi\left(I_0,\omega_0\right)$ is a constant of proportionality incorporating the initial excitation beam irradiance, I_0, and its corresponding optical frequency ω_0, noting that overbars again denote complex conjugation. In the above expression, the first two terms are essentially identical to equation (4.20) and as before, signify the expected response for one-photon fluorescence, whilst subsequent terms represent the leading corrections produced by the probe. The equation is explicitly cast in terms of the

three distinct angles between each pair of polarisation vectors, for the incident, off-resonant probe and emitted light: $\theta = \cos^{-1}\left(\boldsymbol{e}_0(\boldsymbol{p}_0)\cdot\boldsymbol{e}(\boldsymbol{p})\right)$, $\varphi = \cos^{-1}\left(\boldsymbol{e}(\boldsymbol{p})\cdot\boldsymbol{e}'(\boldsymbol{p}')\right)$ and $\phi = \cos^{-1}\left(\boldsymbol{e}_0(\boldsymbol{p}_0)\cdot\boldsymbol{e}'(\boldsymbol{p}')\right)$. To describe the products of molecular transition moments, the result utilizes a similar shorthand notation to that established in Chapter 4, where for example T_{ij} represents $\mu_i^{\nu 0}(\xi)\mu_j^{0\alpha}(\xi)$, whilst $T_{i(ij)j}$ corresponds to $\mu_i^{\nu 0}(\xi)\chi_{(ij)j}^{0\alpha}(\xi)$, noting that the first index of each $\boldsymbol{T}$ tensor is associated with the initial molecular excitation. It is worth highlighting that the third-rank response tensor in this and all ensuing expressions, relates to the form of equation (5.5). The equivalent quantum dot response tensor presented as equation (5.9) represents a significant and relevant result, but its inclusion for now would significantly complicate the analysis to follow.

As shown in the previous Section, taking the two-level form of the nonlinear response tensors has the effect of introducing Kleinman symmetry in each of the optically nonlinear response tensor contributions. It emerges that the six nonlinear response tensor products that feature in equation (5.11) are no longer linearly independent under such conditions, and the result can be recast in a simpler form involving just three such products:

$$\left\langle I'_{flu}\left(\Omega'\right)\right\rangle = \frac{\Xi\left(I_0,\omega_0\right)}{15}\Big[T_{ii}\bar{T}_{jj}\left(3\cos^2\phi-1\right)-T_{ij}\bar{T}_{ij}\left(\cos^2\phi-2\right)$$
$$+\frac{I}{7c\varepsilon_0}\Big(T_{i(ijj)}\bar{T}_{kk}\left(6\cos\theta\cos\varphi\cos\phi-2\cos^2\theta-2\cos^2\varphi+5\cos^2\phi-1\right)$$
$$+T_{i(ijk)}\bar{T}_{jk}\left(6\cos\theta\cos\varphi\cos\phi+5\cos^2\theta-2\cos^2\varphi-2\cos^2\phi-1\right)$$
$$+T_{i(jjk)}\bar{T}_{ik}\left(-4\cos\theta\cos\varphi\cos\phi-\cos^2\theta+6\cos^2\varphi-\cos^2\phi+3\right)\Big)\Big], \tag{5.12}$$

where the following have been applied, $T_{i(ij)j}\bar{T}_{kk}+T_{i(jj)i}\bar{T}_{kk}=2T_{i(ijj)}\bar{T}_{kk}$, $T_{i(ij)k}\bar{T}_{jk}+T_{i(ij)k}\bar{T}_{kj}=2T_{i(ijk)}\bar{T}_{jk}$ and $T_{i(jj)k}\bar{T}_{ik}+T_{i(jk)j}\bar{T}_{ik}=2T_{i(jjk)}\bar{T}_{ik}$. In deriving specific results for independent polarisation components, further simplification can now be achieved by writing each of the above molecular tensors explicitly in terms of components of the two transition dipole moments, the photo-selected $\boldsymbol{\mu}^{\nu 0}\left(\xi\right)$, the emission $\boldsymbol{\mu}^{0\alpha}\left(\xi\right)$ and the angle between these two moments, β. Assuming that the initial excitation has plane polarisation and remembering that it is arbitrarily aligned in the *z*-direction, the resulting fluorescence is now resolved for polarisations $e'_z\left(p'_z\right)$ and $e'_x\left(p'_x\right)$ respectively. Utilizing equation (5.12), the results where $\phi=0,\varphi=\pi/2,\theta=\pi/2$, define the probe input alignment in the x-direction, and are as follows:

$$\left\langle I'_{\parallel}\left(\Omega'\right)\right\rangle = \frac{\Xi\left(I_0,\omega_0\right)\left|\boldsymbol{\mu}^{0\alpha}\left(\xi\right)\right|^2\left|\boldsymbol{\mu}^{\nu 0}\left(\xi\right)\right|^2}{15}$$
$$\times\left[2\cos^2\beta+1+\frac{2I\left|\boldsymbol{\mu}^{0\alpha}\left(\xi\right)\right|^2\left(\cos^2\beta+2\right)}{7c\varepsilon_0\hbar^2\left(\omega^2-\omega'^2\right)}\right], \tag{5.13}$$

and for $\phi = \pi/2, \varphi = 0, \theta = \pi/2$:

$$\left\langle I'_{\perp}(\Omega')\right\rangle = \frac{\Xi(I_0,\omega_0)\left|\boldsymbol{\mu}^{0\alpha}(\xi)\right|^2\left|\boldsymbol{\mu}^{\nu 0}(\xi)\right|^2}{15} \times\left[2-\cos^2\beta+\frac{2I\left|\boldsymbol{\mu}^{0\alpha}(\xi)\right|^2\left(9-6\cos^2\beta\right)}{7c\varepsilon_0\hbar^2\left(\omega^2-\omega'^2\right)}\right]. \tag{5.14}$$

Hence, upon substitution of equations (5.13) and (5.14) into the general anisotropy expression, the following is determined:

$$r' = \frac{3\cos^2\beta - 1 + KI\left|\boldsymbol{\mu}^{0\alpha}(\xi)\right|^2\left(\cos^2\beta-1\right)}{5+KI\left|\boldsymbol{\mu}^{0\alpha}(\xi)\right|^2\left(20-11\cos^2\beta\right)/7}, \tag{5.15}$$

where $K = 2\left(c\varepsilon_0\hbar^2\left(\omega^2-\omega'^2\right)\right)^{-1}$. In the limiting case where $I = 0$, the well-known expression $r = \frac{1}{5}\left(3\cos^2\beta - 1\right)$ is recovered. Generally, however, a change in fluorescence anisotropy can be seen to result from the interaction with the probe beam, although it is to be re-emphasized that the state of the latter beam is unaffected.

5.3.2 Inclusion of Higher-order Correction

Up to this point, the third term in equation (5.1), quadratically dependent on probe laser intensity, has not been considered in detail as its contribution to the overall

fluorescence intensity is generally expected to be negligible. Nevertheless, there can be circumstances in which the third term alone provides the fluorescence response, typically when the first and second contributions are null. Addressing this case requires the theory to progress beyond the two-level approximation. Consider for example a system where following optical excitation, population is efficiently transferred to a state $\left|\xi^{\alpha}\right\rangle$ that might normally decay non-radiatively, transitions from $\left|\xi^{\alpha}\right\rangle$ to $\left|\xi^{0}\right\rangle$ being weak or entirely precluded, for example as a result of inherent geometric or symmetry constraints. Terms in equation (5.1) that feature $\boldsymbol{\mu}^{0\alpha}\left(\xi\right)$ will no longer contribute to the observed emission, which instead is activated solely in response to the off-resonant throughput. Clearly, such a two-level model would also predict a vanishing response from the probe laser, due to the associated structure of the third-rank response tensor portrayed as equation (5.5). However, the more general analysis accommodating higher energy levels in the sum over states, allows the possibility of a decay transition that is symmetry allowed by three-photon selection rules.

An outline for an all-optical switch based on laser-controlled fluorescence may be described as follows: (i) an individual molecule is indirectly excited to a “dark” state, *i.e.* one whose direct dipolar excitation from the ground state is forbidden; (ii) precluded by the one-photon dipole selection rules, fluorescence occurs from this “dark” state through optical nonlinear activation only; (iii) this activation arises due to the presence of the intense non-resonant laser field, the relevant molecular transitions are therefore assumed three-photon allowed, but single-photon

forbidden. Whilst specific systems described in the introduction of Chapter 3 may be suitable, more general examples are afforded by excited states of A_2 symmetry, in molecules of C_{2v} or C_{3v} symmetry, or states of A_u symmetry in D_{2h} species. In such cases, the switching action is enabled since the throughput or absence of the laser input will cause activation or deactivation of the fluorescence, respectively. Clearly it is necessary for the radiation to be delivered in a pulse whose duration and delay, both with respect to the initial excitation, are sufficiently short that it can engage with the system before there is significant non-radiative dissipation of the excited state.

The result for this case is secured on completion of a rotational-average requiring the eighth-rank isotropic tensor average. The calculation leads to the result:

$$\begin{aligned}\left\langle I'_{flu}\left(\Omega'\right)\right\rangle = \Xi\left(I_0,\omega_0\right)\left(\frac{I^2}{1260c^2{\varepsilon_0}^2}\right)\Big[&3T_{i(ijj)}\overline{T}_{k(kll)}\left(3\cos^2\theta\cos^2\varphi-\cos^2\theta-\cos^2\varphi\right.\\&\left.+\cos^2\phi\right)+6T_{i(ijk)}\overline{T}_{j(kll)}\left(6\cos\theta\cos\varphi\cos\phi-\cos^2\theta-2\cos^2\varphi-2\cos^2\phi\right.\\&\left.+1\right)+3T_{i(ijk)}\overline{T}_{l(jkl)}\left(\cos^2\theta\cos^2\varphi-4\cos\theta\cos\varphi\cos\phi+5\cos^2\theta+\cos^2\varphi\right.\\&\left.+4\cos^2\phi-3\right)+3T_{i(jjk)}\overline{T}_{i(kll)}\left(-\cos^2\theta\cos^2\varphi-4\cos\theta\cos\varphi\cos\phi+\cos^2\theta\right.\\&\left.+5\cos^2\varphi+\cos^2\phi-1\right)+T_{i(jkl)}\overline{T}_{i(jkl)}\left(-\cos^2\theta\cos^2\varphi+4\cos\theta\cos\varphi\cos\phi\right.\\&\left.-5\cos^2\theta+\cos^2\varphi-4\cos^2\phi+7\right)\Big].\end{aligned} \tag{5.16}$$

Here, the $\boldsymbol{T}$ tensors accommodate sums over products of transition moments that specifically exclude $\boldsymbol{\mu}^{0\alpha}\left(\xi\right)$, on the basis of the decay transition being symmetry-

forbidden under electric dipole selection rules, however for simplicity we retain the assumption of Kleinman index symmetry in the embedded $\boldsymbol{\chi}^{0\alpha}(\xi)$ tensors.

5.3.3 Complete Result for a Two-level System

For completeness, although the above expression must apply to emission from an indirectly excited state, one can adopt the corresponding result for a case of E1-allowed emission and thereby provide a completely general result for the probe-modified fluorescence anisotropy, accommodating all of the terms arising from equation (5.1). Taking once again the two-level model for the emission, we then have:

$$r' = \frac{3\cos^2\beta - 1 + KI\left|\boldsymbol{\mu}^{0\alpha}(\xi)\right|^2\left(\cos^2\beta - 1\right) + \left(K^2I^2\left|\boldsymbol{\mu}^{0\alpha}(\xi)\right|^4/84\right)\left(15\cos^2\beta - 17\right)}{5 + \left(KI\left|\boldsymbol{\mu}^{0\alpha}(\xi)\right|^2/7\right)\left(20 - 11\cos^2\beta\right) + \left(K^2I^2\left|\boldsymbol{\mu}^{0\alpha}(\xi)\right|^4/84\right)\left(43 - 30\cos^2\beta\right)}. \tag{5.17}$$

In a case where the absorption and transition moments are parallel, we secure the very simple result:

$$r' = \frac{2 - 2\left(K^2I^2\left|\boldsymbol{\mu}^{0\alpha}(\xi)\right|^4/84\right)}{5 + 9\left(KI\left|\boldsymbol{\mu}^{0\alpha}(\xi)\right|^2/7\right) + 13\left(K^2I^2\left|\boldsymbol{\mu}^{0\alpha}(\xi)\right|^4/84\right)}, \tag{5.18}$$

showing that with increasing intensity of the probe beam, the first departures from the probe-free result, $r' = 0.4$, can be anticipated in the linear-response regime

5.4 Conclusion

Developing earlier pioneering work by Bradshaw and Andrews, the theory of laser-modified molecular fluorescence has been developed in order to elicit a number of features of particular experimental significance.[7-10] Use of the two-level emission model is widely valid for systems including those that incorporate common fluorescent markers, such as quantum dots, and here it proves to offer succinct and experimentally tractable results of broad applicability, whose simplified form without further approximation is consistent with the adoption of Kleinman symmetry. Whilst commonly adopted, the casual interchangeability of indices within nonlinear polarisability tensors, such as in those described above, should be cautioned. A number of recent reports highlight the general failure of Kleinman symmetry when applied to practical nonlinear systems.[44,45] The method still proves valid in multiple applications, for example in the case of SHG, provided there is no significant dispersion in the nonlinear response over the entire range of frequencies involved. Consequently, many will consider the benefits afforded by the simplicity of the theory greatly outweigh the potential for error.

Equations have been derived for the anisotropy of fluorescence that can be expected from a system responding to the passage of off-resonant light, its leading correction

being linearly dependent on the probe irradiance and manifest as a reduction of the measured anisotropy. It has also been shown that, for some electronic states that normally decay non-radiatively, it is possible to optically switch fluorescent emission using the off-resonance probe. In all such respects, the capacity to engage with and to optically control the fluorescence process offers significant new grounds for the interrogation of fluorescent materials.

References

1. Marsh, R.J., Armoogum, D.A. & Bain, A.J. *Chem. Phys. Lett.* **366**, 398 (2002).
2. Hell, S.W. *Science* **316**, 1153 (2007).
3. Willig, K.I., Harke, B., Medda, R. & Hell, S.W. *Nat. Meth.* **4**, 915 (2007).
4. Harke, B., Keller, J., Ullal, C.K., Westphal, V., Schönle, A. & Hell, S.W. *Opt. Express* **16**, 4154 (2008).
5. Armoogum, D.A. Marsh, R.J., Nicolaou, N., Mongin, O., Blanchard-Desce, M. & Bain, A.J. *Proc. SPIE* **7030**, 70300S (2008).
6. Leutenegger, M., Eggeling, C. & Hell, S.W. *Opt. Express* **18**, 26417 (2010).
7. Bradshaw, D.S. & Andrews, D.L. *J. Phys. Chem. A* **113**, 6537 (2009).
8. Andrews, D.L., Leeder, J.M. & Bradshaw, D.S. *Proc. SPIE* **7712**, 7712R (2010).
9. Andrews, D.L. & Bradshaw, D.S. *Opt. Commun.* **283**, 4365 (2010).
10. Bradshaw, D.S. & Andrews, D.L. *Phys. Rev. A* **81**, (2010).

11. Rigneault, H., Capoulade, J., Dintinger, J., Wenger, J., Bonod, N., Popov, E., Ebbesen, T. & Lenne, P. *Phys. Rev. Lett.* **95**, (2005).
12. Anger, P., Bharadwaj, P. & Novotny, L. *Phys. Rev. Lett.* **96**, (2006).
13. Yu, Y.-J., Noh, H., Jhe, W., Noh, H.-R., Nakaoka, T. & Arakawa, Y. *Phys. Rev. B* **82**, 085308 (2010).
14. Kirkpatrick, S.M., Naik, R.R. & Stone, M.O. *J. Phys. Chem. B* **105**, 2867 (2001).
15. Drobizhev, M., Makarov, N.S., Hughes, T. & Rebane, A. *J. Phys. Chem. B* **111**, 14051 (2007).
16. Asselberghs, I. Flors, C., Ferrighi, L., Botek, E., Champagne, B., Mizuno, H., Ando, R., Miyawaki, A., Hofkens, J., Auweraer, M. & Clays, K. *J. Am. Chem. Soc.* **130**, 15713 (2008).
17. Drobizhev, M., Tillo, S., Makarov, N.S., Hughes, T.E. & Rebane, A. *J. Phys. Chem. B* **113**, 12860 (2009).
18. Zrenner, A. Beham, E., Stufler, S., Findeis, F., Bichler, M. & Abstreiter, G. *Nature* **418**, 612 (2002).
19. Klimov, V.I. *Los Alamos Science* **28**, 214 (2003).
20. Allcock, P., Jenkins, R.D. & Andrews, D.L. *Chem. Phys. Lett.* **301**, 228 (1999).
21. Allcock, P., Jenkins, R.D. & Andrews, D.L. *Phys. Rev. A* **61**, 023812 (2000).
22. Andrews, D.L. & Crisp, R.G. *J. Opt. A* **8**, S106 (2006).
23. Andrews, D.L. *Phys. Rev. Lett.* **99**, 023601 (2007).
24. Andrews, D.L., Crisp, R.G. & Li, S. *J. Chem. Phys.* **127**, 174702 (2007).
25. Bradshaw, D.S. & Andrews, D.L. *Appl. Phys. B* **93**, 13 (2008).

26. Bradshaw, D.S. & Andrews, D.L. *J. Chem. Phys.* **128**, 144506 (2008).

27. Bradshaw, D.S. & Andrews, D.L. *Laser Phys.* **19**, 125 (2009).

28. Kleinman, D.A. *Phys. Rev.* **126**, 1977 (1962).

29. Andrews, D.L., Dávila Romero, L.C. & Meath, W.J. *J. Phys. B* **32**, 1 (1999).

30. Dávila Romero, L.C. & Andrews, D.L. *J. Phys. B* **32**, 2277 (1999).

31. Andrews, D.L. & Dávila Romero, L.C. *J. Phys. B* **34**, 2177 (2001).

32. Prasad, P.N. *Nanophotonics*. (Wiley: Hoboken, N.J., 2004).

33. Walling, M.A., Novak, J.A. & Shepard, J.R.E. *Int. J. Mol. Sci.* **10**, 441 (2009).

34. Hutter, E. & Maysinger, D. *Microsc. Res. Techniq.* **74**, 592 (2011).

35. Guenther, T., Lienau, C., Elsaesser, T., Glanemann, M., Axt, V., Kuhn, T., Eshlaghi, S. & Wieck, A. *Phys. Rev. Lett.* **89**, (2002).

36. Prasanth, R., Haverkort, J.E.M., Deepthy, A., Bogaart, E.W., van der Tol, J.J.G.M., Patent, E.A., Zhao, G., Gong, Q., van Veldhoven, P.J., Nötzel, R. & Wolter, J.H. *Appl. Phys. Lett.* **84**, 4059 (2004).

37. Wesseli, M., Ruppert, C., Trumm, S., Krenner, H.J., Finley, J.J. & Betz, M. *Appl. Phys. Lett.* **88**, 203110 (2006).

38. Curutchet, C., Franceschetti, A., Zunger, A. & Scholes, G.D. *J. Phys. Chem. C* **112**, 13336 (2008).

39. Lunz, M., Bradley, A.L., Chen, W. & Gun'ko, Y.K. *J. Phys. Chem. C* **113**, 3084 (2009).

40. Sun, Z., Juriani, A., Meininger, G.A. & Meissner, K.E. *J. Biomed. Opt.* **14**, 040502 (2009).

41. Bradshaw, D.S. & Andrews, D.L. *Superlattices Microst.* **47**, 308 (2010).

42. Klimov, V.I. *Los Alamos Science* **28**, 214 (2003).

43. Valeur, B. *Molecular Fluorescence*. (Wiley-VCH: Weinheim, 2002).

44. Dailey, C.A., Burke, B.J. & Simpson, G.J. *Chem. Phys. Lett.* **390**, 8 (2004).

45. Xu, M. & Jiang, S. *J. Phys. Condens. Mat.* **18**, 8987 (2006).